F.W. Klaiber
D.J. Dedic
K.F. Dunker
W.W. Sanders, Jr.

Final Report—Part I

Strengthening of Existing Single Span Steel Beam and Concrete Deck Bridges

February 1983

Sponsored by the Highway Division,
Iowa Department of Transportation
and the Iowa Highway Research Board

Iowa DOT Project HR-238
ERI Project 1536
ISU-ERI-Ames-83185

DEPARTMENT OF CIVIL ENGINEERING
ENGINEERING RESEARCH INSTITUTE
IOWA STATE UNIVERSITY, AMES

TABLE OF CONTENTS

LIST OF FIGURES

LIST OF TABLES

INTRODUCTION

1.1 General Background

A considerable number of single span, composite concrete deck and steel beam bridges in Iowa, as well as in most states, presently cannot be rated to carry today's design loads. This problem was initially addressed in the research project, HR-214, "Feasibility Study of Strengthening Existing Single Span Steel Beam Concrete Deck Bridges" [18,19], henceforth referred to as Phase I. The research of Phase I verified that post-tensioning can be used to provide strengthening of the composite bridges in question. This was determined analytically, using a modification of the orthotropic plate theory, and experimentally, through testing of various post-tensioning schemes on a half-scale model bridge.

Because of the importance of the strengthening problems and the wide range of variables, a second research study was undertaken. The second study involved two parts. As the second study was a continuation of the feasibility study (Phase I), the two parts, henceforth, will be referred to as Phases II and III. The primary emphasis of Phase II involved the strengthening of two full-scale prototype bridges. One of the bridges was a prototype of the model bridge tested during Phase I; the other bridge was larger and skewed.

In addition to this field work, Phase II also involved a considerable amount of laboratory work. A literature search revealed that only minimal data existed on the angle-plus-bar shear connectors. Thus, several specimens utilizing angle-plus-bars, as well as channels,

studs and high strength bolts utilized as shear connectors were fabricated and tested. To obtain additional shear connector information, the bridge model of Phase I was sawed into four composite concrete slab and steel beam specimens. Two of the resulting specimens were tested with the original shear connection, while the other two specimens had additional shear connectors added before testing. In this way, the effect of the additional shear connectors could be determined.

As previously mentioned, one of the bridges selected for strengthening was a 45° skewed bridge. Although orthotropic plate theory was shown in Phase I to predict vertical load distribution in bridge decks and to predict approximate distribution of post-tensioning for right-angle bridges, we questioned whether the theory could also be used on skewed bridges. Thus, a small plexiglas model was constructed and used in vertical load distribution tests and post-tensioning force distribution tests for verification of the theory.

Phase III of the investigation involves the inspection of the two strengthened bridges approximately every three months for a period of two years. Approximately one year after post-tensioning, both bridges will be tested under service loads to determine if there are any behavioral changes from the initial service load tests. The results of Phase II--laboratory and field investigations--are reported herein; results of Phase III will be presented in a final report at the conclusion of the study.

1.2 Objectives

The overall objective of Phase I of the study was to determine the feasibility of strengthening the type of bridges in question by post-tensioning. As a result of the successful completion of Phase I of the study, Phase II was undertaken with the overall objective of designing and installing post-tension strengthening on two existing bridges. After the bridges were strengthened, they both were tested to determine the effectiveness of the post-tension strengthening systems. Before the field strengthening systems could be designed, additional data were needed on the strength of the angle-plus-bar shear connectors, thus requiring the additional laboratory work in Phase II.

In line with the overall objective of Phase II of this study, the following secondary objectives were established:

- Determine load distribution before and after post-tensioning in actual bridges.
- Determine vertical load and post-tension force distribution in skewed bridges.
- Determine strength and behavior of angle-plus-bar shear connectors and compare with other shear connectors, such as studs and channels.
- Develop a simple method of adding shear connectors to existing construction and evaluate their strength and effectiveness.

- Determine if there are any field problems in employing the post-tensioning scheme developed during Phase I that did not exist in the laboratory.

Field experimental results were compared wth theoretical predictions obtained from orthotropic plate theory. Laboratory experimental results were compared with theoretical predictions using appropriate theories.

1.3 Literature Review

The report on Phase I of the study [19] included a literature review which was organized into four areas: prestressed steel structures, prestressed composite structures, bridge strengthening, and bridge deck analysis. Although the majority of these references are pertinent to the work in Phase II, a review will not be repeated here due to their availability in Ref. [19]. Therefore, the literature review which follows only pertains to shear connectors and skewed bridges.

1.3.1 Mechanical Shear Connectors

Numerous types of mechanical shear connectors have been proposed since the early 1920's for steel and concrete composite construction. Although spirals, channels, and studs found wide acceptance in the United States then, stud connectors are almost exclusively used today because of their ease of installation and low cost.

The use of two-slab push-out tests for the evaluation of shear connector behavior was common [27,29,31]. These early investigations suggested that the strength of shear connectors obtained from push-out

tests was lower than that obtained from beam tests. It was later concluded by Slutter and Driscoll [28] that this relationship was true. Also, the push-out test is still considered to be the most reliable and useful method of determining load-slip and ultimate load capacities of different types of connectors used in beams [5,21].

The use of high strength bolts (ASTM A325) as shear connectors has been tested in several situations [6,7,10]. Dallam [7], in 1968 and 1970, reported the testing of two-slab push-out and composite beam specimens with high strength bolts (ASTM A325, various diameters) as shear connectors. The bolts were loosely attached to the steel beam section and held in place by wire-spring chairs. After the slab concrete was cured for 28 days, the bolts were tightened to the minimum specified bolt tension; the specimens were then tested to failure. It was found that the bolts exhibited a greater useful capacity and ultimate strength than comparable studs. In 1976, Dorton [10] described the use of high strength bolts (ASTM A325 Type 3 weathering steel, 7/8-in. diameter) in push-out specimens and a full-scale test bridge. The bolts were double-nutted to the beam flange of a steel bridge stringer (H-pile section substituted in the push-out specimens), and placed in oversize holes to accommodate movement of the concrete deck due to post-tensioning. Both the push-out specimens and the test bridge were subjected to fatigue and static loading. Dorton concluded that a high strength bolt in this particular configuration could be safely used to replace a welded stud of the same diameter. In the studies described above, the bolts were placed before the concrete slab was cast.

Slutter and Driscoll [28] tested a series of composite beams and push-out specimens. They also re-evaluated the test results from other investigations in order to substantiate their conclusions. Tests were performed on composite beams with varying numbers of shear connectors. A number of different shear connectors (channels, spirals, bent studs, headed studs) were tested in the composite beam and push-out specimens. Test results from this and previous investigations were compared. This was done by utilizing a method of analysis for determining the ultimate moment capacity of beams when a weaker shear connection than that proposed for design existed. Slutter and Driscoll concluded that the ultimate flexural capacity of a beam could be evaluated, even if the number of shear connectors was less than that required to develop the theoretical ultimate bending capacity. The analysis showed that the load-deflection curve of a beam was not significantly affected by slip if there were enough shear connectors provided to develop the theoretical ultimate bending capacity.

In the literature it has been established that push-out tests give reliable and slightly conservative results for the ultimate strength of shear connectors. Properly installed high strength bolts provided a slightly higher strength and therefore can be substituted for welded stud connectors of equal diameter. Load-deflection behavior of a composite beam is not significantly affected by slip of shear connectors, as long as connectors are adequate for ultimate flexural capacity of the beam.

1.3.2 Effect of Skew on Bridge Deck Behavior

Skew generally has a greater effect on isotropic than on orthotropic bridge decks. A rather comprehensive review of skew effects on prestressed slab bridge decks is contained in the publication by Clark and West [4]. The authors tested two 45° skewed, solid slab bridge deck models and compared the model results with separate grillage and finite element analyses. The models represented bridge decks which were essentially isotropic except for longitudinal post-tensioning.

Clark and West separated the prestressing into separate axial and bending components for purposes of analysis. Although the axial component could be treated on a simple force per area basis, the bending component could not be treated so simply. Because a portion of the bending component was dispersed in the slab as torsional and transverse bending stresses, a simple treatment of the bending component applied to a slab strip of unit width would overestimate the effects of the bending component. Increasing skew and increasing aspect ratio (width to length) increased bending component losses, whereas increasing orthotropy (longitudinal to transverse strength) decreased losses.

Due to the post-tensioning, obtuse corners of the bridge deck were subject to uplift, if not tied down. Downward reactions due to application of live load tended to concentrate in the obtuse corners. Minor differences in behavior occurred depending on the sequence of post-tensioning of a slab bridge deck.

For slab bridge decks, Lee and Chaplin [22] reiterated several of the conclusions reached by Clark and West, namely that prestressing could cause uplift at obtuse corners, that maximum reactions due to

live load occurred in obtuse corners and that beam and slab (orthotropic) bridge decks would have reduced skew effects. Lee and Chaplin also noted that, for slab bridges, moments were large in obtuse corners and that the directions of principal moments were dependent on the position of a live load. The variation in direction of principal moments therefore requires additional quantities of reinforcing, beyond that required for right-angle bridges.

Newmark, Siess, and Peckham [23] tested both 30° and 60° skewed, quarter-scale composite beam and slab (orthotropic) bridge models. For a 30° skewed bridge model, deflections and live load distribution to beams were essentially the same as for a right-angle bridge model. Beam strains in the skewed model were up to 5% larger than in right-angle bridge models.

For the 60° skewed model, differences between the skewed and right-angle models became quite apparent. Smaller deflections were measured in the 60° skewed model, and deflections and load distributions were less uniform. Beam strains were up to 14% less. The change in performance can be explained by partial restraint at beam ends and increased torsional stiffness of the bridge deck.

Hondros and Marsh [15] tested a series of right-angle and 30° skewed composite bridge models. They found that in the 30° skewed model strains and deflections were approximately 17% less. It appeared to them that the proportion of load to each beam remained essentially the same for the right-angle and 30° skewed bridge models.

Gustafson and Wright [13] utilized finite element analysis to analyze the effects of skew on an 80-ft span, two-lane steel girder

and concrete slab composite bridge. Their analysis showed almost no change in distribution of moment to the girders for angles of skew less than 30°, and no significant change unless the skew angle exceeded 45°. They found that exterior girders were less sensitive to skew than interior girders. Influence lines for girder reactions which they plotted indicated that exterior girders carried a large percentage of midspan concentrated loads--even when interior girders rather than exterior girders were loaded.

DeCastro and Kostem [8] conducted a rather extensive finite element analysis of composite, prestressed concrete I-beam bridges of moderate span. Their results were quite comparable to those of Gustafson and Wright. Exterior beams were less affected by skew than were interior beams, and the effect of skew was not significant until the angle of skew exceeded 45°. For relatively closely spaced beams (small S/L ratios), the authors found that the distribution factor actually increased slightly. The effect of skew decreased as the span of the bridge increased.

Kennedy and Gupta [17] correlated orthotropic plate theory (modified to account for skew) with model tests. They concluded that for orthotropic plates, skew had a greater effect for uniform load than for a concentrated load. For a concentrated load at midspan, their charts can be interpreted to show results similar to those contained in other research reviewed above. For an interior beam, skew had the effect of decreasing moment to the beam, and the reduction became significant at angles of skew greater than 45°. For an exterior beam, the charts indicated a slight increase in moment with increasing skew.

Bakht, Cheung, and Aziz [3] described the use of charts for load distribution in the Ontario bridge code. Although their charts are for right-angle bridges, they indicated that bridges with angles of skew to 15° may be treated as right-angle bridges.

The review of literature on skewed bridge decks indicated several potential problem areas. Both moments and reactions tended to concentrate in obtuse corners. In particular, uplift could occur at obtuse corners due to prestressing. These effects were more pronounced for isotropic than for orthotropic bridge decks. The various authors considered skew to have a significant effect at angles of 15° to 45°, depending on the type of bridge deck. Truck load distribution for orthotropic, composite beam and slab bridges is quite similar for angles of skew of 0° to 45°, but changes significantly for angles of skew greater than 45°.

1.4 General Testing Program

As previously stated, Phase II of the study consisted of both a laboratory investigation and a field investigation. Brief descriptions of each of these investigations are presented in the following sections; detailed information about the various tests will be presented later in this report.

1.4.1 Laboratory Testing Program

The laboratory investigation consisted of three programs: one involved the determination of the strength and load-slip characteristics of various shear connectors; the second involved testing of the composite

beams cut from the bridge model of Phase I; and the third involved the testing of a small scale plexiglas model to determine vertical load and post-tensioning force distribution in a skewed bridge.

Push-out specimens were utilized to investigate the strength and behavior of various shear connectors. Deflection dials were used in each test to measure relative slip and separation between the concrete and steel. A total of 22 specimens were fabricated and tested to failure. The types of shear connector used in the specimens were as follows: six angle-plus-bar connectors, five channel connectors, three stud connectors, four epoxied high strength bolt connectors, and four double-nutted high strength bolt connectors.

The model bridge utilized in Phase I was sawed into four composite concrete slab and steel beam specimens. Two of the specimens, one interior and one exterior, were tested in the "as fabricated" condition, while the remaining two specimens had additional shear connectors added before testing. All tests employed two equal concentrated loads positioned about the span centerline so that a region of pure moment existed. After several tests were performed, each specimen was post-tensioned and loaded to failure with vertical loading. Strain gages utilized in the testing of the model bridge in Phase I were again utilized to collect strain data for each specimen. Deflection dials were used to measure vertical deflection of the specimens, as well as relative slip between the concrete slab and steel beam.

A plexiglas model of the skewed bridge selected for field strengthening was fabricated and instrumented with strain gages for load distri-

bution testing. The bridge model was subjected to vertical concentrated loads, simulated truck loading, and various post-tensioning schemes.

1.4.2 Field Testing Program

After several meetings with the Iowa DOT Office of Bridge Design, two bridges were selected on which the post-tension strengthening technique could be applied. One of the bridges, henceforth referred to as Bridge 1, is located in Dickinson County (2.2 miles north of Terrill on county road N14), and is on the secondary road system. The other bridge, henceforth referred to as Bridge 2, is located in Greene County (a few yards south of the Greene-Webster County line on Iowa 144), and is on the primary highway system.

Bridge 1 is a four beam 50 ft × 30 ft I-beam right-angle bridge, which is essentially identical to the prototype for the model bridge used in Phase I. Thus, Bridge 1 is essentially twice the size of the laboratory model bridge.

Bridge 2 is a four beam 70 ft × 30 ft I-beam 45° skewed bridge which was used as the prototype of the plexiglas model bridge.

Both bridges were instrumented with strain gages and deflection dials. Although essentially the same instrumentation was employed on both bridges, more strain gages and deflection dials were used on Bridge 2 to determine the effects of the skew and to measure the end restraint present.

The testing program employed, which was essentially the same for both bridges, consisted of determining the response of the bridge:

- To an overloaded truck before post-tensioning

- To post-tensioning
- To an overloaded truck after post-tensioning.

2. DESCRIPTION OF TESTS

2.1 Push-Out Tests

2.1.1 Description of Specimens

The push-out specimens were of two sizes: one full-scale and the other half-scale. Dimensions of the specimens are shown in Fig. 1. As is shown, each specimen consisted of a wide-flange beam, 2 ft long, with concrete slabs attached to each flange of the beam. The size of the wide-flange beams utilized (W10×22 in the half-scale specimens and W10×68 in the full-scale specimens) was chosen on the basis of flange thickness of the beam sections. The flange thickness of the full-scale specimens closely approximated that of the exterior beams in existing bridges; the flange thickness in the half-scale specimens nearly equalled that of the exterior beams in the model bridge. As shown in Figs. 2 through 6 and also described in Table 1, shear connectors were rigidly attached to the beam flanges by bolting or welding. Load was applied to the upper portion of the beam and transmitted into the slabs through the shear connectors. Thus, both the slabs and beam were subjected to compression.

The push-out specimens were grouped into two categories:

1) Type A specimens (as shown in Figs. 2, 3, and 4) employed welded connectors installed before the concrete was poured.
2) Type B specimens (Figs. 5 and 6) had high strength bolts inserted and tightened after the slabs had cured.

Thus, Type A specimens were modeled as shear connectors currently in use on various composite bridges and on the half-scale bridge of

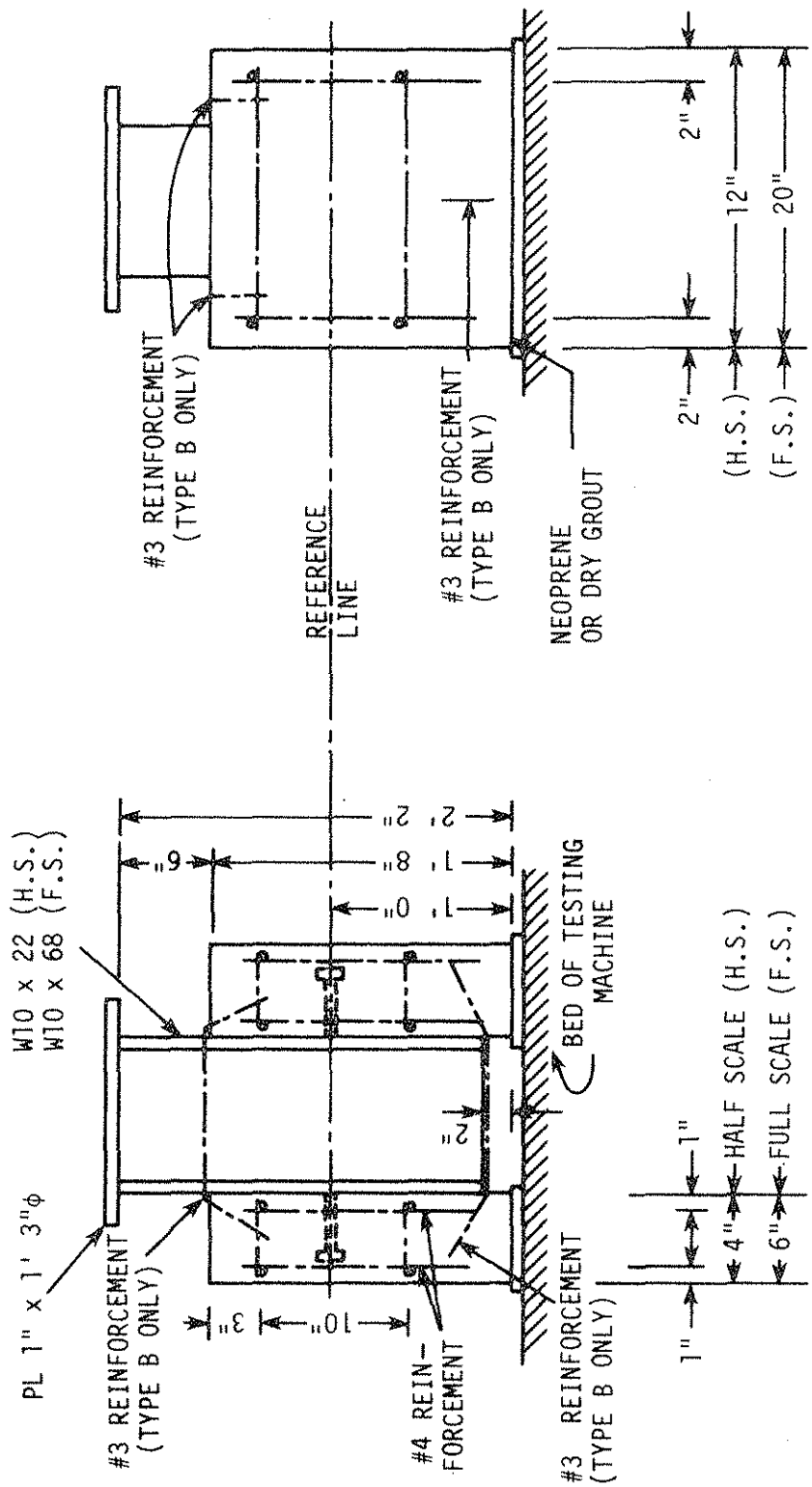

Fig. 1. Details and dimensions of the push-out specimen.

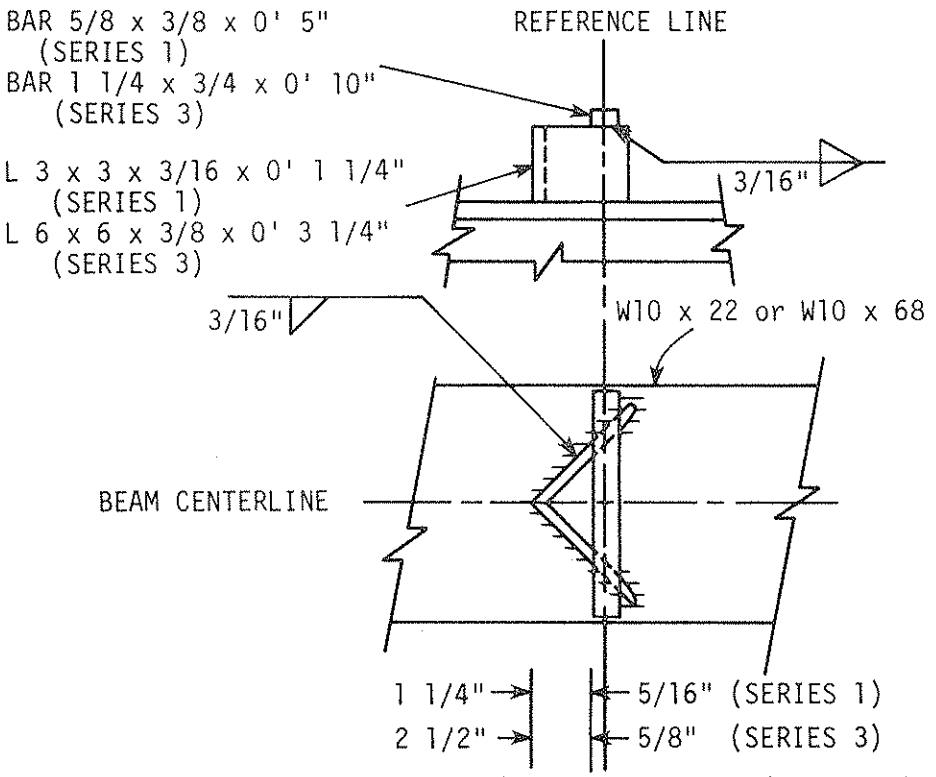

a. Details of half-scale (SERIES 1) and full-scale (SERIES 3) connector.

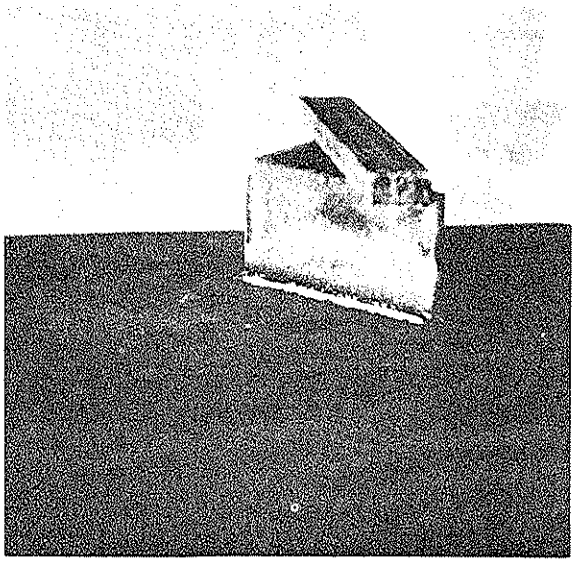

b. Photograph of full-scale connector.

Fig. 2. Angle-plus-bar shear connector (Series 1 and 3).

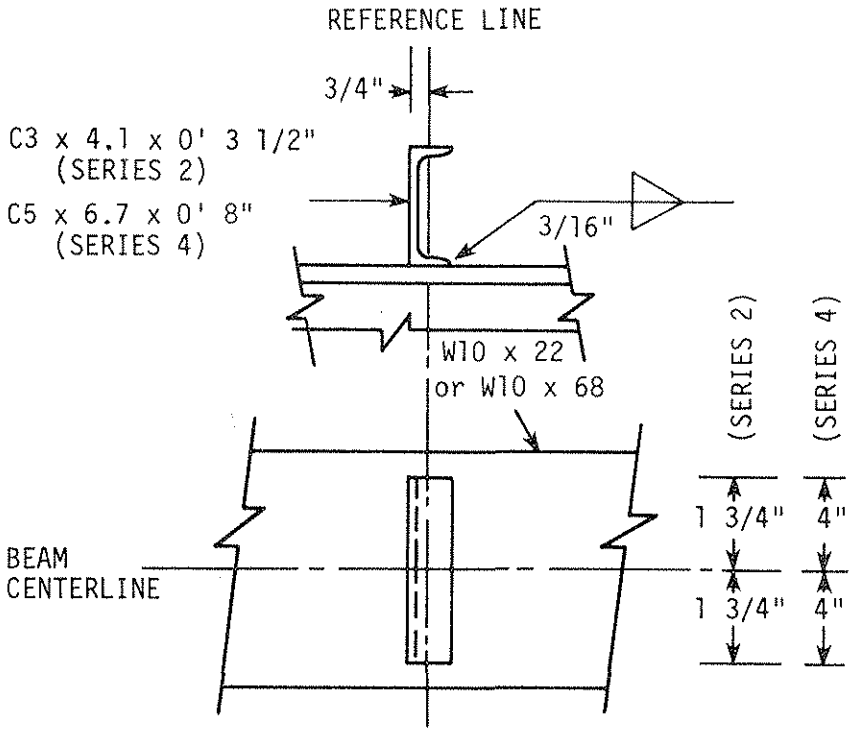

a. Details of half-scale (SERIES 2) and full-scale (SERIES 4) connector.

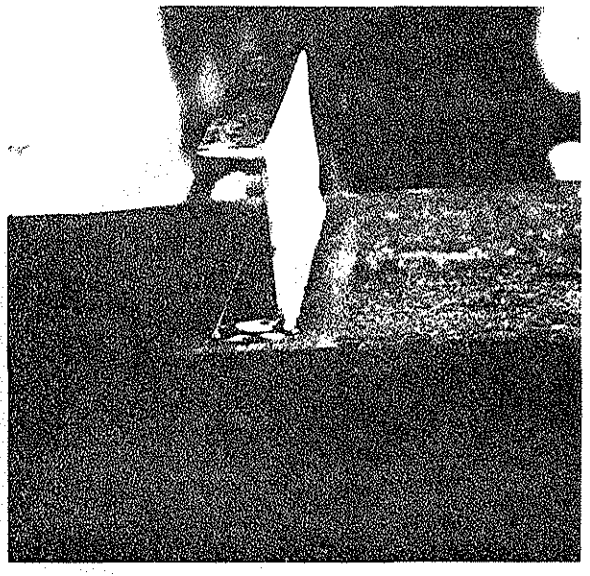

b. Photograph of full-scale connector.

Fig. 3. Channel shear connector (Series 2 and 4).

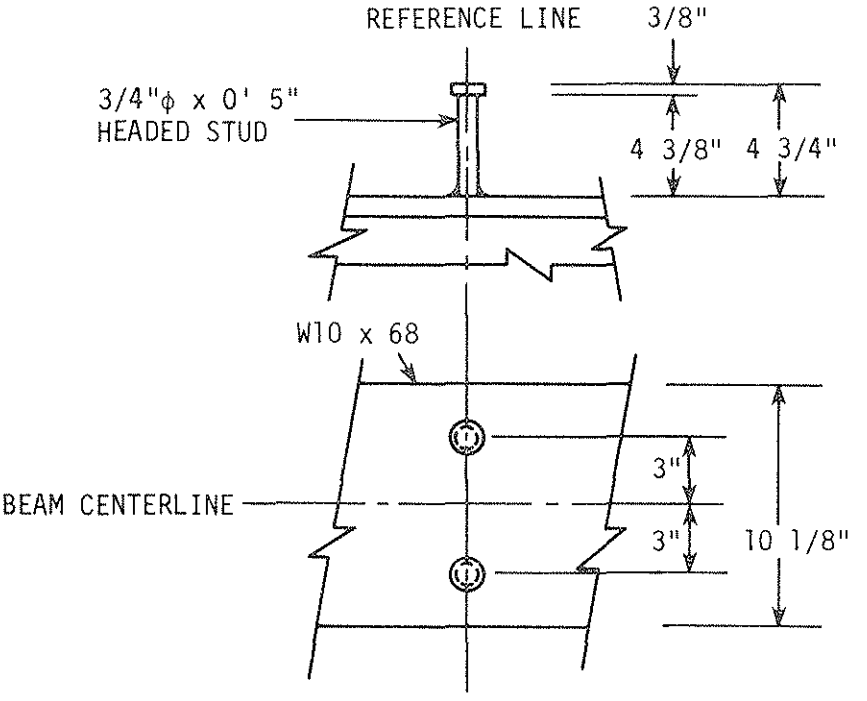

a. Details of full-scale stud connector.

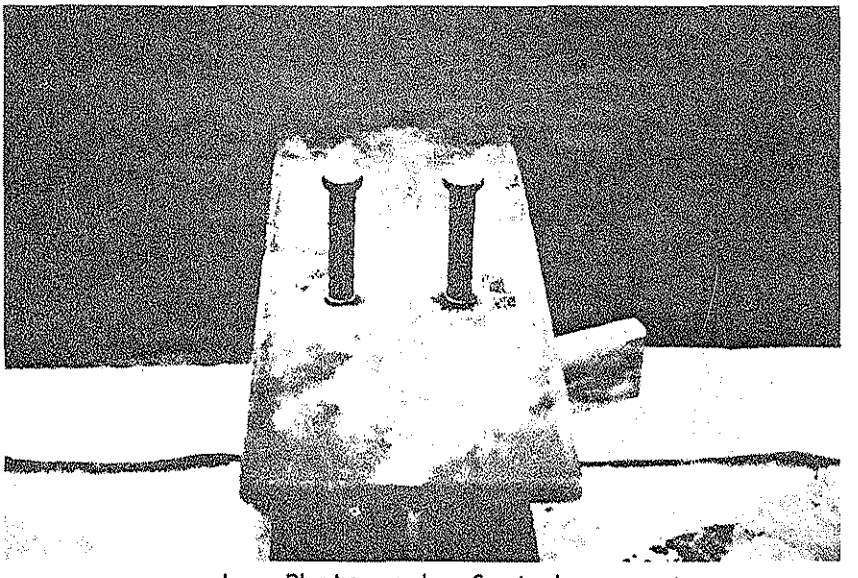

b. Photograph of stud connector.

Fig. 4. Stud shear connector (Series 5).

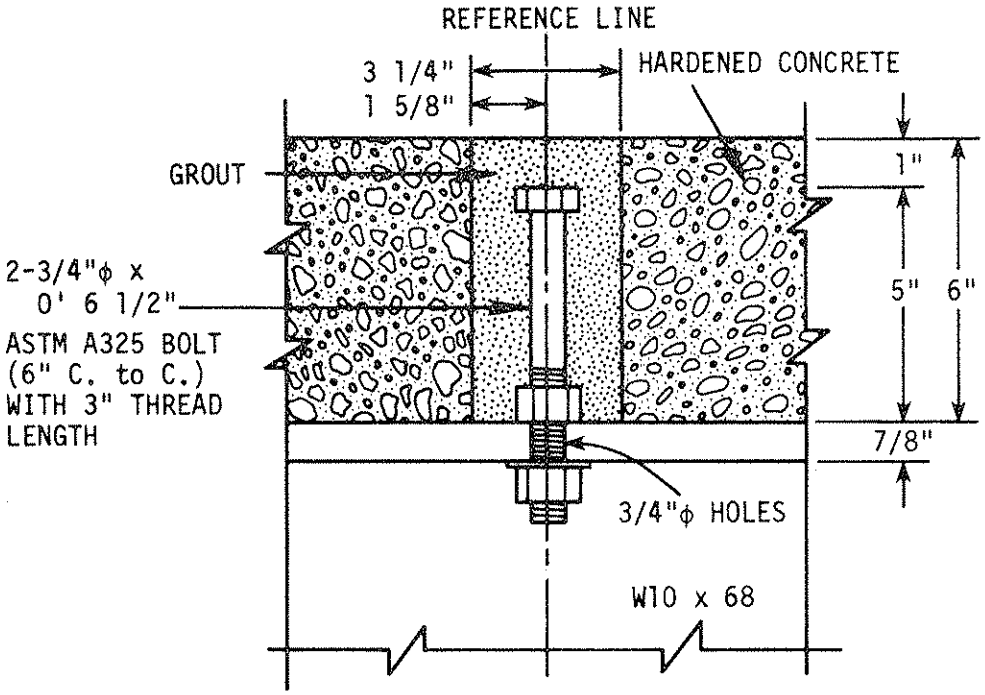

a. Details of double-nutted high strength bolt shear connector.

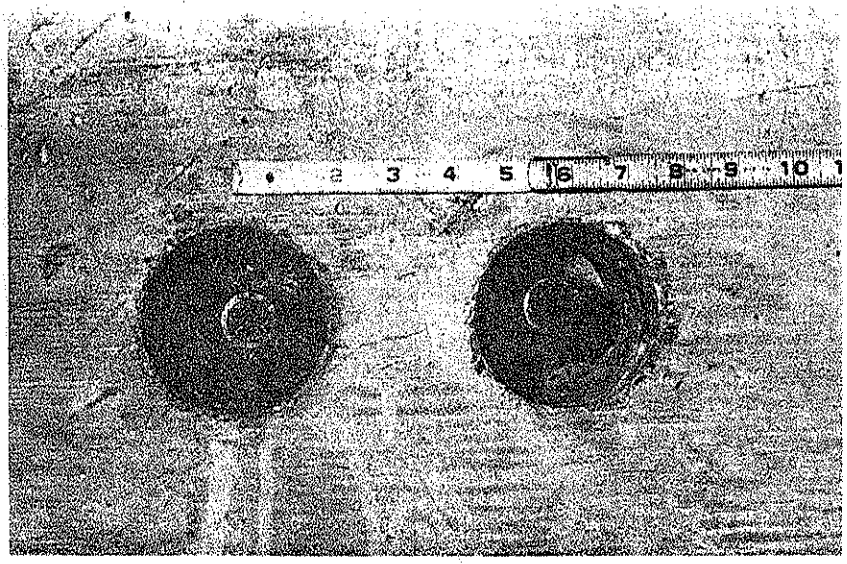

b. Photograph of double-nutted connector prior to placement of grout.

Fig. 5. Double-nutted high strength bolt shear connector (Series 6).

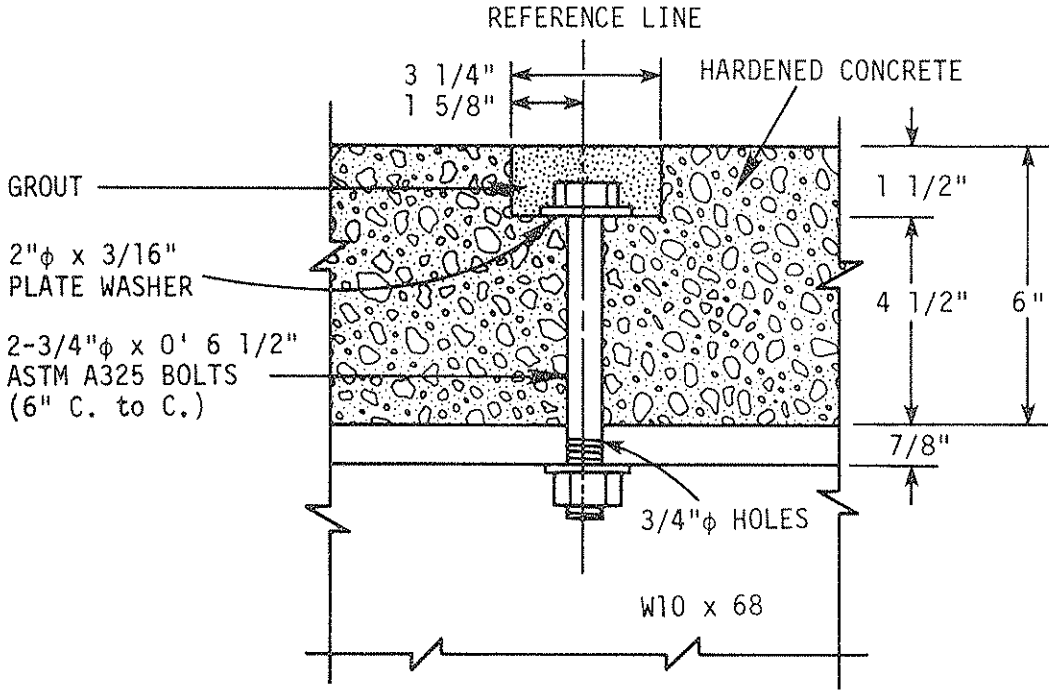

a. Details of epoxied high strength bolt connector.

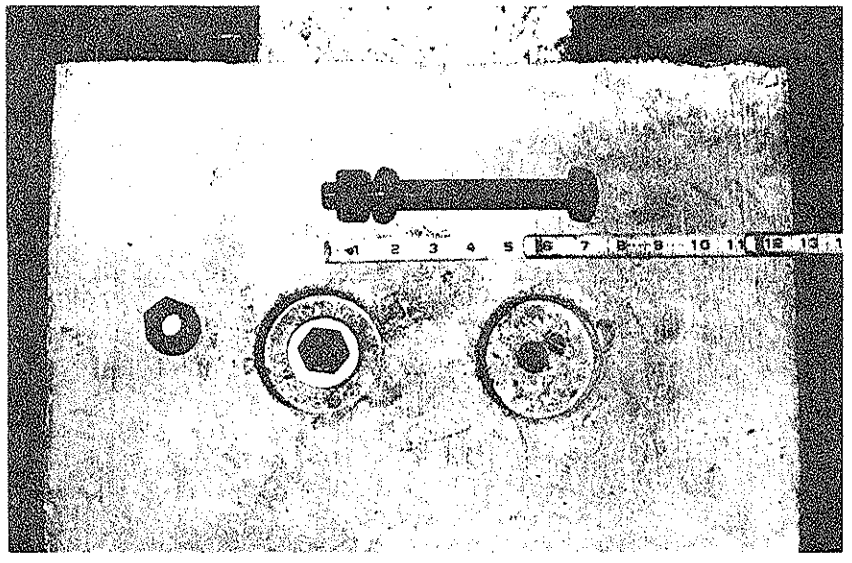

b. Photograph of connector prior to installation of the bolts.

Fig. 6. Epoxied high strength bolt shear connector (Series 7).

Table 1. Summary of push-out specimens tested.

Series	Type	Connector Description	Specimens
1	A	Half-scale angle-plus-bar	HA1 HA2 HA3
2	A	Half-scale channel	HC1 HC2 HC3
3	A	Full-scale angle-plus-bar	FA1 FA2 FA3
4	A	Full-scale channel	FC1 FC2
5	A	Full-scale stud	FS1 FS2 FS3
6	B	Double-nutted high strength bolt	N1 N2 N3 N4
7	B	Epoxied high strength bolt	E1 E2 E3 E4

Phase I, while Type B specimens were modeled as techniques of adding shear connectors to existing bridges. Because the type of steel on several of the bridges requiring strengthening was unknown, only shear connectors that could be added by bolting rather than welding were considered and tested.

Table 1 presents a breakdown of the push-out specimens grouped according to series and type. As shown, Type A specimens were designated by two letters and one number. The first letter designates the specimen size: H for half-scale and F for full-scale. The second letter represents the type of connector welded to the flange: S for stud, A for angle-plus-bar, and C for channel. The number distinguishes between the various specimens in a given series.

Type B specimens were all full-scale specimens and, therefore, designated by just one letter and one number. The letter represents the process used for attaching the slab to the beam flange by bolting: E for epoxied and N for double-nutted. The number distinguishes between specimens within a series. As may be seen, there were five series of Type A specimens (Series 1-5) and two series of Type B specimens (Series 6 and 7).

Earlier research had shown that the bond does not change the specimen's ultimate strength [27]. Thus, although the beam flanges and shear connectors were thoroughly cleaned with a wire brush and then with acetone, no attempt was made to destroy the natural bond between the concrete and steel.

2.1.2 Fabrication of Specimens

A general description of the push-out specimens was given in the previous section. The following two sections, Sec. 2.1.2.1 and Sec. 2.1.2.2, present the fabrication procedures used for the Type A and the Type B specimens, respectively.

2.1.2.1 Type A Specimens

The first step in the fabrication of the specimens was welding the shear connectors to the beams. Channel and angle-plus-bar connectors were welded utilizing a standard weld, while the studs were installed using a stud welder. The location of the shear connectors in the various specimens may be determined by correlating the reference lines in Figs. 2 through 6 with the reference line in Fig. 1.

The push-out specimens were cast vertically, rather than horizontally, so that both slabs could be cast from the same batch of concrete to reduce the chance for variation in concrete strength from one slab to another. Concrete was mixed in a 9-cu-ft mixer and cast into the forms in three individual lifts. Each lift was thoroughly vibrated; care was taken to minimize the formation of voids adjacent to the shear connectors. Forms were fabricated so that three specimens could be cast simultaneously as shown in Fig. 7. Each slab was provided with a small amount of reinforcement, that is, two layers of #4 reinforcement, arranged as shown in Fig. 1.

A minimum of three 6-in.-diameter × 12-in.-long standard ASTM quality test cylinders were made during each pour. The specimens, as well as the control cylinders, were covered with burlap and plastic, then wet cured for five to seven days. Due to time constraints, the

Fig. 7. Formwork used for constructing the push-out specimens.

specimens needed to be tested before 28 days had elapsed. Therefore, a high strength concrete was employed. From the nine-day cylinder compressive strength determined, the push-out specimens were determined to be sufficiently strong for testing at an age of 14 days.

2.1.2.2 Type B Specimens

Fabrication of Type B specimens began with the vertical casting of slabs in the same formwork used for Type A specimens (see Fig. 7). A nominal amount of reinforcement was provided, as well as three #3 reinforcing bars as labeled and shown in Fig. 1. The #3 reinforcing bars provided temporary connection of the slab to the beam flanges until the high strength bolt shear connectors were in place. Prior to testing, the #3 reinforcing bars were removed, so that the only connection between the slabs and wide-flange beam sections was provided by the high strength bolts. Because all the specimens were full-size, concrete was purchased from a local ready-mix plant rather than mixing it in the laboratory as was done for the half-scale, Type A specimens which required smaller aggregate. The concrete was placed in two lifts, each of which was properly vibrated to prevent honeycombing.

Four 6-in.-diameter × 12-in.-long standard ASTM quality test cylinders were made for each set of three specimens. The specimens and cylinders were then covered with burlap and plastic and wet-cured for seven days. Due to the time required for the more involved fabrication of Type B specimens, Series 6 and Series 7 specimens were tested 41 days and 52 days respectively after casting.

After the formwork was removed, each specimen was rotated so that one slab was resting on the floor and the other resting on the beam

section so the desired shear connectors could be added. Two different methods of adding high strength bolt shear connectors to existing beams were investigated for ease of installation, ultimate strength, and characteristics of load-slip and load-separation.

The first fabrication technique examined was the double-nut configuration depicted in Fig. 5. Two 3 1/4-in.-diameter × 6-in.-deep cores at 6 in., center to center, were drilled into each slab of the Series 6 specimens. Location of the cores along the length of the beam is given by the reference lines in Figs. 1 and 5. The concrete cores were removed and a 3/4-in.-diameter hole was drilled through the beam flange at the center of each core. The side walls of the core holes were then roughened and cleaned to improve the bonding between the non-shrink grout and the hardened concrete. Acetone was used to remove the oil residue left from drilling the steel beams; water was used to remove the cementitious materials resulting from the coring.

High strength bolts (ASTM A325 3/4-in. diameter × 6 1/2-in. long) were then placed in the holes through the beam flange and adjusted for an overall length of 5 in. above the flange. Bolts were then tightened to the beam flange in the double-nut configuration. To retard the hydration process in the grout, the core walls were rinsed with water immediately prior to placement of the grout.

When the grouting was placed, three 3-in.-diameter × 6-in.-long standard ASTM quality test cylinders were made for determining the compressive strength. The grouting and cylinders were wet-cured for four to five days.

The addition of shear connectors to Series 7 specimens followed a different procedure, as portrayed in Fig. 6. Two 3 1/4-in.-diameter × 1 1/2-in.-deep cores at 6 in., center to center, were drilled into each slab. The reference lines of Figs. 1 and 6 locate the core holes along the length of the beam. At the center of each core, a 3/4-in.-diameter core was drilled to the beam flange. After removal of all core material, a 3/4-in.-diameter hole was drilled through the beam flange at each core location. The build-up of steel shavings in the 3/4 in. core caused the drilling to be halted frequently in order to remove the shavings. To provide an even bearing surface for the 1/8 in. plate washer and bolt combination, grout was placed in the 3 1/4-in.-diameter core and leveled off 1 1/2 in. below the top surface of the slab. The grout used for leveling was allowed to wet cure for a minimum of four days.

In order to fill voids and provide bonding between the bolt and the slab, a concrete-steel epoxy was employed. The epoxy was spread thoroughly over the shaft of a 3/4-in.-diameter × 6 1/2-in.-long ASTM A325 high strength bolt. The epoxy-covered bolt was then placed in the 3/4-in.-diameter core and moved vertically up and down to provide an even coating of epoxy between the core walls and bolt shaft. The bolts were immediately tightened, thus forcing out any voids in the viscous epoxy and providing uniform bonding between the steel and concrete.

The epoxy was allowed to cure for a minimum of 24 hours before grout was placed in the remaining 3 1/4-in.-diameter cores. Two 3-in.-diameter × 6-in.-long standard ASTM quality test cylinders were

made of the grout used in the previously described patching process. The patching on all specimens and the control cylinders was wet-cured for a minimum of four days.

2.2 Composite Beam Specimens

The four composite, concrete slab and steel beam specimens were sawed from the half-scale model bridge of Phase I. The model bridge framing plan and midspan cross-section may be found in Ref. 19. The composite beam specimens were obtained by making five longitudinal cuts in the model bridge, as depicted in Fig. 8. The cuts were made with a gasoline-engine-powered concrete saw which was provided and operated by personnel from the Iowa DOT.

Two of the beams, Beams 1 and 4 (see Fig. 8), had a nominal slab width of 1 ft 5 in. and were exterior-type composite beams with a flange on one side only. The remaining beams, Beams 2 and 3, had a nominal flange width of 4 ft 10 in. and were interior-type composite beams with equal widths of slab on each side of the beam centerline. Flange widths on Beams 2 and 3 were made equal to the beam spacing, thus minimizing the number of saw cuts required. Flange widths on Beams 1 and 4 were determined by calculating the width of slab needed to locate the centroid of the slab about a vertical axis through the centerline of the steel beam. This was done to decrease the possibility of unsymmetrical bending. The actual composite beam slab widths were the result of inaccuracies in the cutting process; these, along with the average slab thicknesses, are given in Fig. 9 and Table 2.

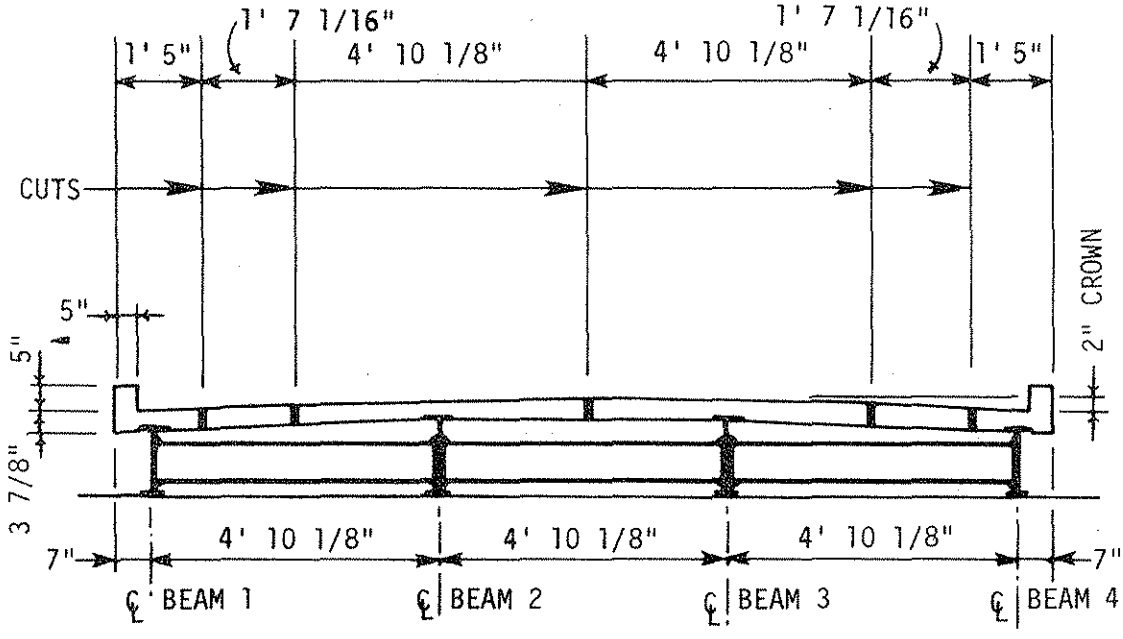

Fig. 8. Cross-section of model bridge showing the location of longitudinal cuts.

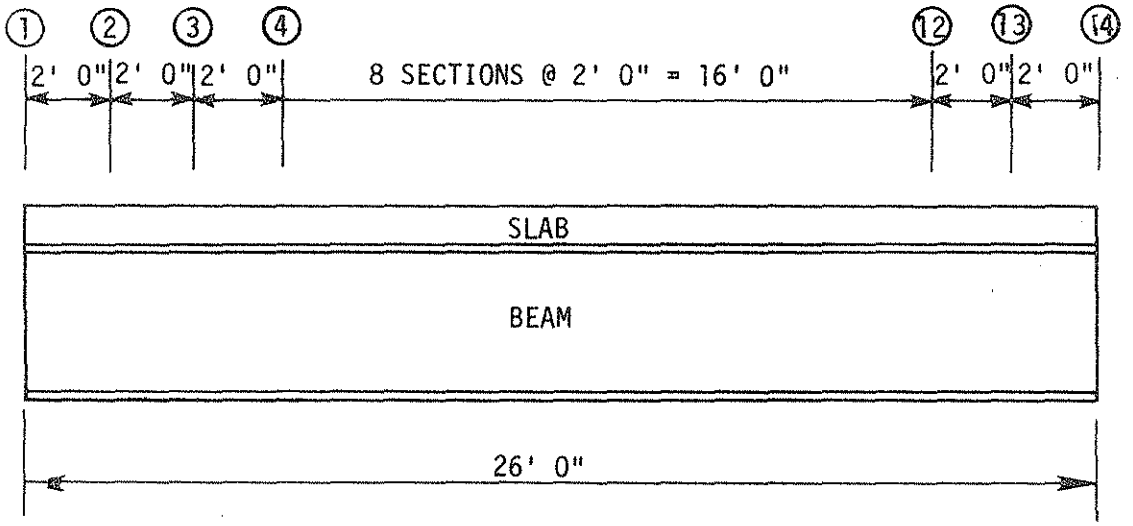

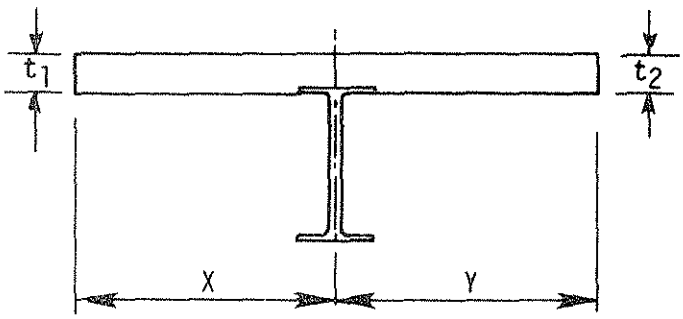

TYPICAL SECTION FOR
BEAMS 2 AND 3

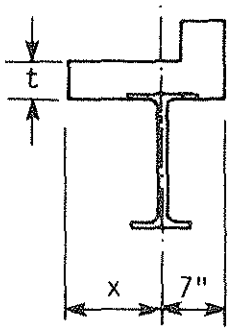

TYPICAL SECTION FOR
BEAMS 1 AND 4

where, $T = \frac{t_1 + t_2}{2}$

Fig. 9. Location of composite beam sections where measurements of slab width and thickness were determined. (See Table 2 for values of each variable.)

Table 2. Actual widths for each composite beam tested. (Refer to Fig. 9 for definition of x, t, X, Y, and T.)

Beam 1			Beam 2			
Point	x(in.)	t(in.)	Point	X(in.)	Y(in.)	T(in.)
1	10.50	4.25	1	31.12	28.50	4.22
2	10.25	4.25	2	31.12	28.62	4.25
3	10.25	4.38	3	31.12	28.62	4.19
4	9.62	4.25	4	31.00	28.50	4.16
5	9.25	4.12	5	31.00	28.50	4.09
6	9.62	4.12	6	31.12	28.38	4.09
7	10.25	4.12	7	31.00	28.25	4.06
8	10.38	4.25	8	31.00	28.12	4.16
9	10.50	4.12	9	30.75	28.12	4.16
10	10.62	4.12	10	30.62	28.25	4.06
11	10.38	4.12	11	30.38	28.25	4.03
12	10.62	4.12	12	29.88	28.38	4.00
13	11.00	4.12	13	29.62	28.75	4.06
14	11.25	3.88	14	29.50	29.00	4.12
Ave.	10.32	4.16	Ave.	30.66	28.45	4.12

Table 2. Continued.

Beam 3				Beam 4		
Point	X(in.)	Y(in.)	T(in.)	Point	x(in.)	t(in.)
1	28.00	28.62	4.06	1	10.00	4.00
2	28.62	28.62	4.06	2	10.00	4.00
3	28.75	28.25	4.00	3	10.00	4.12
4	28.62	27.88	4.06	4	10.00	4.00
5	28.50	27.62	4.06	5	10.00	4.12
6	28.50	27.38	4.19	6	10.00	4.25
7	28.50	27.25	4.19	7	10.25	4.12
8	28.38	27.00	4.12	8	10.12	4.12
9	28.62	27.00	4.06	9	10.00	4.12
10	29.00	27.12	4.06	10	9.75	4.00
11	28.88	27.12	4.19	11	9.50	4.12
12	28.88	27.12	4.12	12	9.75	4.00
13	28.62	27.00	4.19	13	10.12	4.00
14	28.62	27.25	4.12	14	10.62	3.88
Ave.	28.61	27.52	4.11	Ave.	10.01	4.07

All four beams were equipped with the post-tensioning system used in the testing of the model bridge of Phase I. Details of the post-tensioning system employed may be found in Ref. 19.

The properties of the concrete and steel in the four beams, although also available in Ref. 19, are presented in Tables 3 and 4 for convenient reference.

The shear capacity of the beams was less than that required by AASHTO bridge standards [1]. Therefore, additional shear connectors (high strength bolts double-nutted to the top flange) were added to one interior beam, Beam 3, and one exterior beam, Beam 4. The locations of the existing angle-plus-bar shear connectors for all four composite beams are given in Ref. 19; the locations of the shear connectors added to Beams 3 and 4 are shown in Fig. 10. These locations were dictated by the location of the existing angle-plus-bar connectors. Core holes were located on either side of the beam centerline. However, this placement was varied slightly on the exterior-type beams so that the cores did not have to pass through the curbs. For ease of construction, the core holes (3 1/4 diameter) were drilled before the bridge was cut into individual beams.

The additional shear connectors were 1/2-in.-diameter × 4-in.-long ASTM A325 high strength bolts. The bolts were double-nutted to the beam flange similar to the configuration (shown in Fig. 5) used in the Series 5 push-out specimens. An ultimate strength value for the existing angle-plus-bar shear connector was computed using data obtained from the push-out tests. The total resisting force of the angle-plus-bar connectors was then determined for each beam and was found to be less

Table 3. Physical properties of concrete.

	f'_c(psi)	E(ksi)
Deck	3300	2830
Curb	7450	5080

Table 4. Physical properties of steel.

	σ_y(ksi)	σ_{ult}(ksi)	E(ksi)
Reinforcement			
#3	69.8	110.8	29,110
#4	70.8	109.7	-
Prestressing	-	156.1	24,100
W16 × 26	44.1	66.9	29,990
W14 × 22	44.7	69.4	28,990

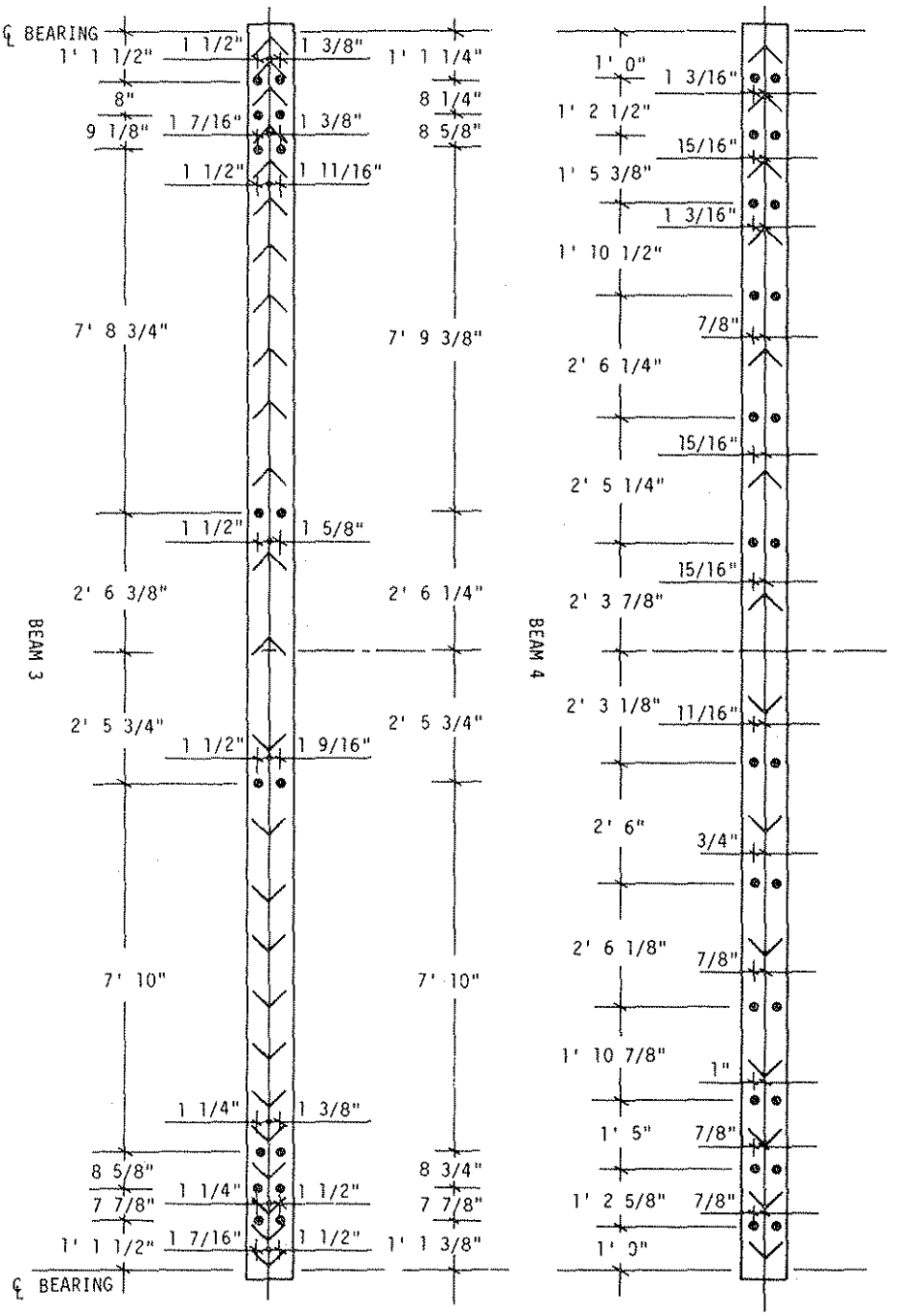

Fig. 10. Location of high strength bolt shear connectors added to Beams 3 and 4.

than that required. Therefore, sufficient bolt connectors, 16 to the interior beam (Beam 3) and 24 to the exterior beam (Beam 4), were added to increase the shear capacity to the required level. The ultimate strength of the bolts was calculated using the welded stud formula for shear connectors in the AASHTO standards [1]. From the laboratory work performed on the push-out specimens, this was found to be a slightly conservative assumption.

2.3 Plexiglas Bridge Model

To determine approximately how Bridge 2 would respond to post-tensioning, a small scale model of the bridge was fabricated and tested. As elastic behavior was the primary interest, plexiglas was chosen for the model material rather than reinforced concrete and structural steel, as was done in Phase I. Not only was there considerable saving in expense but also in fabrication time. The model fabricated is shown in Fig. 11. The loading shown on the bridge is to simulate the correct dead load stresses.

The size of the model was governed by the thickness of available plexiglas. Since 3/8 in. plexiglas was readily available and Bridge 2 had a deck thickness of 8 in., a model scale factor of 21.33 resulted. This was close to the range of scale factors generally selected for highway bridge models. Using the 21.33 scale factor, the overall bridge dimensions were to be 40 1/2 in. long and 17 5/8 in. wide; however, due to a fabrication error the bridge was made 40 in. long. Because of the two different materials (reinforced concrete deck and

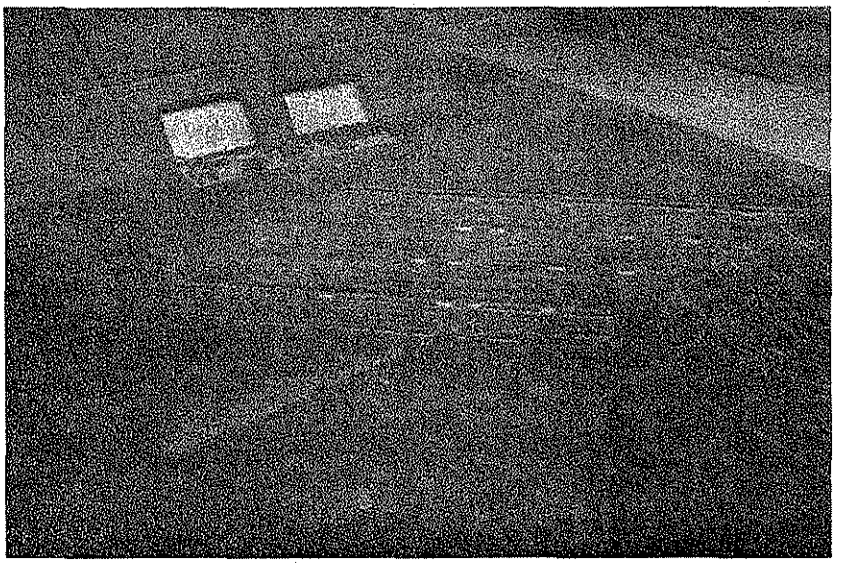

Fig. 11. Photograph of plexiglas model bridge with additional dead load in place.

steel I-beams) in the prototype, a unique problem existed in modeling the remaining portion of the bridge. The modeling was accomplished by transforming the steel beams into equivalent concrete areas through use of the modular ratio concept. Beam depths were determined through use of the scale factor. As may be seen in Fig. 12a, all beams also were fabricated from 3/8-in.-thick plexiglas. The curbs shown in Fig. 12a were attached to the deck by set-screws, so that the behavior with and without curbs could be studied. Flange widths were varied to obtain the correct moment of inertia and, thus, a good model for deflection behavior. The variation in lower flange widths shown in Fig. 12b was made to model the presence of cover plates (thus, larger moments of inertia) on the exterior and interior beams of the prototype. Support conditions were modeled using pin supports at one end of the span and roller supports at the other end.

Due to the small size of the model, the post-tensioning arrangement also had to be modified from that used on the prototype. For post-tensioning, a single 1/4-in.-diameter aluminum rod was attached to the ends of each exterior beam by means of aluminum angles (2 in. × 2 in. × 1/4 in.) attached to the bottom of the lower flange. Thus, the rod on the model was located at a greater distance from the neutral axis of the cross-section and had a significantly larger moment arm than the post-tensioning system used on the prototype. As may be seen in Fig. 13a, three holes were drilled in the outstanding legs of the brackets so that various moment to axial load ratios could be investigated. Another variable incorporated into the model was the series of holes drilled into the lower flange of the exterior beams, thus making

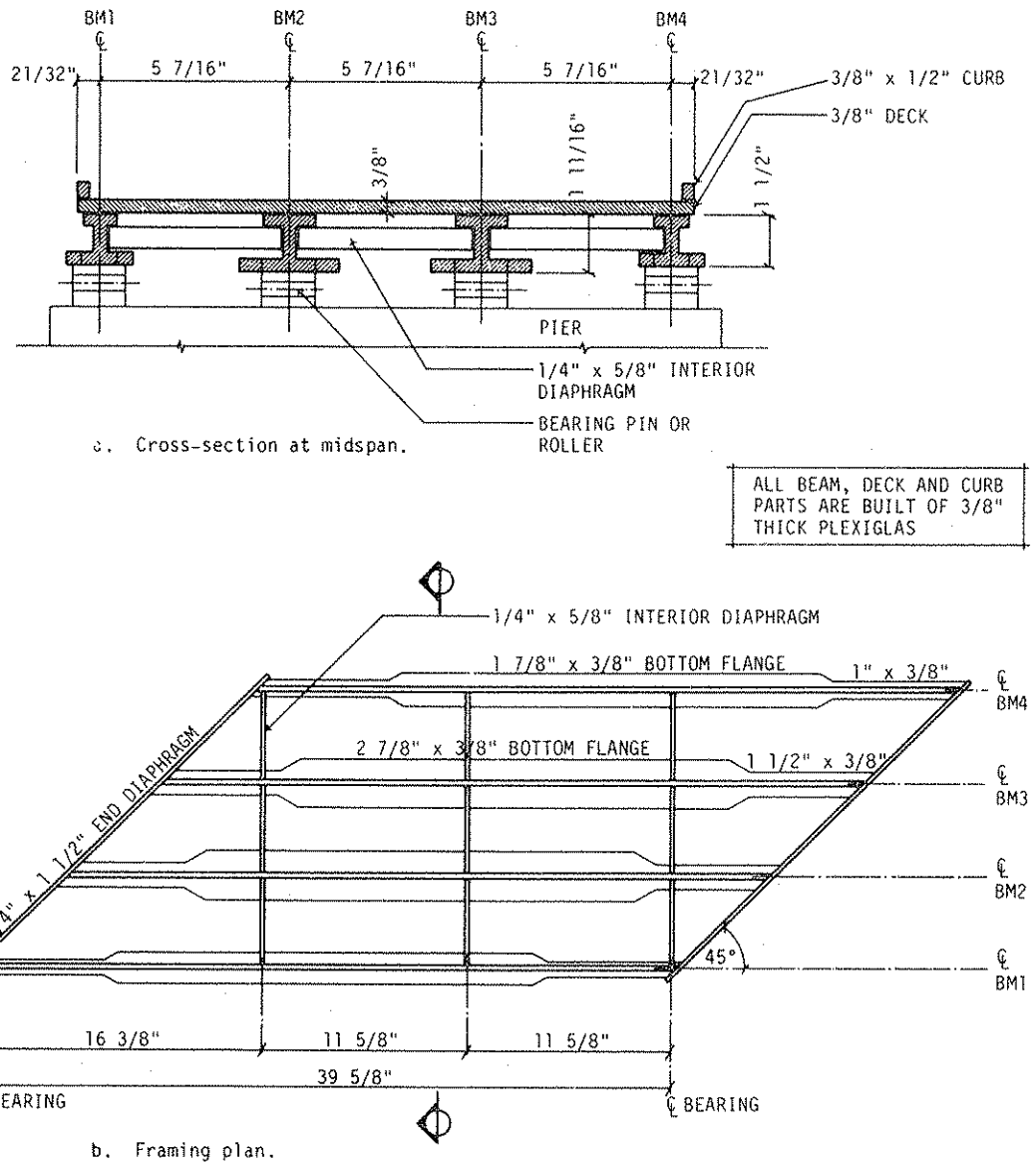

Fig. 12. Plexiglas model bridge.

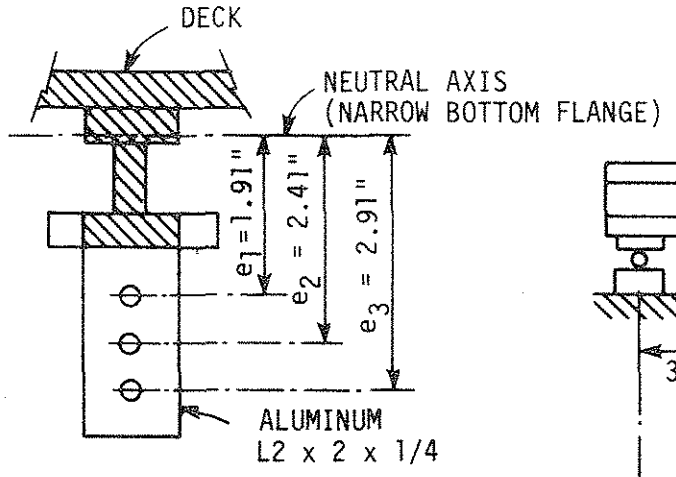

a. Cross section.

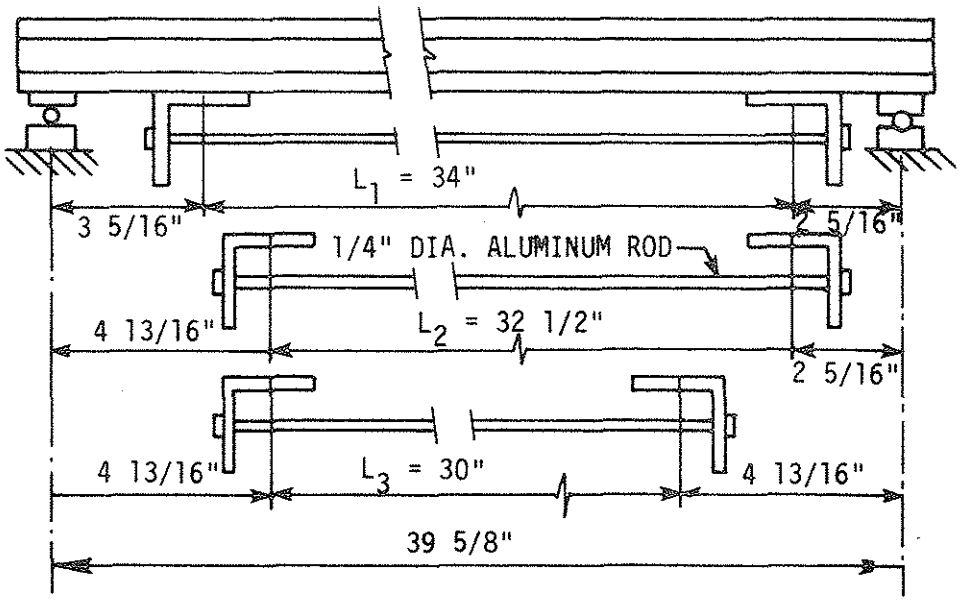

b. Side view.

Fig. 13. Bracket detail -- plexiglas model bridge.

possible variations in length of the post-tensioned regions of the beams. Three different post-tensioning lengths may be seen in Fig. 13b; these were obtained by positioning the brackets in the various holes in the lower flanges of the exterior beams.

2.4 Field Bridges

2.4.1 Description of Bridges

As previously mentioned, two bridges were chosen to be post-tensioned: Bridge 1, a 50 ft × 30 ft right-angle bridge, and Bridge 2, a 70 ft × 30 ft, 45° skewed bridge. An overall view of each bridge with the post-tension strengthening system in place is shown in Fig. 14. The framing plans and midspan cross-sections for Bridge 1 and Bridge 2 are presented in Figs. 15 and 16, respectively. The overall condition of both bridges was generally good. On both bridges, the abutments had been undercut as the elevation of the stream bed dropped, but otherwise they were in excellent condition with minimal cracks visible and no spalling. The deck on Bridge 1 was in excellent condition; the steel frame, although not corroded, needed painting. The top surface of the deck on Bridge 2 was badly deteriorated; however, the underneath deck surface was in good condition. The bridge is now scheduled for a concrete overlay in the near future. Its steel frame was in excellent condition; the painting appeared to be relatively recent.

Since material properties for the bridges were unknown, testing or some approximations were required. A number of 4-in.-diameter cores were taken from each bridge (three from Bridge 1 and six from

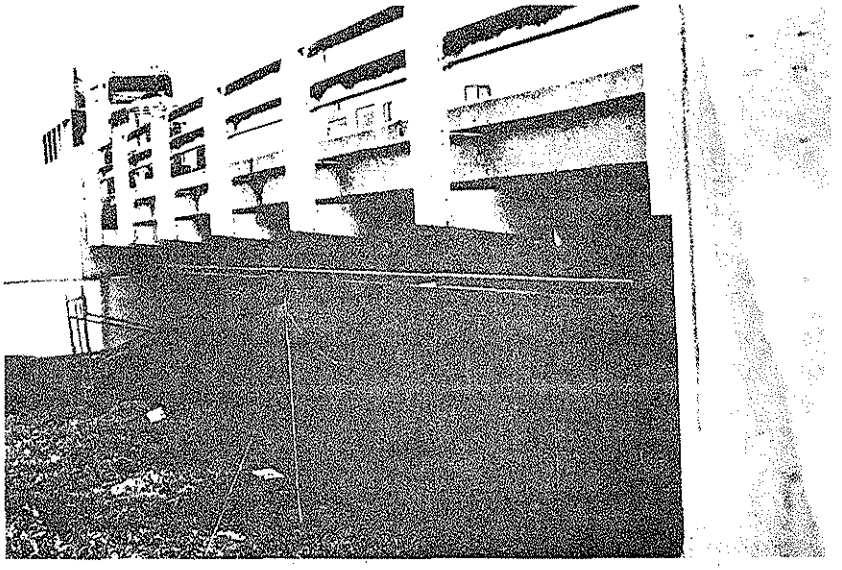

a. Bridge 1--Dickinson County.

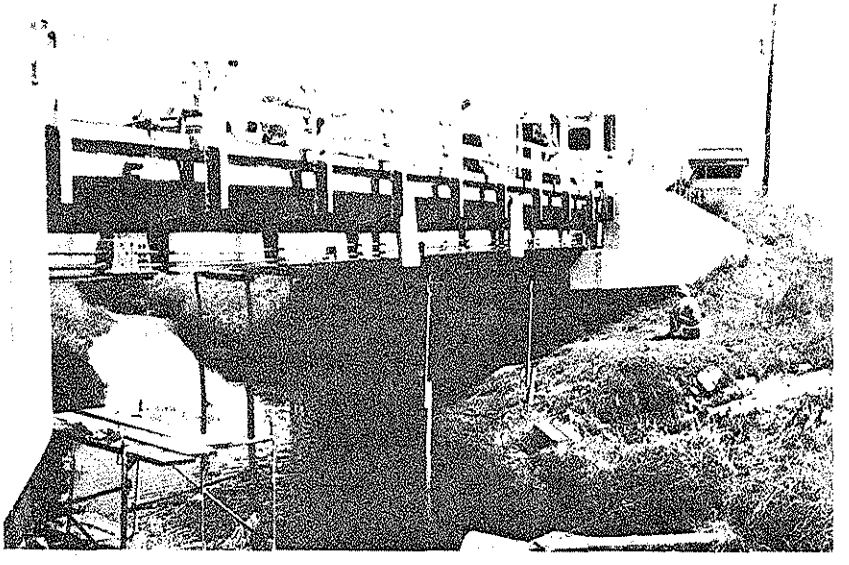

b. Bridge 2--Greene County.

Fig. 14. Photographs of prototype bridges.

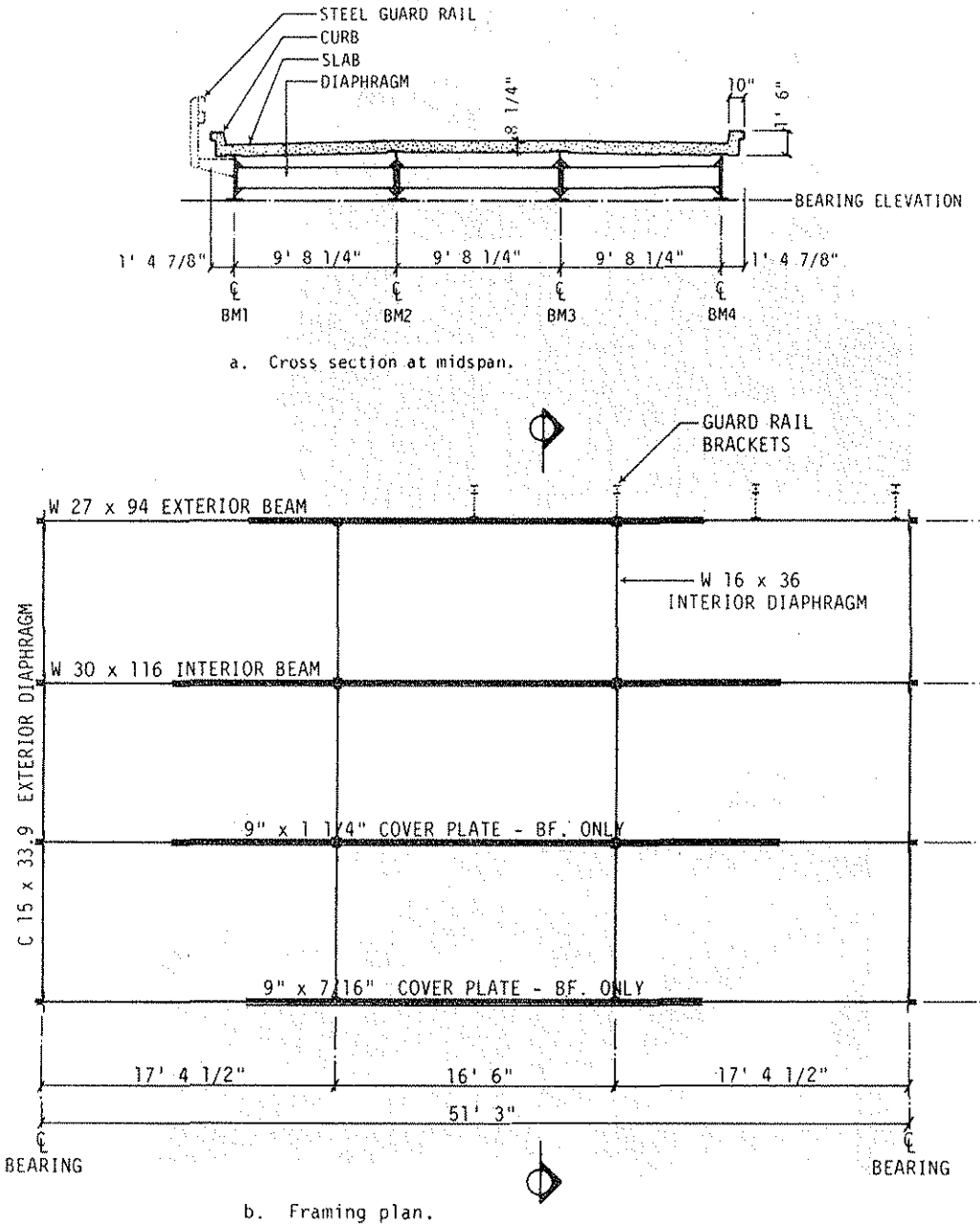

Fig. 15. Framing plan -- Bridge 1.

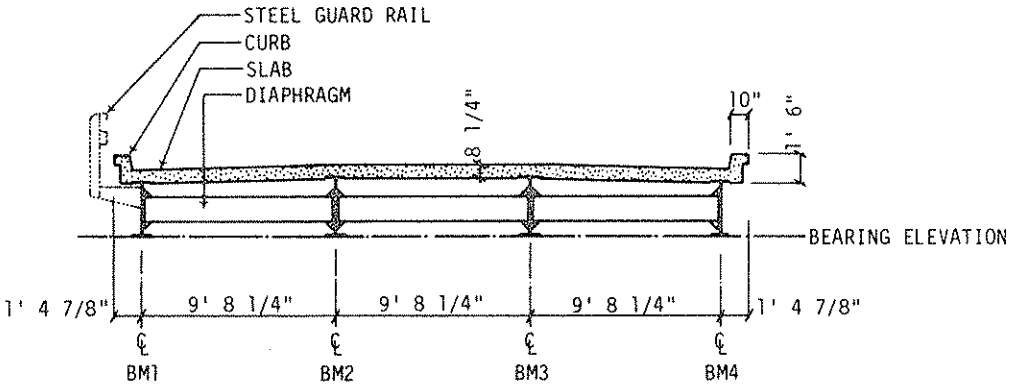

a. Cross section at midspan.

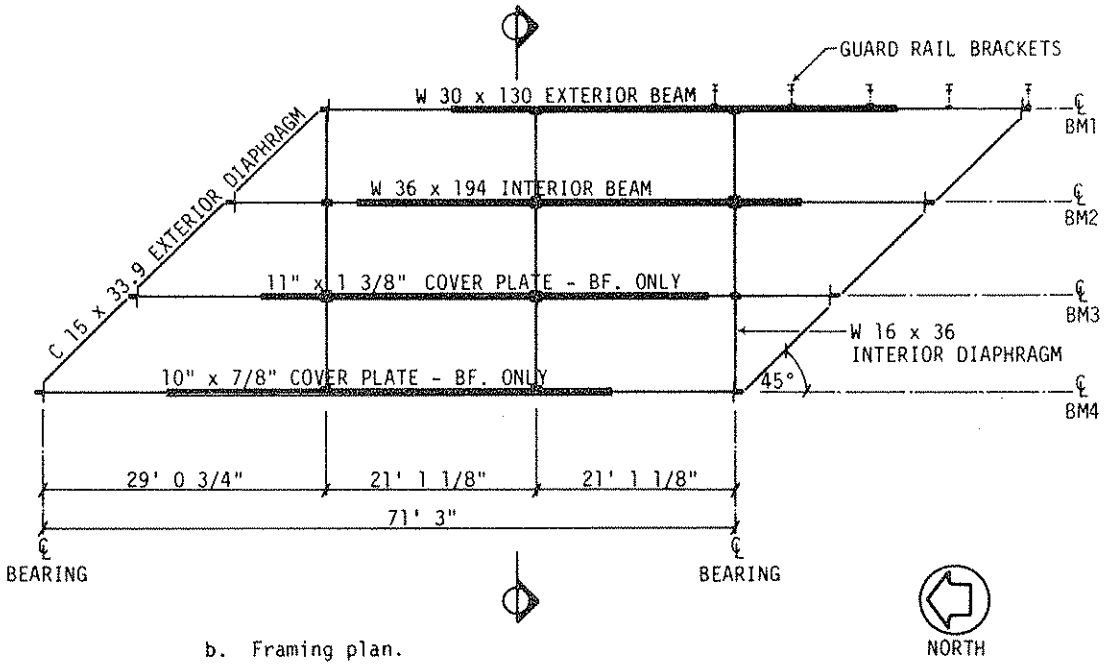

b. Framing plan.

Fig. 16. Framing plan -- Bridge 2.

Bridge 2) and tested. The average deck concrete strength for Bridge 1 was 7140 psi and for Bridge 2 it was 6430 psi. The reinforcing steel and A7 structural steel properties were estimated for each bridge, at 40,000 psi for the yield stress of the reinforcing steel and 33 ksi for the yield point of the A7 structural steel.

Each bridge required approximately two weeks of preparatory work before any testing took place. This work consisted mainly of installation of shear connectors, application of strain gages, construction of frames for deflection dials, and placement of the post-tensioning system. Most of the work was performed by crews working from scaffolding under the bridge, while the bridge was open to traffic. However, when strain gages were applied, shear connectors attached, and obviously when testing was in progress, it was necessary to close the bridge. The shear connectors were installed employing the procedure for double-nutted bolt connectors described in Sec. 2.1.2.2 and shown in Fig. 5. The 4-in.-diameter cores for the 1-in.-diameter × 8-in.-long high strength bolts (ASTM A325) were located as shown in Figs. 17 and 18 based on computations in Sec. 2.4.2. Also shown are the locations of the existing angle-plus-bar shear connectors for each bridge. Bridge 1 had 26 high strength bolts added to each exterior beam, while Bridge 2 had 28 added to each exterior beam and 26 to each interior beam for a total of 108. The angle-plus-bar configuration for both bridges is similar to that used on the Series 3 push-out specimens (see Fig. 2).

2.4.2 Design of Strengthening for Bridges

Details of the post-tensioning system employed on each bridge are presented in the following two sections. Due to the uncertainty about

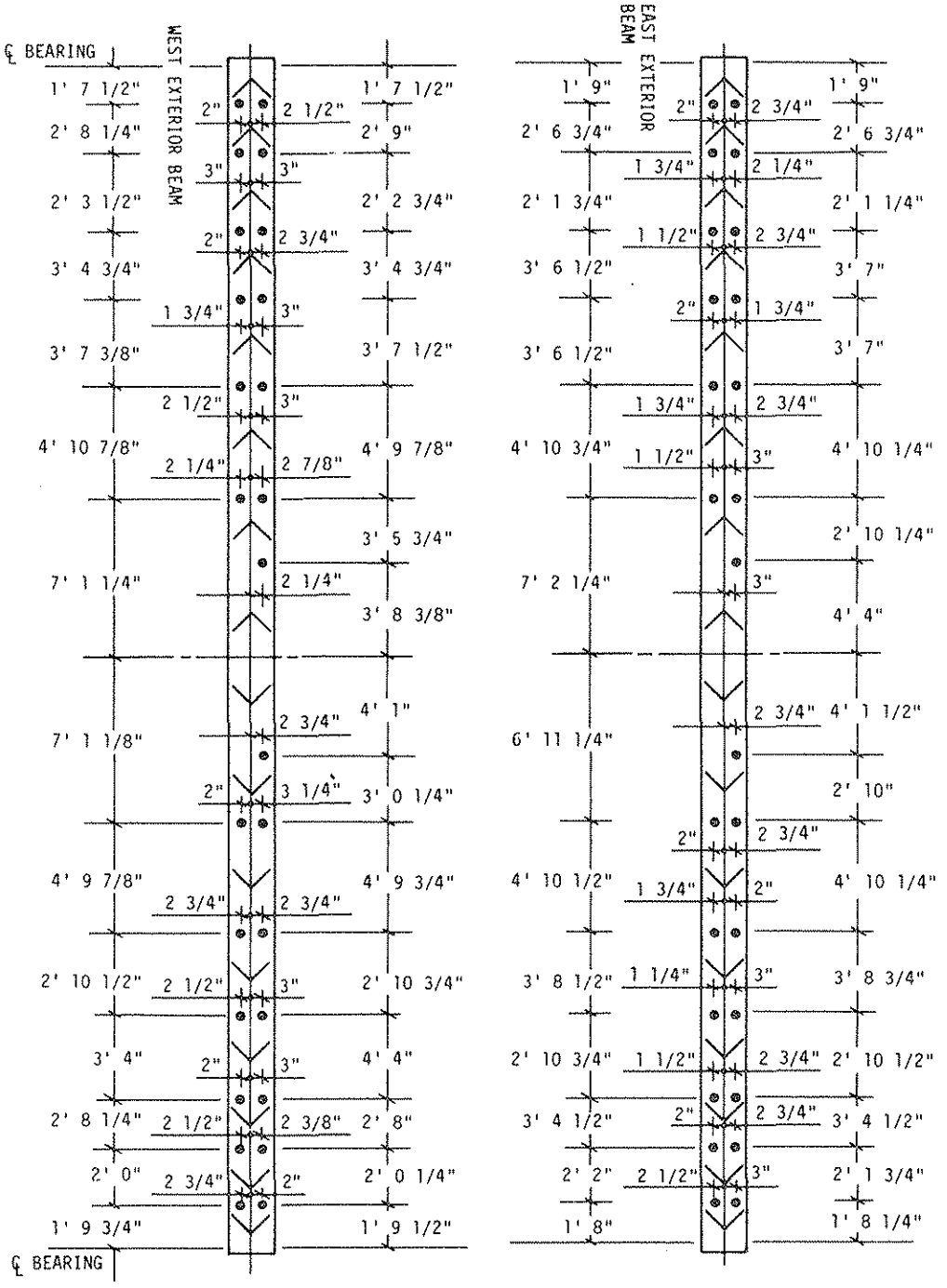

Fig. 17. Location of shear connectors on Bridge 1.

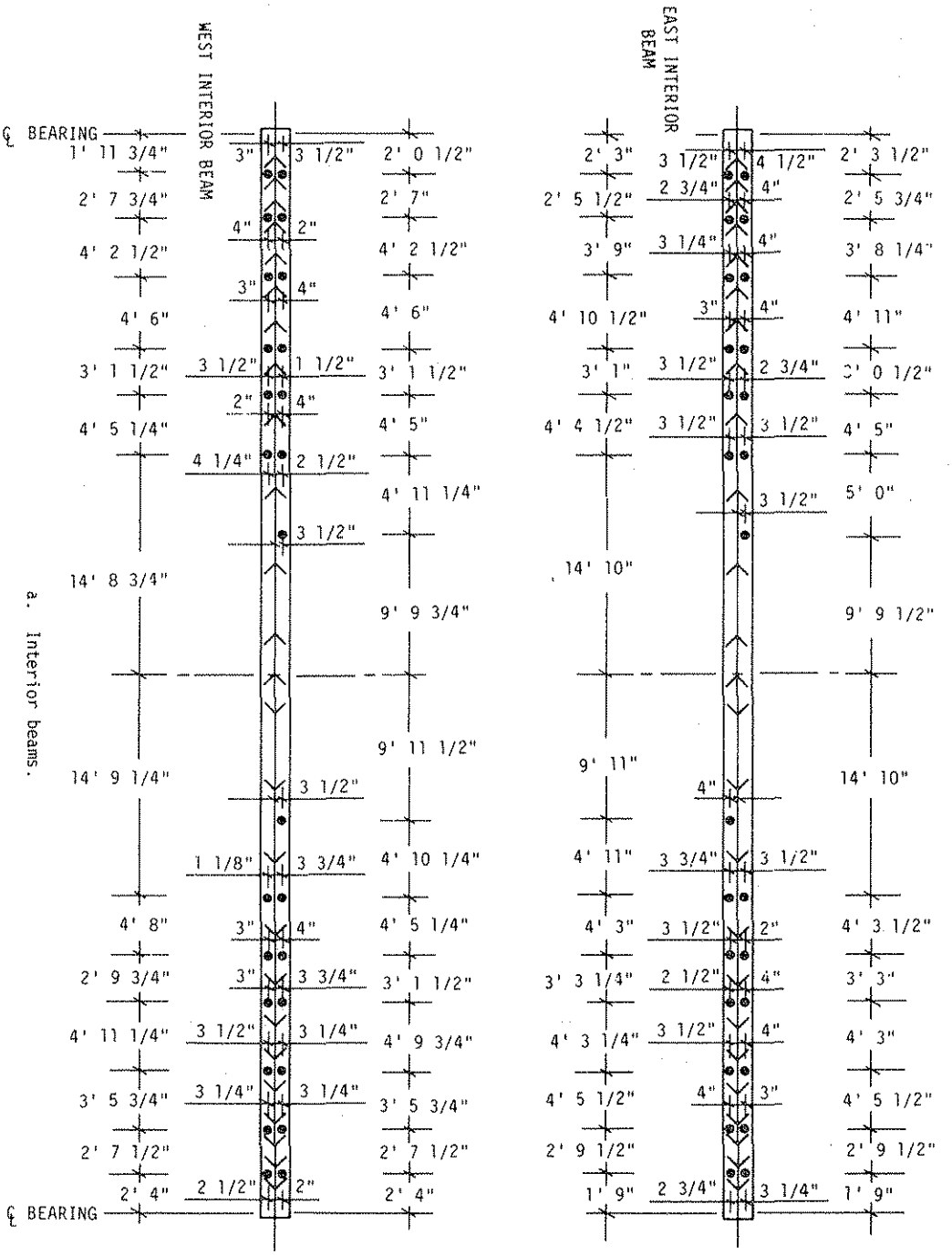

a. Interior beams.

Fig. 18. Location of shear connectors on Bridge 2.

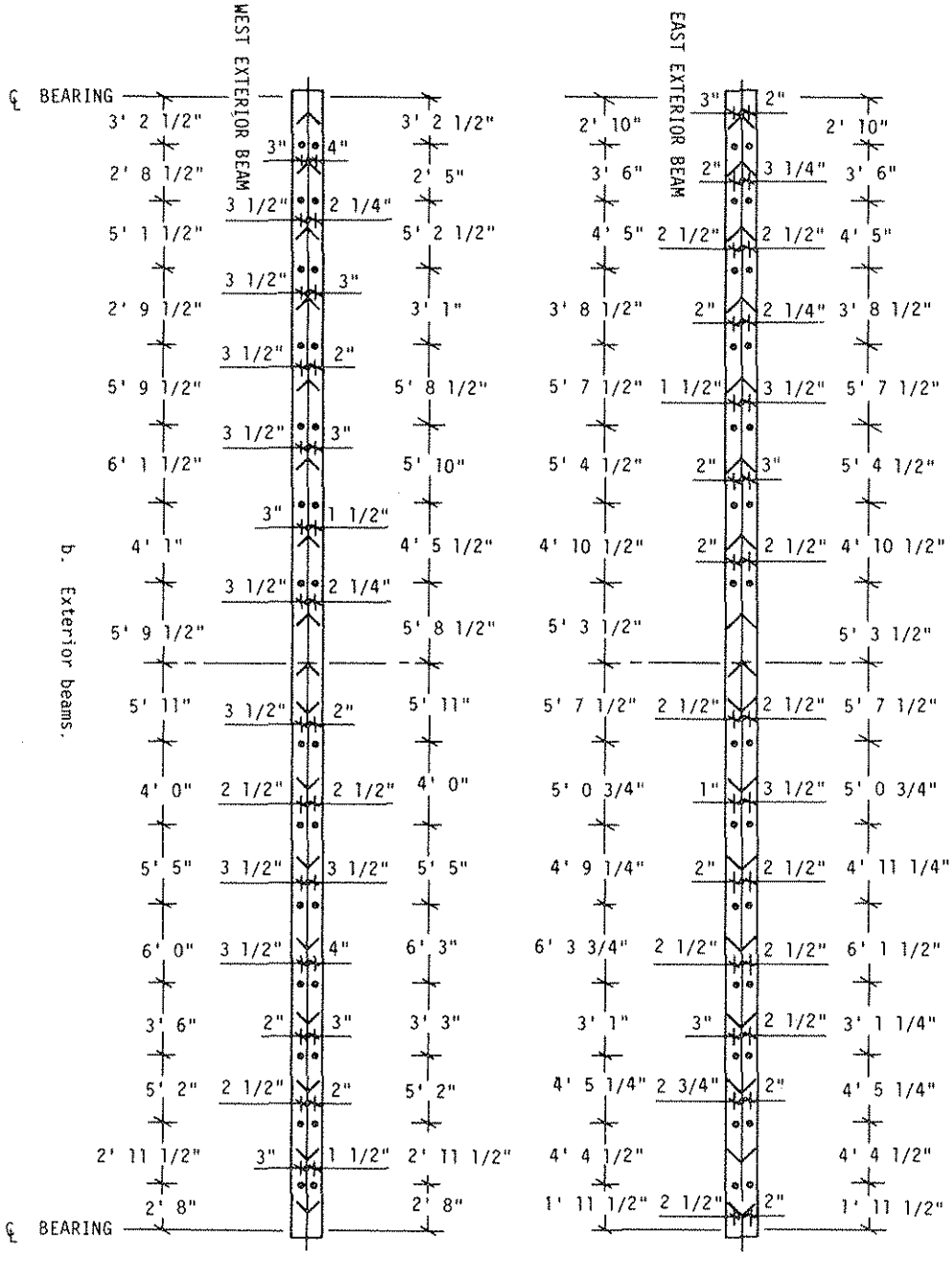

Fig. 18. Continued.

b. Exterior beams.

the type of steel in these bridges, as well as in others requiring strengthening, the brackets were designed for bolted connection to the bridges (as was done in Phase I).

2.4.2.1 Strengthening for Bridge 1

A Fortran program, BRIDGE02, developed under Phase I of this research, was used to determine the extent of overload in the existing bridge. The basic set-up for the data and program included:

- Simple span support conditions
- Iowa DOT truck loads (which give results that lie between those for an H20 truck and an HS20 truck)
- Impact increase as required by AASHTO
- 1 1/2 in. overlay on an 8 in. slab (only the 8 in. slab was included in the composite section computations)
- Wheel load fractions for beams as required by AASHTO
- Effective flange widths as determined by AASHTO rules (curb parts were included in exterior beam composite section)
- n = 10 (based on estimated minimum deck concrete strength of 3000 psi)

For data listed above, BRIDGE02 gave the following results for maximum tension stresses in the bottom flange or coverplate:

	Exterior Beam	Interior Beam
In bottom flange at cover plate cutoff	25.28 ksi	18.85 ksi
In cover plate near midspan	24.49 ksi	18.25 ksi

The allowable stress for inventory rating for A7 steel is 18 ksi [2]. Consequently, the post-tensioning was required to remove 7.28 ksi from the bottom flange at the cover plate cutoff and 6.49 ksi from the cover plate at midspan.

Based on the good correlation between results obtained from orthotropic plate theory for vertical loading and distribution of post-tensioning forces and moments in Phase I, ORTHCO02, a Fortran program utilizing a series solution to the orthotropic plate equation, was used to determine the approximate post-tensioning distribution. When both exterior beams were post-tensioned, ORTHCO02 indicated that each exterior beam would retain approximately 0.35 of the effects of the total post-tensioning applied to the bridge. Because 0.15 of the total post-tensioning effects would be applied to each interior beam, the slight bottom flange and cover plate overstresses there are obviously relieved by post-tensioning of the exterior beam.

In order to allow for possible upward adjustment of post-tensioning force, the maximum allowable force in post-tensioning tendons was set at 0.60 f_{pu}, where f_{pu} is the ultimate tension strength of the tendons.

In order to reduce the midspan tension stress of the exterior beam cover plate by 6.49 ksi, it was determined that two of the 1 1/4-in.-diameter post-tensioning tendons, 3 1/4 in. above the bottom flange, would be required for each exterior beam. The force to be applied to each tendon was computed as 92 kips, for a total of 184 kips for each exterior beam.

A check of post-tensioning losses and gains showed that losses due to concrete shrinkage, elastic shortening, and concrete creep either did not apply or were insignificant. The loss due to steel relaxation was estimated to be 3.8 kips per tendon. If a maximum temperature difference of 20° F occurred between post-tensioning tendons and beam, a temporary temperature-caused loss of 3.9 kips per tendon could occur. These two losses essentially would be offset by an estimated 5.4 kips increase in tension per tendon as a truck passed over the bridge. Since estimated losses and gain were essentially compensated, the initial computation of 92 kips per tendon was retained.

For the exterior beam and simple span conditions, the computed deflection after full post-tensioning was 0.34 in. upward. An eccentric truck on the bridge would cause a computed deflection of 0.64 in., which is less than 0.77 in. or L/800, the allowable deflection.

Shear stress on the exterior beam was checked during preliminary computations and found to be approximately 60% of the allowable and, consequently, no further shear checks were performed.

Fatigue on coverplate welds was checked. The check indicated that the welds would be adequate for 100,000 total cycles, but inadequate for 500,000 total cycles.

Location of post-tensioning brackets was set so that the average stress in the bottom flange of the beam would be 18 ksi, or less, after deduction for holes for 1 in. diameter bolts. Computations showed that no bolt hole should be farther from the support than 6.04 ft, and brackets were located accordingly.

For purposes of computing the force applied to each bracket, the post-tensioning tendon was considered to be a member. Under AASHTO requirements, the connection (bracket) design force then must be increased; thus the bracket was designed for 144.25 kips.

The thickness for bracket parts was set to be at least the thickness of the beam flange, 3/4 in. The bracket end plate thickness was computed assuming a uniform load on a simply supported plate with a central hole. Welds and bolts were designed for both force and moment caused by the eccentric force of the post-tensioning tendon. The complete post-tensioning tendon and bracket design is shown in Fig. 19. Detail drawings for the bracket are in Appendix A.

The statement on the Bridge 1 plans that surface bond between the top beam flanges and concrete deck had been considered in design indicated the need for an increased number of shear connectors, as did our preliminary computations. Often, fatigue controls design of the shear connectors [14]; however, fatigue data on the bridge itself and on the angle-plus-bar type of shear connector were not available. Consequently, the shear connectors were checked on the basis of ultimate strength.

For computing the capacity of existing angle-plus-bar connectors, the angle-plus-bar was converted to an equivalent channel, based on

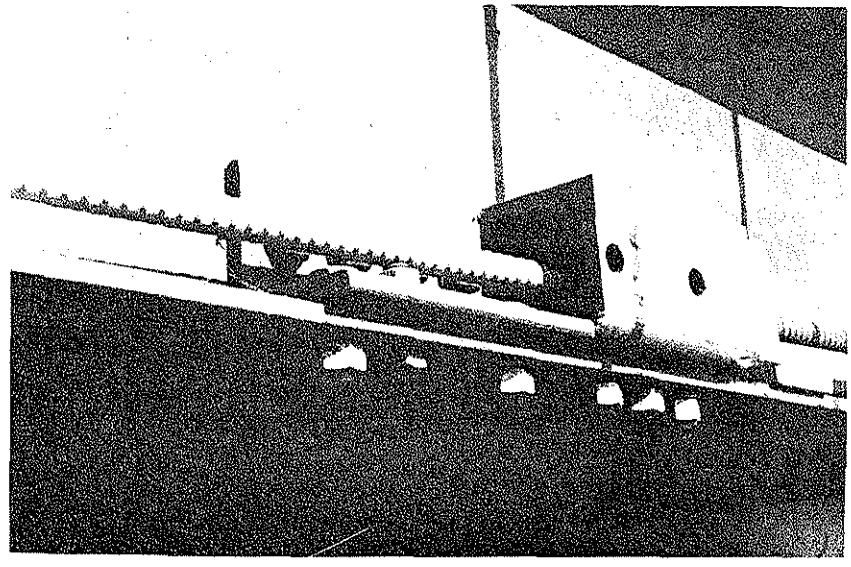

a. Post-tensioning bracket & tendon in position.

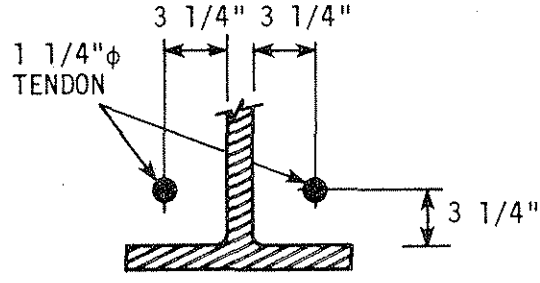

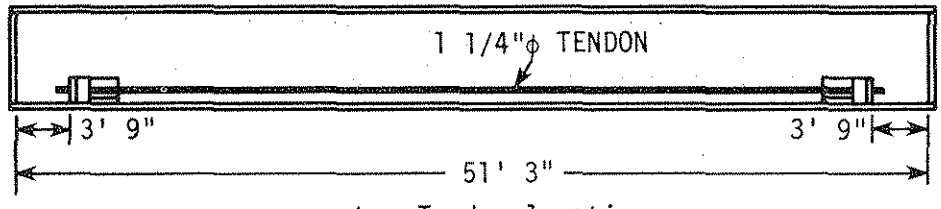

b. Tendon location.

Fig. 19. Post-tensioning details -- Bridge 1.

laboratory push-out tests, and the AASHTO channel formula was applied. On that basis, each existing angle-plus-bar connector was computed to have an ultimate strength of 143.8 kips.

Shear connector computations are summarized below:

Exterior beam

$P_2 > P_1 = 1289$ kips

ϕS_u for 7 connectors = 856 kips

ϕS_u for 13-1" ϕ bolts (studs) = 428 kips

1284 kips TOTAL $\cong$ 1289 kips $\therefore$ OK

Interior beam

$P_2 > P_1 = 1498$ kips

ϕS_u for 12.5 connectors = 1528 kips (including central connector at one-half value)

1528 kips > 1498 kips $\therefore$ OK

where

P_1 = force in the slab due to steel beam and tendon yield strength

P_2 = force in the slab due to concrete slab ultimate compression strength

ϕ = a reduction factor, 0.85

S_u = the ultimate strength of the shear connector

2.4.2.2 Strengthening for Bridge 2

Since the literature review indicated that the behavior of 45° skewed beam and slab bridges was similar to that for right angle bridges, Bridge 2 was analyzed as a right angle bridge. BRIDGE02 data

were the same as those for Bridge 1 given in Sec. 2.4.2.1, except that Bridge 2 was treated as a right-angle bridge with a span of 71.25 ft.

Results for tension stresses were:

	Exterior Beam	Interior Beam
In bottom flange at cover plate cutoff	24.97 ksi	18.80 ksi
In cover plate near midspan	24.37 ksi	18.58 ksi

To meet the allowable inventory stress of 18 ksi, the post-tensioning was required to reduce the exterior beam cover plate stress at midspan by 6.37 ksi.

Even though ORTHCO02 is directly applicable only to right-angle bridges, our review of the literature indicated that load distribution could be expected to be within 15% of the correct solution. ORTHCO02 applied to a right-angle bridge with a 71.25 ft span indicated, then, that each exterior beam would retain approximately 0.32 of the effects of the total post-tensioning applied to the bridge. Post-tensioning of the exterior beams easily compensated for the slight overstress in the interior beams.

In order that stresses in post-tensioning tendons would not exceed 0.60 f_{pu}, and to keep forces within 120 kip jack capacity, four tendons were required for each exterior beam as follows:

- Two tendons of 1 1/4 in. diameter, stressed to 91 kips at 3 1/4 in. above the bottom flange
- Two tendons of 1 in. diameter, stressed to 62 kips at 7 3/4 in. above the bottom flange

Based on computations for Bridge 1, no adjustments were made for gains or losses.

In order to keep the average stress in the bottom flange of the exterior beam at 18 ksi or less after deduction of holes for 1 in. diameter bolts, all bolt holes were required to be within 7.51 ft of the center of bearing. Due to expected moment shift toward obtuse corners, the brackets at those corners were located as close as possible to the supports, and the brackets at the acute corners were located with bolt holes ending at 7.50 ft on the span.

The force for each bracket was increased in accordance with AASHTO requirements to 241.50 kips. The bracket was designed to be welded from 3/4 in. plate, except for the end plate, which was to be 2 in. thick of Grade 50. (During fabrication a 2 1/2-in.-thick A36 plate was substituted for the Grade 50 plate.) Welds and bolts were designed for both force and moment. The complete post-tensioning tendon and bracket design is shown in Fig. 20. Detail drawings for the bracket are in Appendix A.

Computations for the shear connectors are summarized below:

Exterior beam

$P_1 > P_2 = 1503$ kips

ϕS_u for 8.5 connectors = 1039 kips (central connector at one-half value)

ϕS_u for 14-1" ϕ bolts (studs) = 461 kips

1500 kips $\cong$ 1503 kips $\therefore$ OK

Interior beam

$P_1 > P_2 = 1958$ kips

ϕS_u for 12.5 connectors = 1528 kips (central connector at one-half value)

ϕS_u for 13-1" ϕ bolts (studs) = 428 kips

1956 kips $\cong$ 1958 kips $\therefore$ OK

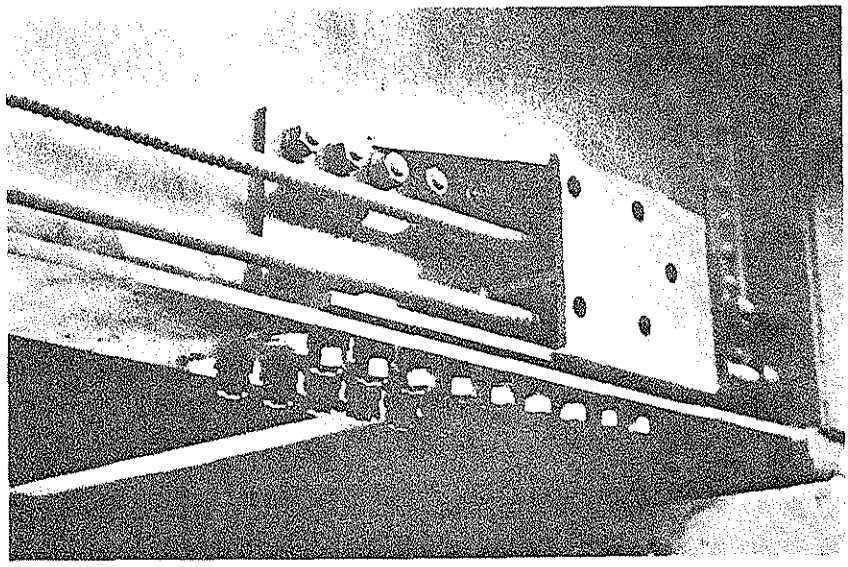

a. Post-tensioning bracket & tendons in position.

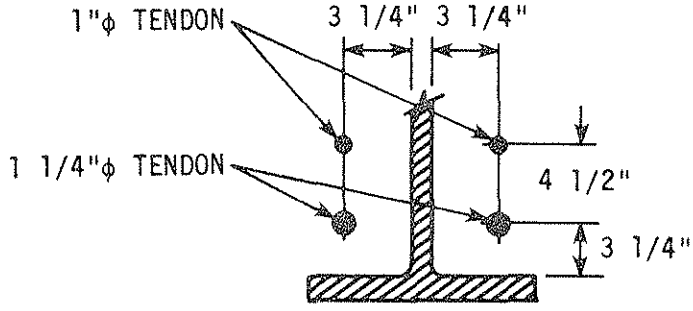

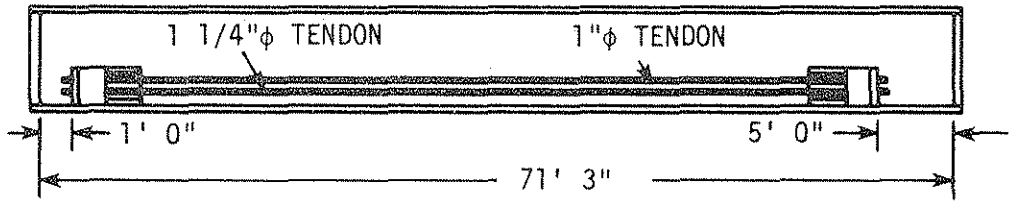

b. Tendon location.

Fig. 20. Post-tensioning detail -- Bridge 2.

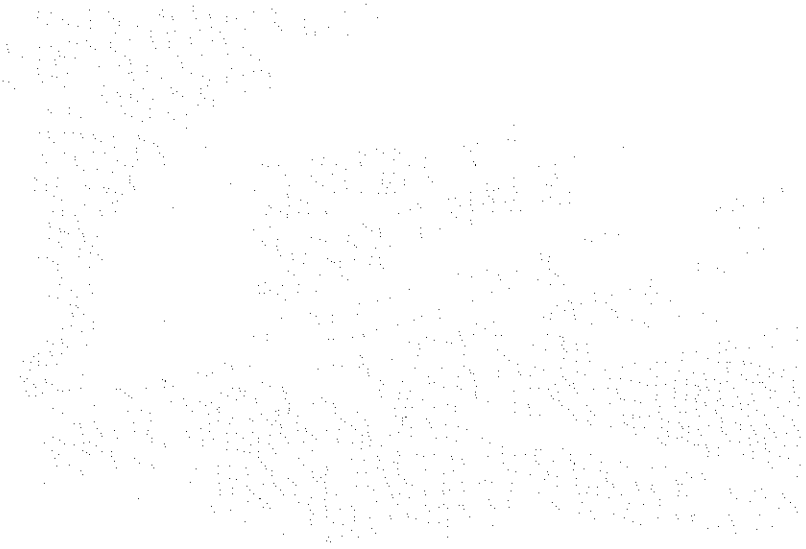

3. TESTS AND TEST PROCEDURES

The following sections outline the details of the specific tests that were conducted in the laboratory, as well as those that were conducted during the field strengthening and testing of Bridges 1 and 2. Only test set-ups, instrumentation utilized, and procedures followed during testing will be presented in this section; discussion and analysis of results, as well as behavior, will be presented in Section 4.

The instrumentation for the tests (laboratory and field) consisted of electrical-resistance strain gages (strain gages), direct current displacement transducers (DCDT's), and mechanical displacement dial gages (deflection dials). Calibration problems with the DCDT's resulted in their only being used in some of the laboratory testing.

Strain gages were attached to the various materials (steel, concrete, plexiglas) of the test specimens, by means of recommended surface preparations and adhesives. All strain gages were appropriately waterproofed and wired to minimize the effects of long lead wires and temperature changes. The majority of the gages attached to the model bridge of Phase I were still operational, and thus were used during the testing of the composite concrete and steel beam specimens cut from the bridge model.

Strains were read and recorded using an automatic data acquisition system (DAS), except for those on the post-tensioning tendons in the laboratory and field, which were read using a Vishay portable strain indicator. The same DAS was used to measure and record the deflections

which were measured using DCDT's; however, deflections measured with deflection dials were read and recorded by hand in all tests.

3.1 Push-out Tests

Slip and separation between the slabs and the beams were measured on all push-out specimens. The instrumentation for all specimens consisted of eight deflection dials, located as shown in Fig. 21. Four deflection dials recorded slip and the remaining four deflection dials measured separation at two elevations along the slab.

The four deflection dials which were used to measure slip were rigidly attached to the web of the beam, as shown in Fig. 21. The stem of each deflection dial was allowed to bear against blocks attached to the slab as shown. Slip was measured relative to the centerline of the various shear connectors.

The remaining four deflection dials, used to measure separation or "uplift", were rigidly attached to the platen of the universal testing machine. As shown in Fig. 21, separation was measured at the connector centerline and 1 in. from the end of the slab bearing on the testing machine platen.

The arrangement for testing in the universal testing machine is shown in Fig. 22. For uniform load distribution, the lower ends of the slabs were bearing either on a 1/4-in.-thick pad of neoprene or a thin layer of dry portland cement. Load was applied to the upper end of the steel beam by the head of the testing machine through a steel distribution plate; care was taken to assure concentric loading.

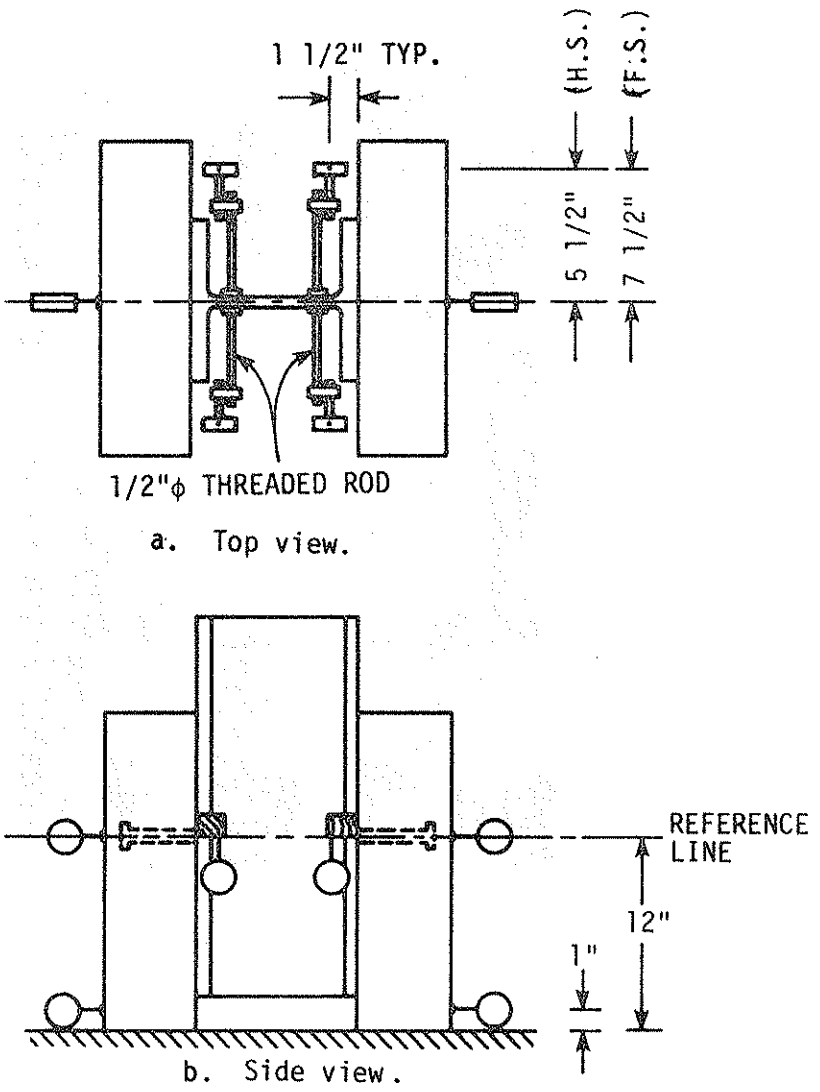

Fig. 21. Location of instrumentation used in the push-out tests.

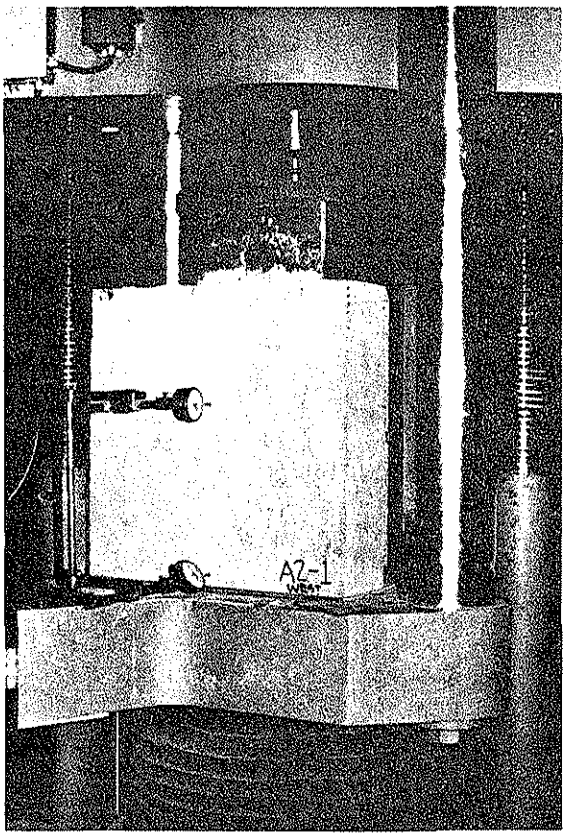

Fig. 22. Full-scale push-out specimen in testing machine.

The tests involving both Type A and Type B push-out specimens proceeded in the same general manner. Testing began with a pre-load of approximately 10% of the predicted ultimate load for each specimen. The pre-load value of 10 to 25 kips was applied for a variety of reasons: to insure an even distribution of force through the proper seating of the steel distribution plate on the beam flanges, to check the operation of the deflection dials, and to break the bond between the concrete and the steel beam.

By destroying the bond, consistent ultimate load results will occur because the entire load is on the connectors [27]. The bond was physically destroyed even though it has been reported that shrinkage of the concrete is sufficient to destroy bond [28]. Previous research [24] has indicated that the load-slip relationship will not be affected by unloading and reloading the specimens.

After the pre-load had been released and equilibrium in the system established, the load was applied in increments of varying magnitude. The magnitude of the increments for the tests varied from 10 kips to 50 kips at the beginning of the tests and 1 to 5 kips when failure was imminent. After each increment of load, slip and separation displacements were recorded. At high values of load, the load was held constant so that behavior (e.g., crack patterns) could be recorded. When failure occurred, photographs were taken to show the final deformed shape, and the ultimate load was recorded. The specimens were then removed from the testing machine and disassembled to determine the effects of the loading on the slabs and shear connection.

3.2 Testing of Composite Beams

3.2.1 Loading Apparatus and Instrumentation

This section outlines the loading apparatus and the instrumentation employed on the four test specimens. The same loading apparatus, except for slight variations in the load point location, was used in all tests. The instrumentation was nearly identical on each of the composite beams.

Load was applied to the beams through two 100 kip hydraulic jacks bearing against a steel frame anchored to the structural testing floor. Photographs of the test set-up used on the interior and exterior beams are shown in Figs. 23a and b, respectively. The load points were nominally 80 in. apart; the exact locations may be found in Fig. 24 along with other details of the test set-up. In order to transmit force uniformly to the slab, a combination of steel plates and neoprene pads was placed between the jacks and the slab. To transmit force through the curb and slab on the exterior-type composite beams, a concrete block was placed under the neoprene pads. Force was then transmitted through the concrete block and curb, which were at the same elevation. To prevent horizontal restraint at the load points, pin and roller supports were provided under the jacks. The jack pin support coincided with the beam's roller support and the jack roller support with the beam's pin support; details of the load points are provided in Fig. 24.

The load on the specimen was measured by a 100 kip load cell and checked by hydraulic jack pressure. The load cell was placed under

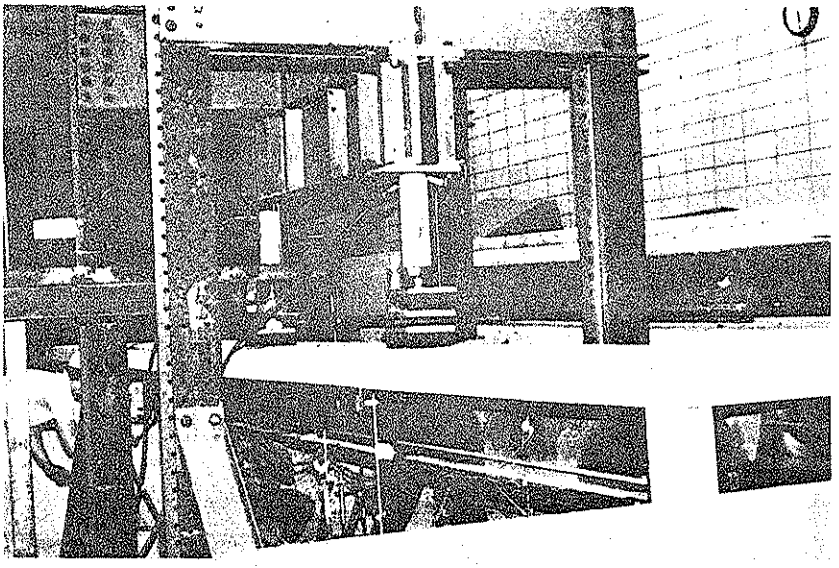

a. Example of interior beam test set-up.

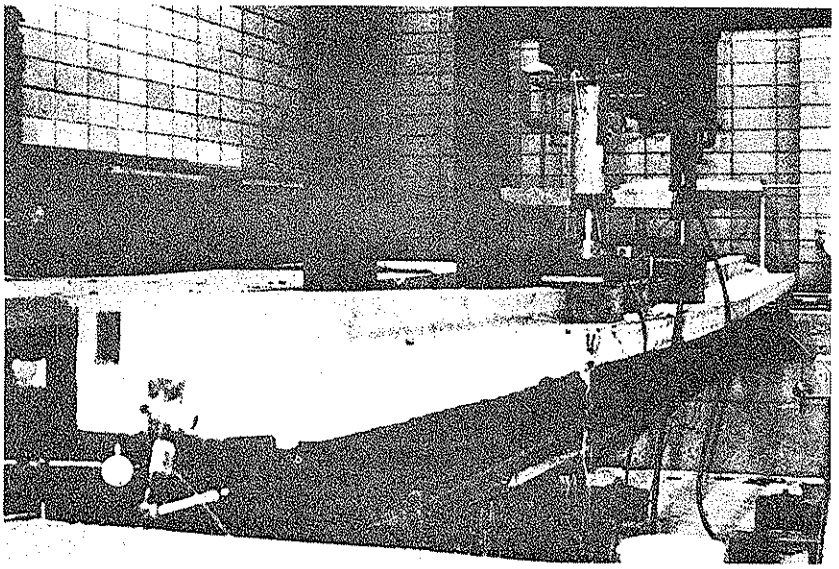

b. Example of exterior beam test set-up.

Fig. 23. Photographs of composite beam test set-up.

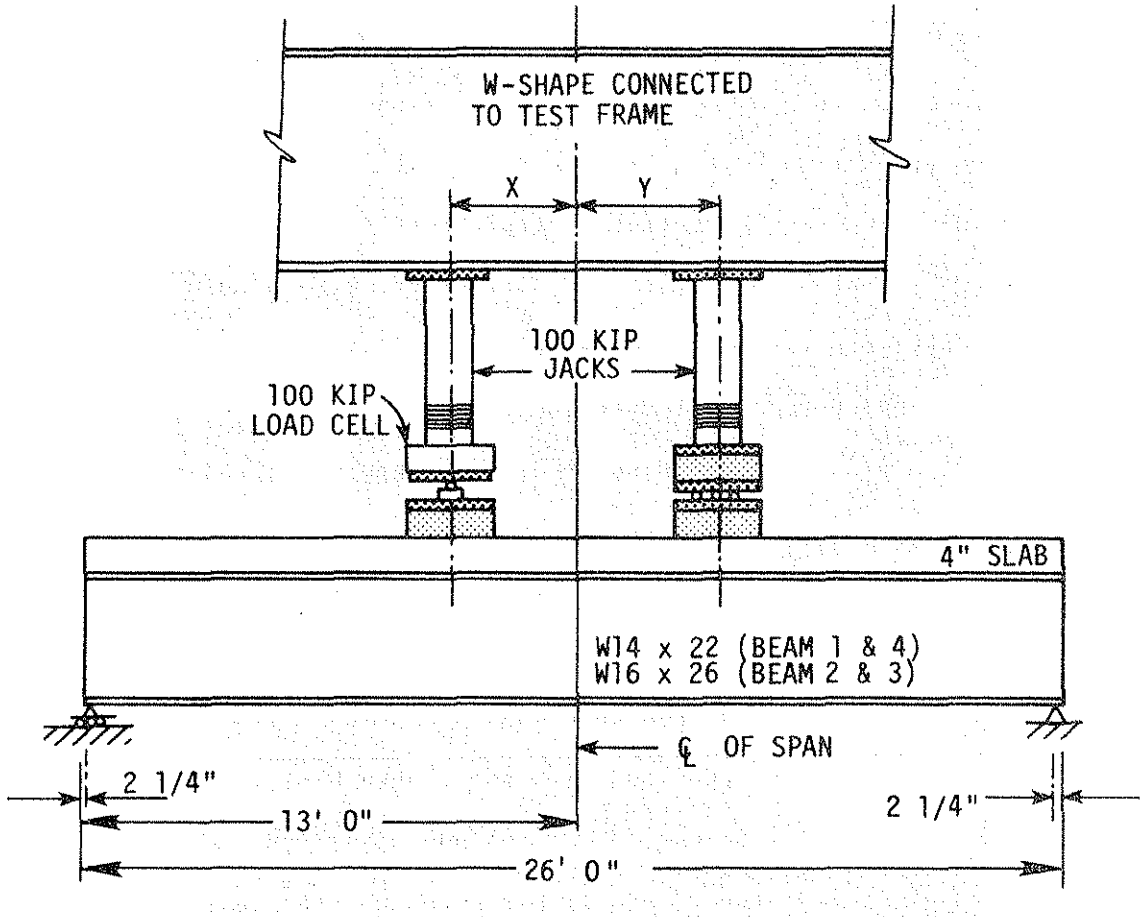

BEAM	X	Y
1	39 3/4"	40"
2	40"	40"
3	38 7/8"	40 1/2"
4	39 1/2"	39 3/4"

Fig. 24. Loading apparatus employed for testing the composite beams.

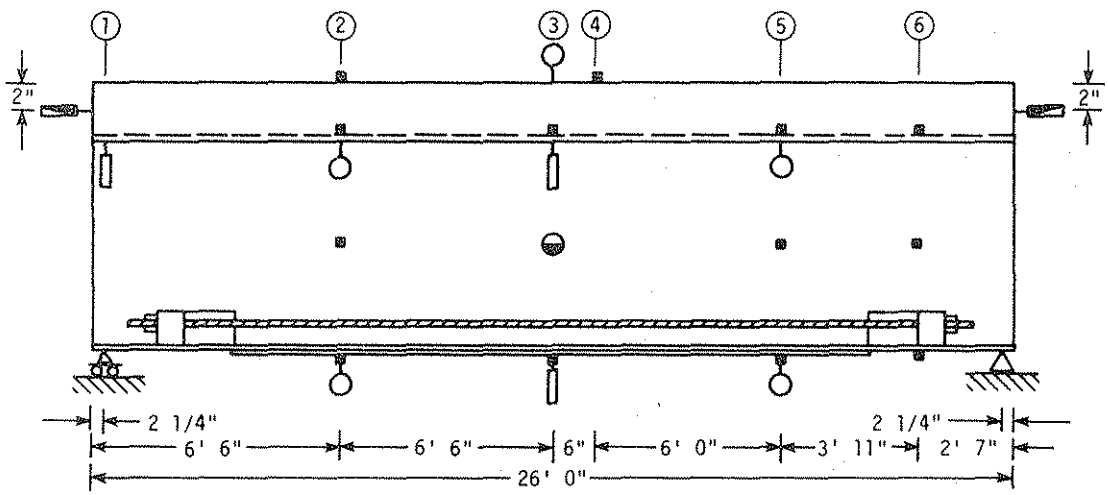

SIDE VIEW

SYMBOL	TYPE OF MEASUREMENT	GAGE
▭	VERTICAL DISPLACEMENT	DCDT
▱	RELATIVE SLIP	DCDT
○	VERTICAL DISPLACEMENT	DEFLECTION
●	HORIZONTAL DISPLACEMENT	DEFLECTION
▪	STRAIN	STRAIN

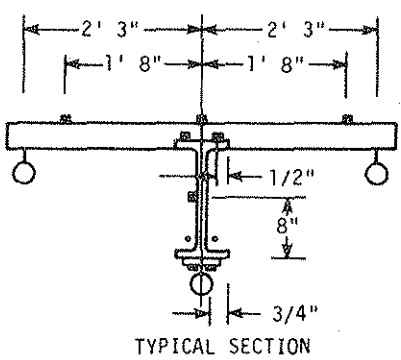

TYPICAL SECTION

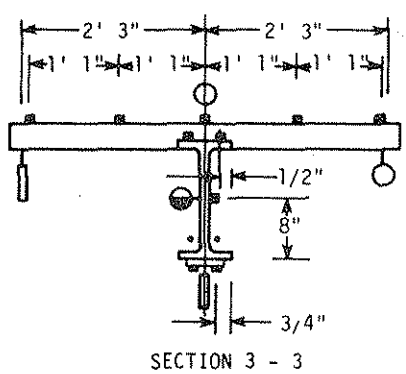

SECTION 3 - 3

Fig. 25. Location of instrumentation on Beams 2 and 3.

Table 5. Total number of DCDT's, deflection dials, and strain gages on each composite beam.

Beam	DCDT's	Deflection Dials	Strain Gages
1	5	8	16
2	5	7	18
3	5	7	26
4	5	8	29

post-tensioning force and magnitude of vertical load. Four tests were performed on each beam; the magnitude of test variables as well as the combination of variables in each test is summarized in Table 6. Note that Tests A, B, and C for each of the beams were elastic tests, while Test D for each of the beams was an ultimate strength test. A description of the four tests performed on each beam and test set-ups unique to the individual composite beams is provided in the following paragraphs.

To distinguish between tests, a number and a letter are used to designate each test. Thus, Test 3A indicates Test A of Beam 3.

Initially, in Test A, each composite beam was loaded with a preload of one to two kips to insure proper seating at the load points and to check the performance of all gages and DCDT's. After the preloading, initial "zero" readings for all strain gages, deflection dials, and DCDT's were recorded. As loading progressed, strain and displacement readings were taken after each load increment. Behavior was noted and photographs were taken throughout the test. After the load was released, beams were allowed to sit unloaded for a few minutes before final zero readings were recorded.

Tests B and C were slightly different from Test A in that a predetermined force was applied to the post-tensioning tendons (see Table 6 for magnitude of post-tensioning force). Composite beam specimens were then pre-loaded, vertical load applied, and readings taken as was done during Test A. The procedure used to "lock in" the post-tensioning force was similar to that used in Phase I.

The ultimate test performed on each beam, Test D, consisted of applying vertical load to the post-tensioned beam until the ultimate

Table 6. Summary of tests performed on the composite beam specimens.

Beam	Test	Post-tensioning Force (kips)	Vertical Load per Load Point (kips)	
			Maximum	Increment
1	A	0	9	1
	B	12	9	1
	C	24	9	1*
	D	34	35.0	1
2	A	0	18	1
	B	16	15	1
	C	32	15	1**
	D	48	48.3	1
3	A	0	15	1
	B	16	15	1
	C	32	15	1**
	D	48	50.4	1
4	A	0	9	1
	B	12	9	1
	C	24	9	1*
	D	34	38.1	1

*Increment was increased to 2 kips after the vertical load per load point reached 9 kips.

**Increment was increased to 2 kips after the vertical load per load point reached 15 kips.

capacity of the beam was reached. The test procedure up to the calculated elastic limit of the steel beam was identical to Tests B and C except that a higher post-tensioning force (see Table 6) was locked into each composite beam. At the calculated elastic limit of the steel beam, the loading increment was increased to two kips per load point. Behavior of the beam was noted and photographs taken when significant deformations occurred and when failure occurred.

3.3 Plexiglas Bridge Model

Although using plexiglas for the model of Bridge 2 did save time and money, it did have one undesirable characteristic, creep. If this is not properly accounted for, all results may be invalid. The most common method for handling creep in constant stress situations, such as the tests on the bridge model, is to determine a cyclic loading time to use in all tests. At a specified time increment, loads are applied and then all strain and deflection readings are taken. It is important to use the same time increment in all tests as there is a certain modulus of elasticity associated with that time. Through experimenting with a test specimen of the plexiglas in the model bridge, a time increment of one minute was selected. This same test specimen was used to determine the modulus of elasticity of the plexiglas. After loading was removed from the model, it was found that a period of time (at least twice the time it was loaded) was required for the model to relax and be ready for another loading cycle.

Figure 27 indicates the location of the 32 strain gages mounted on the model. At each of the 16 locations, there were two gages with their axes parallel to the axis of the beams--one on the top of the deck and one on the bottom of the lower flange. As seen in Fig. 27, the skewed centerline, as well as a perpendicular centerline, were instrumented for strain measurements. However, only the skewed centerline was instrumented for deflection measurements.

Table 7 lists the combination of variables in each of the ten different tests. Clarification of the various loading positions and the truck loading position is presented in Figs. 28 and 35. As previously stated, the bridge model was fabricated so that it could be tested with and without curbs; however, all testing done to date has been with the curbs in place. Load points shown in Fig. 28 were 1/2 in. off the centerline and quarter span line to avoid the strain gages on the deck.

For clarity, the testing program will be presented in three sections: vertical load tests (Tests 1 and 2 in Table 7), post-tensioning load tests (Tests 3-5 and 8-10), and tests involving a combination of vertical load and post-tensioning load (Tests 6 and 7).

3.3.1 Vertical Load Tests

Tests involving vertical loads only are designated in Table 7 as Tests 1 and 2. A single concentrated load of 14.2 lbs was systematically placed at each of the eight load points shown in Fig. 28. The 14.2 lbs concentrated load (equivalent to 41.9 kips on the prototype) produced strains of sufficient magnitude that measurement problems were minimal. Steel plates were placed on bolts, so that only the

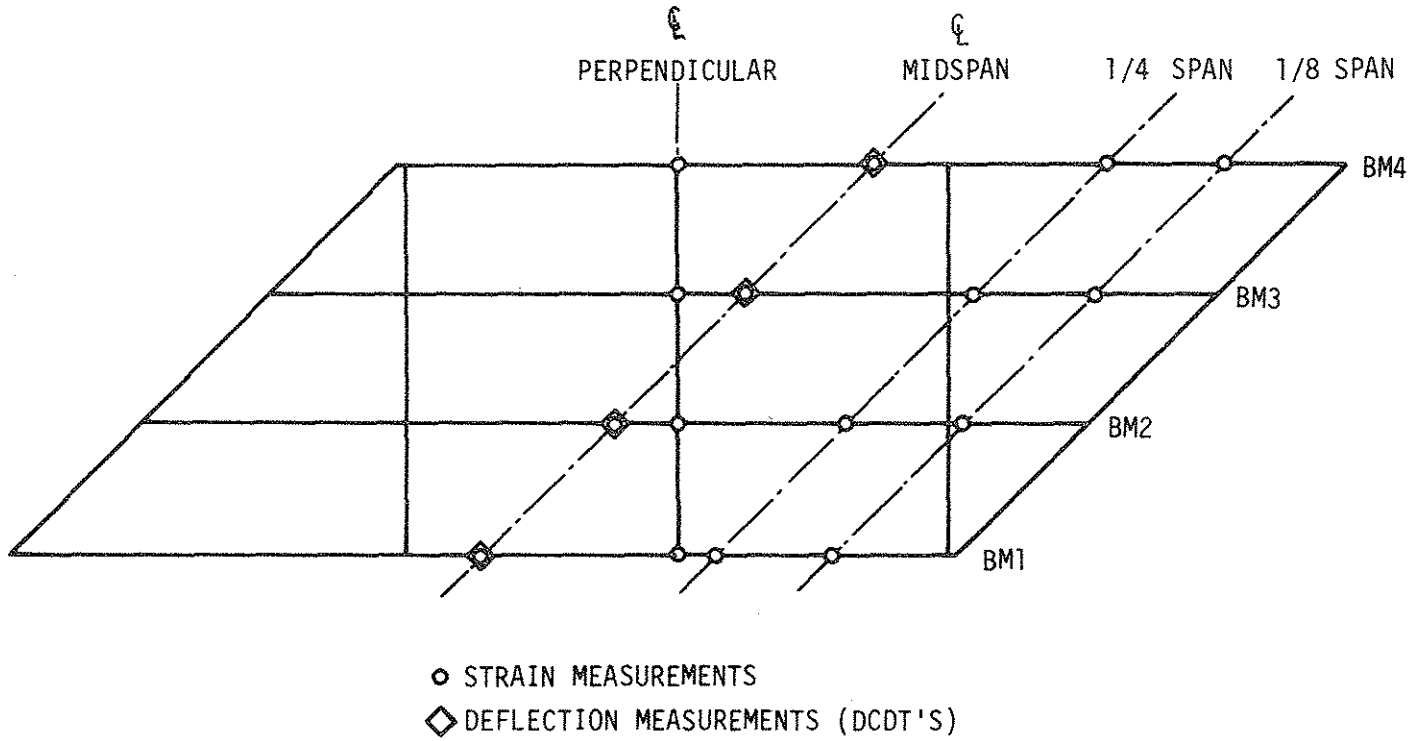

Fig. 27. Location of instrumentation -- plexiglas model.

Table 7. List of tests with variables used--plexiglas model.

Test No.	Post-tensioning Scheme		Post-tensioning Eccentricity			Post-tensioning Length			Vertical Loads								
									14.2 lb load @								
	PTS-1	PTS-2	e_1	e_2	e_3	L_1	L_2	L_3	1	2	3	4	5	6	7	8*	T**
1									●	●	●	●	●	●	●	●	
2																	●
3	●		●			●											
4	●			●		●											
5	●				●	●											
6	●			●		●			●	●	●	●					
7	●			●		●											●
8	●			●			●										
9	●			●				●									
10		●		●		●											

*Positions at which load was applied (see Figure 28).

**Simulated truck loading (see Figure 29).

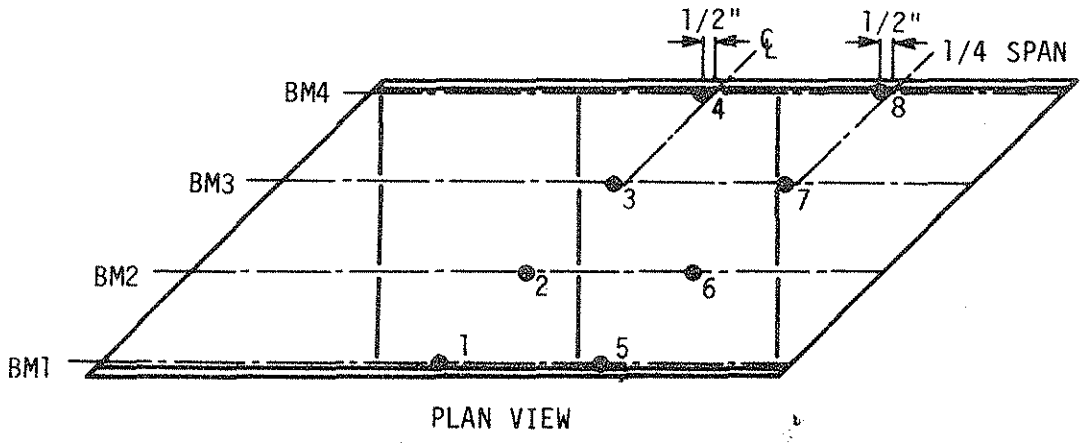

Fig. 28. Locations of concentrated vertical load points -- plexiglas model.

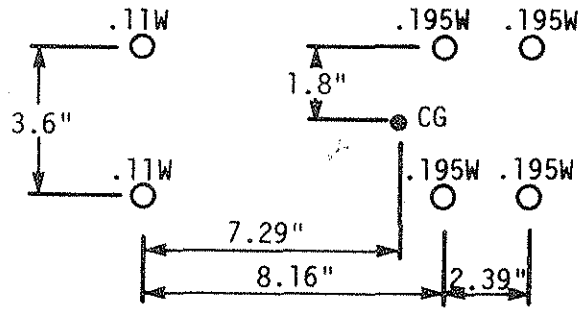

AXLE LOADS: 4.53 LB 7.99 LB 7.99 LB

TOTAL : 20.51 LB

Fig. 29. Simulated truck loading -- plexiglas model.

head of the bolt came in contact with the bridge (approximately 1/2 square in. of contact area). These were used to simulate the concentrated load.

In Fig. 29 the simulated truck loading used on the model bridge is shown; it is a scaled-down version of the truck actually used on Bridge 2. Thus, the model truck weighed 20.51 lbs, while the actual truck weighed 60,500 lbs. Shown in Fig. 35 are quarter span and centerline points where the center-of-gravity of the truck was positioned on the model. As was the case in the field testing (see Section 3.4), the truck was placed in six different lanes--three one direction and three the other direction--across the bridge. Lanes 1 and 6 were at minimum distance from curb (1.13 in. model; 2 ft prototype); lanes 2 and 5 were at minimum distance from bridge centerline; and lanes 3 and 4 were both centered on the longitudinal bridge centerline--lane 3 with the truck headed one direction and lane 4 with the truck headed opposite. Thus, the truck was placed at 18 different locations.

The procedure used in each vertical load test was as follows:

(1) Record zero strain gage and DCDT readings utilizing the DAS. Read and record initial reading of deflection dial for creep determination.

(2) Apply load (concentrated or truck) at desired location.

(3) Wait one minute and take strain and deflection readings as in step 1.

(4) Remove loading, wait a minimum of two minutes (noting deflection dial reading for creep behavior) and take second set of zero readings as in step 1.

(5) Repeat above steps until all vertical load cases have been completed.

3.3.2 Post-tensioning Tests

Tests involving post-tension forces only are listed in Table 7 as Tests 3, 4, 5, 8, 9, and 10. The only difference in post-tensioning schemes 1 and 2 (listed as Tests 9 and 10 in Table 7; henceforth referenced as PTS-1 and PTS-2) was in PTS-1, where the force was symmetrically incremented in each rod to the desired value, and in PTS-2 the force was increased to the desired value in one rod and then increased to the same value in the second rod. The three different eccentricities (e_1, e_2, and e_3) used, as well as their distance from the composite neutral axis, are shown in Fig. 13a. Figure 13b indicates the location of the brackets used to obtain the three different post-tensioning lengths (L_1, L_2, and L_3). Length L_1 was obtained by placing the brackets close to the location they will be on the prototype, Bridge 2. By moving the bracket at the acute angle of the bridge closer to the other bracket, length L_2 was obtained. Length L_3, the shortest length, was obtained by moving both brackets away from the end supports.

The post-tensioning force required for each exterior beam--to reduce the bottom flange strains to the desired level--was found by using the requirements of similitude to be 104.1 lbs. This is the force required, assuming the post-tensioning rods have the same eccentricity as those in the prototype. However, in the model the post-tensioning rods are actually below the lower flange; thus, a smaller force was required to obtain the same moment effect. As is normally

the case, the axial load effects are small compared to the flexural effects resulting from post-tensioning. Thus, the axial load stresses were ignored when the force necessary to produce the same moment as the 104.1 lbs in the correct position was determined. Using eccentricity e_2, a force of 50.0 lbs was determined to result in the desired moment.

In the tests involving PTS-1, the post-tensioning force was increased in increments of 12.5 lbs until 62.5 lbs was reached. The tests in which the post-tensioning force was incremented were conducted as follows:

(1) Record zero strain gage and DCDT readings utilizing the DAS.

(2) Tighten nuts at one end of each post-tensioning rod until the desired strain is reached, thus indicating the desired force has been obtained.

(3) Allow creep effects to occur in the model for approximately 30 sec. Adjust tension in post-tensioning rods until the desired force is once again obtained.

(4) Take final strain gage readings using the DAS.

(5) Remove post-tensioning force and allow bridge to relax for a period of time at least twice that in which the force was applied.

(6) Repeat steps 1 through 5 except each time increase the post-tensioning force one increment. For the higher post-tensioning force, considerably longer periods of time are required for the model to relax.

3.3.3 Vertical Loads Plus Post-tensioning

Tests involving a combination of vertical load and post-tensioning (Tests 6 and 7 in Table 7) were conducted at eccentricity e_2 and length L_1, with a post-tensioning force of magnitude, 50.0 lbs. As presented in the previous sections, the 50.0 lbs of force at an eccentricity e_2 were required to reduce lower flange stresses to the desired level. The procedure of applying the vertical loads and post-tensioning forces, as well as their locations, were the same as has already been presented. Post-tensioning forces were applied first, when vertical loads (concentrated or truck) were applied to the model. The bridge strains, as well as the change in strains in the post-tensioning rods, were recorded utilizing procedures similar to those previously described.

3.4 Field Bridge Tests

In the following paragraphs the instrumentation, type of loading, location of loading, testing program, and so forth for Bridges 1 and 2 will be presented. Due to the similarities in the bridges, instrumentation and the like will be discussed together for both bridges.

Figure 30 indicates the location of the strain gages and deflection dials used on Bridge 1. At each of the four sections instrumented for strain detection, four strain gages were oriented with their axes parallel to the axis of the beam. Two of the four gages were on the lower surface of the top flange, and two were on upper surface of the bottom flange; all were 1/2 in. in from the flange edges. The strain gages were so positioned on the beam cross-section to facilitate their

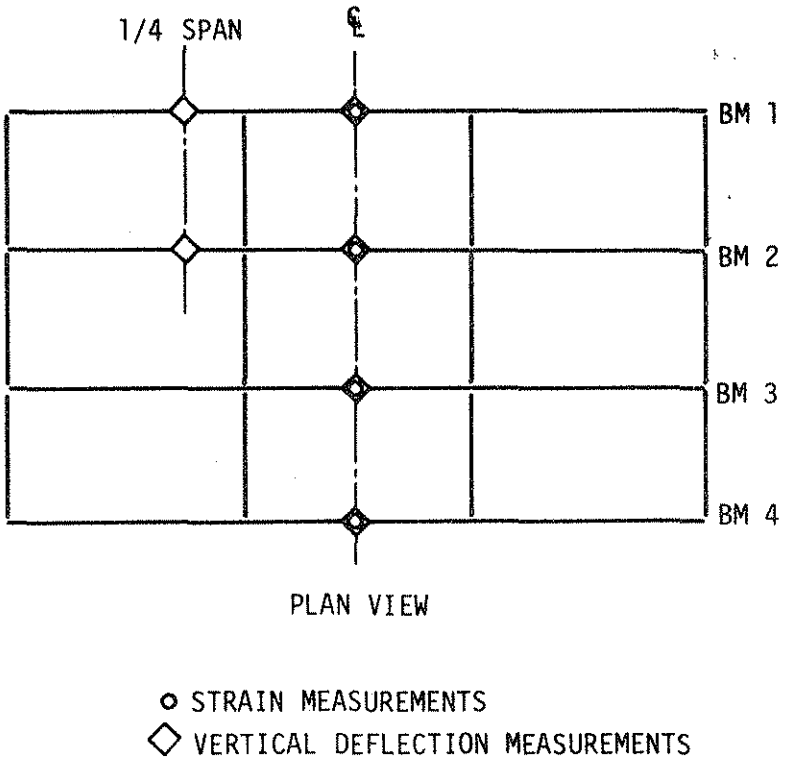

Fig. 30. Location of instrumentation -- Bridge 1.

installation. Since the strain gages were not on the top and bottom of the beams, strains slightly less than the maximum at the various sections were recorded. However, with the measured strains, the maximum strains at the given section can be determined.

The six deflection dials indicated in Fig. 30 were positioned to measure vertical deflection at the centerline of each beam and the quarter point of Beams 1 and 2. Due to the large distance between the bridge and the ground, it was necessary to construct wooden frames to support the deflection dials. To prevent movement of the frames, they were guyed with several small cables.

The instrumentation (strain gages and deflection dials) utilized on Bridge 2 is shown in Fig. 31. At each of the eight sections instrumented for strain measurement, four strain gages were placed and oriented as on Bridge 1. The majority of the strain gages were placed on Beams 3 and 4; however, the centerline of Beams 1 and 2 was also instrumented. Two sections were instrumented 15 in. from the centerline of bearing of Beams 3 and 4; this was done as a result of the end restraint detected during the strengthening of Bridge 1. With the instrumentation of these two sections, it was possible to determine the approximate end restraint present. More details on the end restraint in the two bridges is presented later. The eight deflection dials used for the measurement of vertical deflections were attached to wooden frames similar to those used on Bridge 1. As previously stated for post-tensioning the bridges, two 1 1/4 in. diameter Dywidag Threadbars were required on each exterior beam of Bridge 1 and four Dywidag Threadbars--two of 1 in. diameter and two of 1 1/4 in. diameter--were

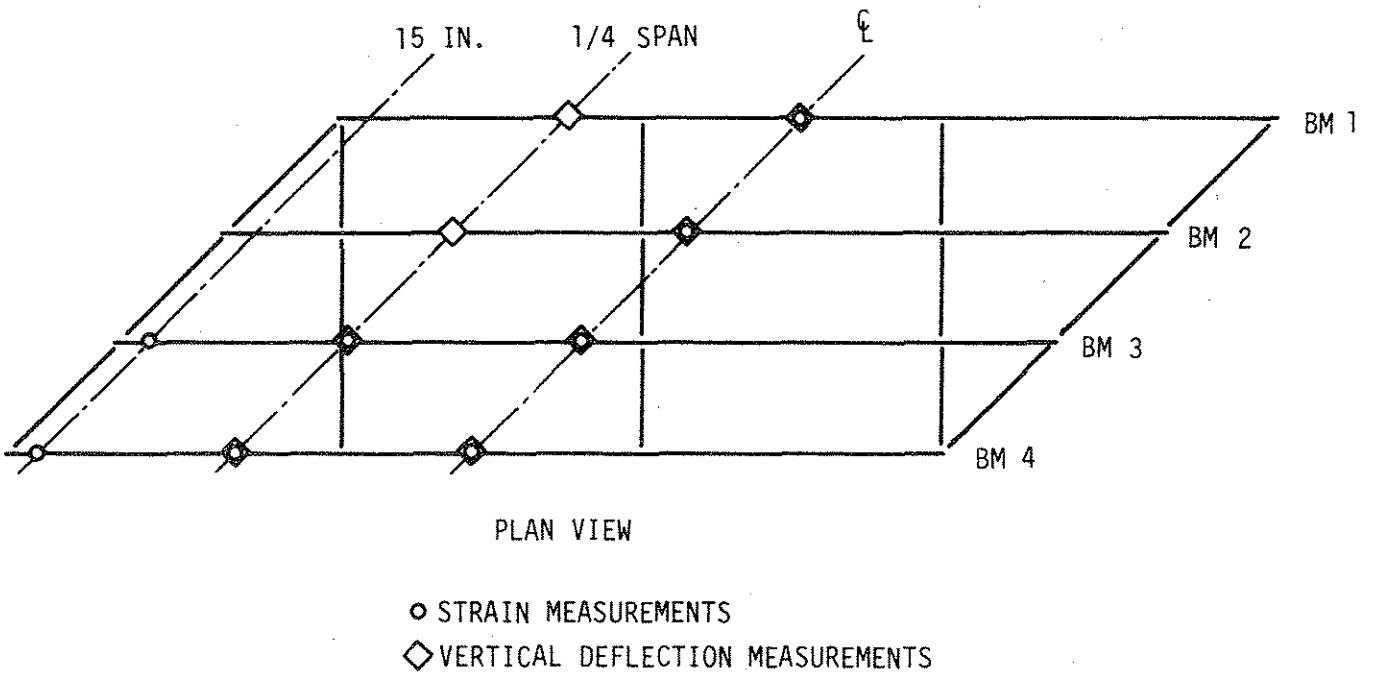

Fig. 31. Location of instrumentation -- Bridge 2.

required on the exterior beams of Bridge 2. For accurate measurement of the post-tensioning force, two longitudinal strain gages (wired to cancel bending and detect twice the axial strains) were attached to each tendon (Dywidag Threadbars). For corrosion protection, all tendons were given a fusion bonded powder epoxy coating using 3M, SK213 material; coating thickness was 8 mils ± 2 mils. As the tendons were factory coated, they were inspected after they were in place to recoat any areas that had been scratched during shipping or handling. Post-tensioning brackets for both bridges were painted with red oxide Type 2 primer before installation. After they were bolted in place, the bolts were painted and the brackets "touched-up" with the primer. Brackets and attaching bolts were then painted with Iowa DOT approved second field coat: Foliage Green. On both bridges, it was necessary to remove a portion of the interior diaphragm brackets for tendon clearance.

The field testing program on each bridge involved the determination of each bridge's response, strains, and deflections, to the following three loading conditions:

(1) An overloaded truck at various predetermined locations on the bridge

(2) The various stages of the post-tensioning sequence

(3) Same overloaded truck at the same locations after the post-tensioning of the bridge had been completed.

The trucks (configuration and weights) used to load the bridges are presented in Figs. 32 and 33. Although the trucks had different wheel spacing, their weights (60,540 lbs for Bridge 1 and 60,500 lbs

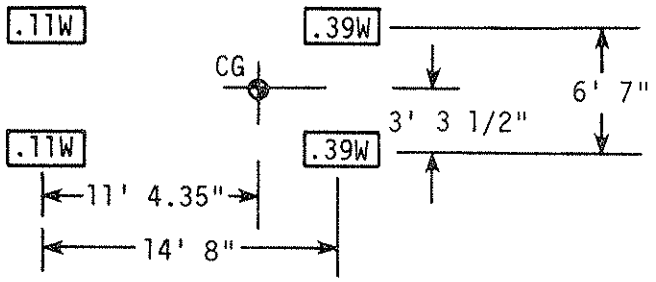

AXLE LOADS: 13.64^{K} 46.90^{K}
TOTAL: 60.54^{K}

a. Wheel configuration and weight distribution.

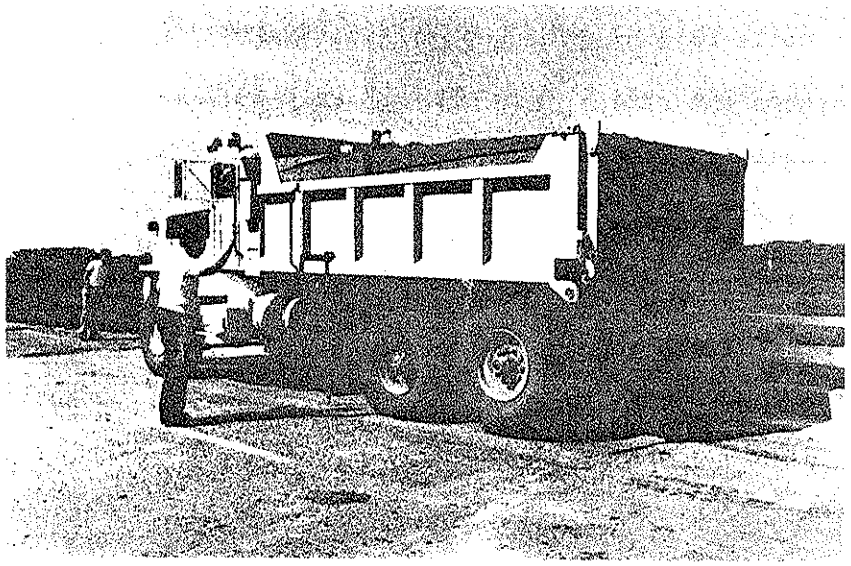

b. Photograph of test vehicle at predetermined location on bridge.

Fig. 32. Field test vehicle used to load Bridge 1.

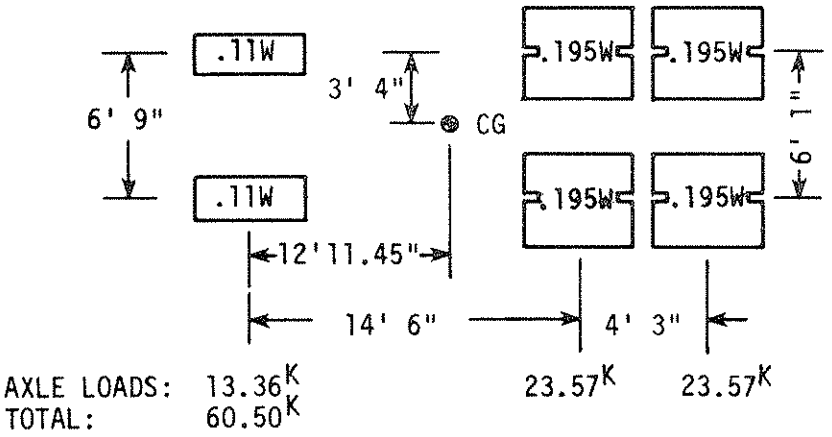

a. Wheel configuration and weight distribution.

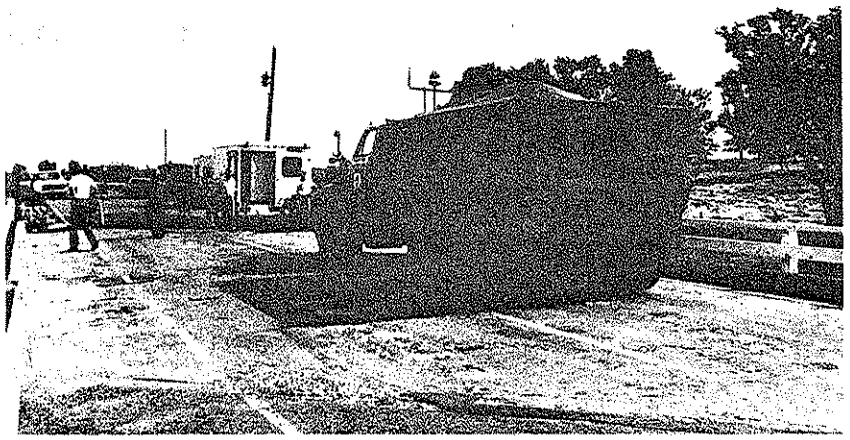

b. Photograph of test vehicle at predetermined location on bridge.

Fig. 33. Field test vehicle used to load Bridge 2.

for Bridge 2) were essentially the same. As may be seen in Figs. 32b and 33b the sand load in both trucks was covered to reduce evaporation, which would change the truck weight. Although the photograph of the truck used on Bridge 1 (Fig. 32b) shows rear tandem wheels, the rear wheels were actually raised, thus creating the wheel spacing shown in Figure 32a.

The load points shown in Figs. 34 and 35 indicate where the center-of-gravity of trucks (see Fig. 32a for Bridge 1 and Fig. 33a for Bridge 2) used in the loading of Bridges 1 and 2, respectively, were positioned. Trucks were positioned at these locations before (loading condition 1) and after (loading condition 3) post-tensioning.

On Bridge 1, the truck was positioned over the 12 loading points shown in Fig. 34b by having the truck heading south and crossing the bridge in three different lanes: lane 1 was with the centerline of the tires 2 ft from the curb, lane 2 was with the centerlines of the tires 2 ft from the longitudinal bridge centerline, and lane 3 was with the truck centered on the longitudinal bridge centerline (see Fig. 34a). As the truck crossed the bridge, it was stopped at the two quarter points, the centerline, and at a section 19.83 in. past the bridge centerline. For this truck, positioning the truck's center-of-gravity at this latter section produces maximum moment in the bridge. Although not shown, testing also included having the truck cross the bridge headed north, in lanes similar to the other three, to check symmetry.

As in the test of Bridge 1, another truck (see Fig. 33) was positioned on Bridge 2 (see Fig. 35b) by having the truck cross the

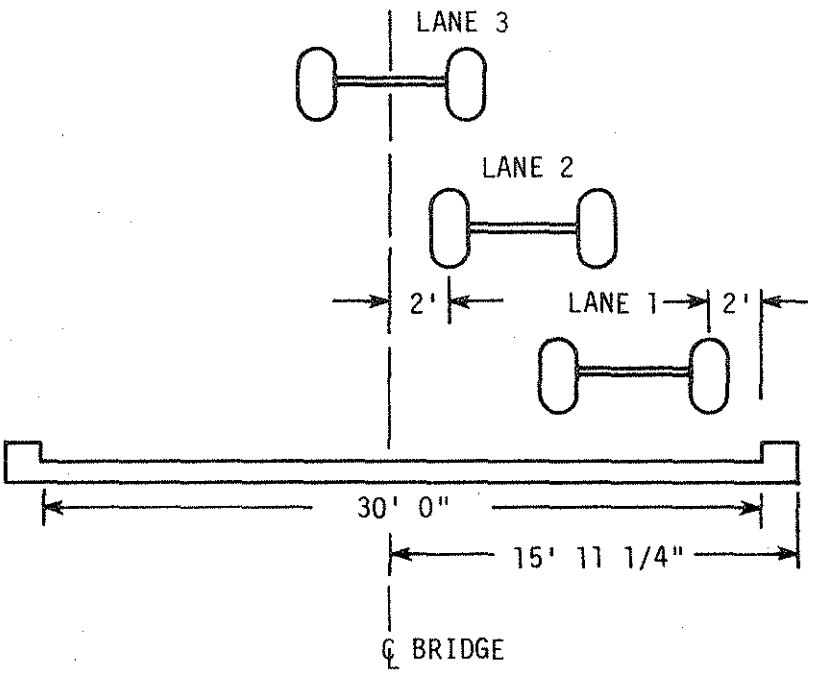

a. Cross-section.

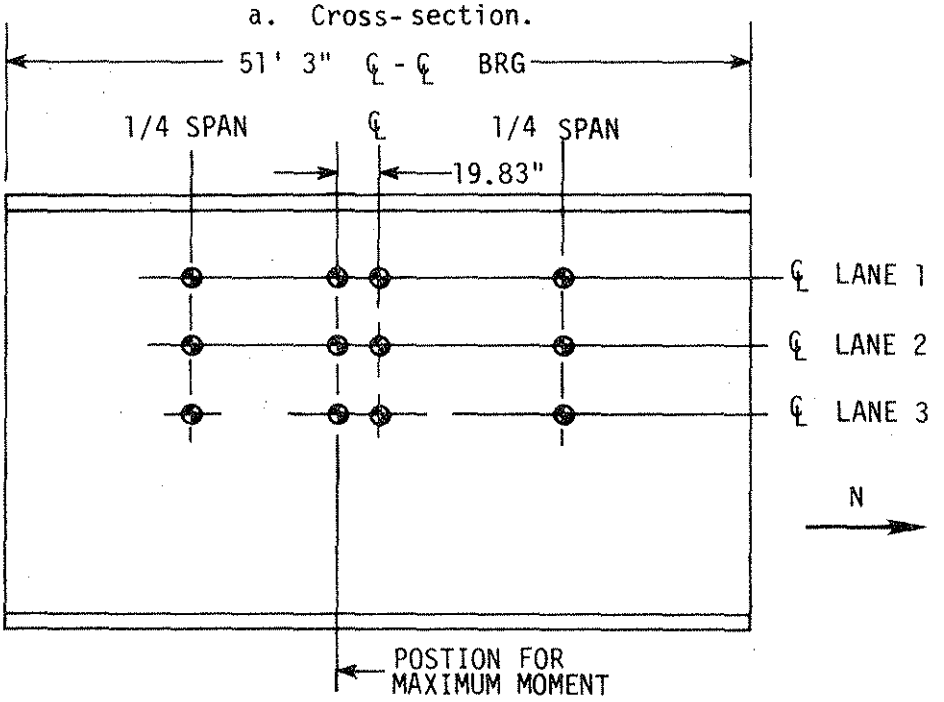

b. Plan view.

Fig. 34. Location of test vehicle -- Bridge 1.

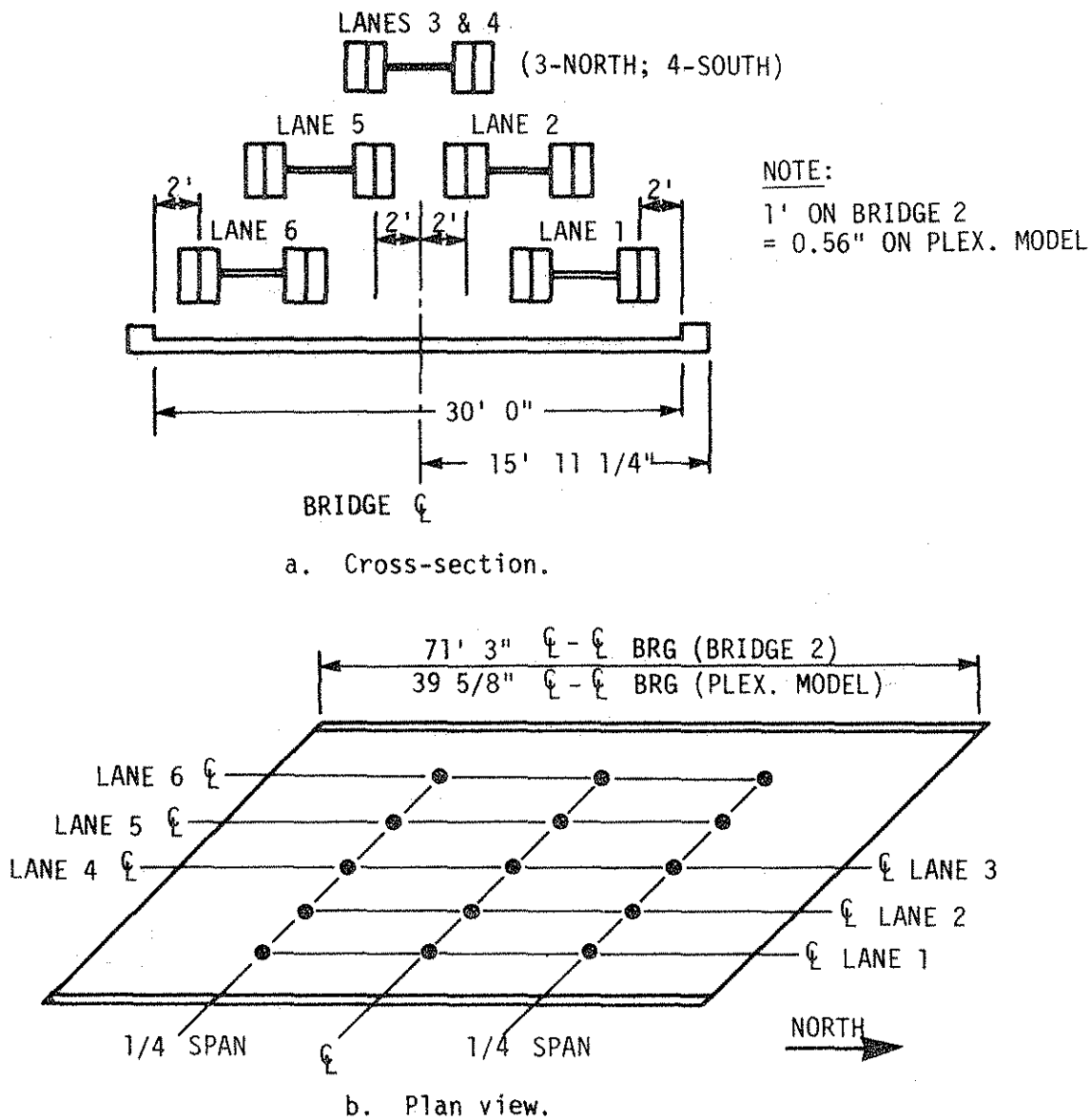

Fig. 35. Location of test vehicle -- Bridge 2 & plexiglas model.

bridge in six different lanes and stop so that the truck's center-of-gravity was at the two quarter points and bridge centerline. The six crossings (three with the truck headed north and three with the truck headed south) were necessary due to the skew of the bridge and the limited amount of instrumentation used. As on Bridge 1 the truck crossed the bridge at a minimum distance from the curb (lanes 1 and 6), at a minimum distance from the bridge centerline (lanes 2 and 5), and with the truck centered on the longitudinal centerline of the bridge (lanes 3 and 4). As expected, the results obtained when the truck was placed in lane 3 (truck headed north) and in lane 4 (truck headed south) were essentially the same.

Post-tensioning force was applied to the exterior beam of the two bridges utilizing 120 kip capacity, 6-in.-stroke hollow-core-hydraulic cylinders, which were 6 1/4 in. in diameter. This diameter was somewhat critical in that it did influence the position of the tendons relative to the beams. As only two hydraulic cylinders were available, it was necessary to post-tension the bridges utilizing a scheme similar to the second post-tensioning scheme (PTS-2) of Phase I. As the actual steps in post-tensioning were different for the two bridges, they will be presented separately in the following paragraphs.

For Bridge 1, in order to reduce by the desired amount the stresses in the exterior beam and cover plate, it was determined that each exterior beam required 184 kips (92 kips per tendon) of post-tensioning force located 3 1/4 in. above the bottom flange (see Sec. 2.3.2.1). Utilizing the two hydraulic-cylinders, the bridge was post-tensioned by applying approximately one-third (60 kips) to each exterior beam in

six steps as shown in Table 8. Note that the values given in Table 8 (as well as in Table 9 which follows) are nominal values rather than actual values.

In steps 5 and 6 the forces in the tendons were increased past the desired values to offset seating losses. As previously noted, the post-tensioning forces could be measured accurately using the strain gages mounted on the individual tendon. After seating losses, Beams 1 and 4 had 181.59 kips and 182.43 kips of post-tension force respectively. Thus, based on the average of the two values, 182.01 kips, there was 1% less post-tensioning force than desired.

To obtain the desired stress reduction in Bridge 2, each exterior beam required 306 kips (91 kips per large tendon and 62 kips per small tendon), located as shown in Fig. 20. As there were only two hydraulic cylinders available and each exterior beam had four tendons (two of 1 1/4 in. diameter and two of 1 in. diameter), the post-tensioning of Bridge 2 was somewhat more involved than Bridge 1. As shown in Table 9, post-tensioning of Bridge 2 was accomplished in steps by applying to the eight tendons approximately one-third the desired force. A graphical representation, as presented in Fig. 36, shows how the post-tensioning force was applied (12 steps). As can be seen, small changes in the post-tensioning force occur on one beam when the other beam is being post-tensioned. In addition to seating losses, the loss of post-tensioning force in one set of tendons on a given beam, caused by the elastic shortening of the beam when the other set of tendons was post-tensioned, had to be taken into account.

Table 8. Post-tensioning sequence--Bridge 1.

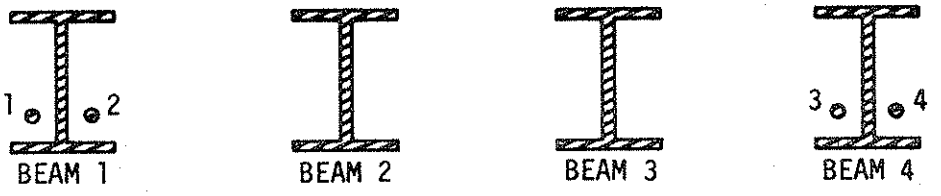

Steps	Force Applied and "Locked in" Tendons (kips)			
	Tendon 1	Tendon 2	Tendon 3	Tendon 4
1	30	30		
2			30	30
3	60	60		
4			60	60
5	92	92		
6			92	92

Table 9. Post-tensioning sequence--Bridge 2.

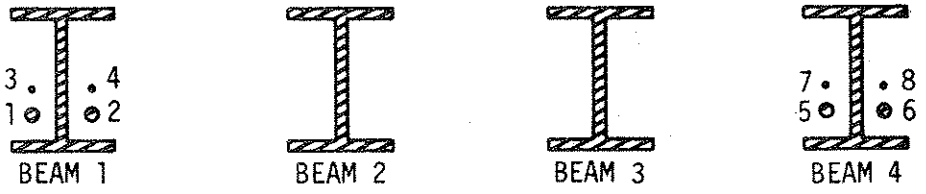

Steps	Force Applied and "Locked in" Tendons (kips)							
	Tendon 1	Tendon 2	Tendon 3	Tendon 4	Tendon 5	Tendon 6	Tendon 7	Tendon 8
1	30	30						
2			20	20				
3					30	30		
4							20	20
5							40	40
6					60	60		
7	60	60						
8			40	40				
9			62	62				
10	91	91						
11					91	91		
12							62	62

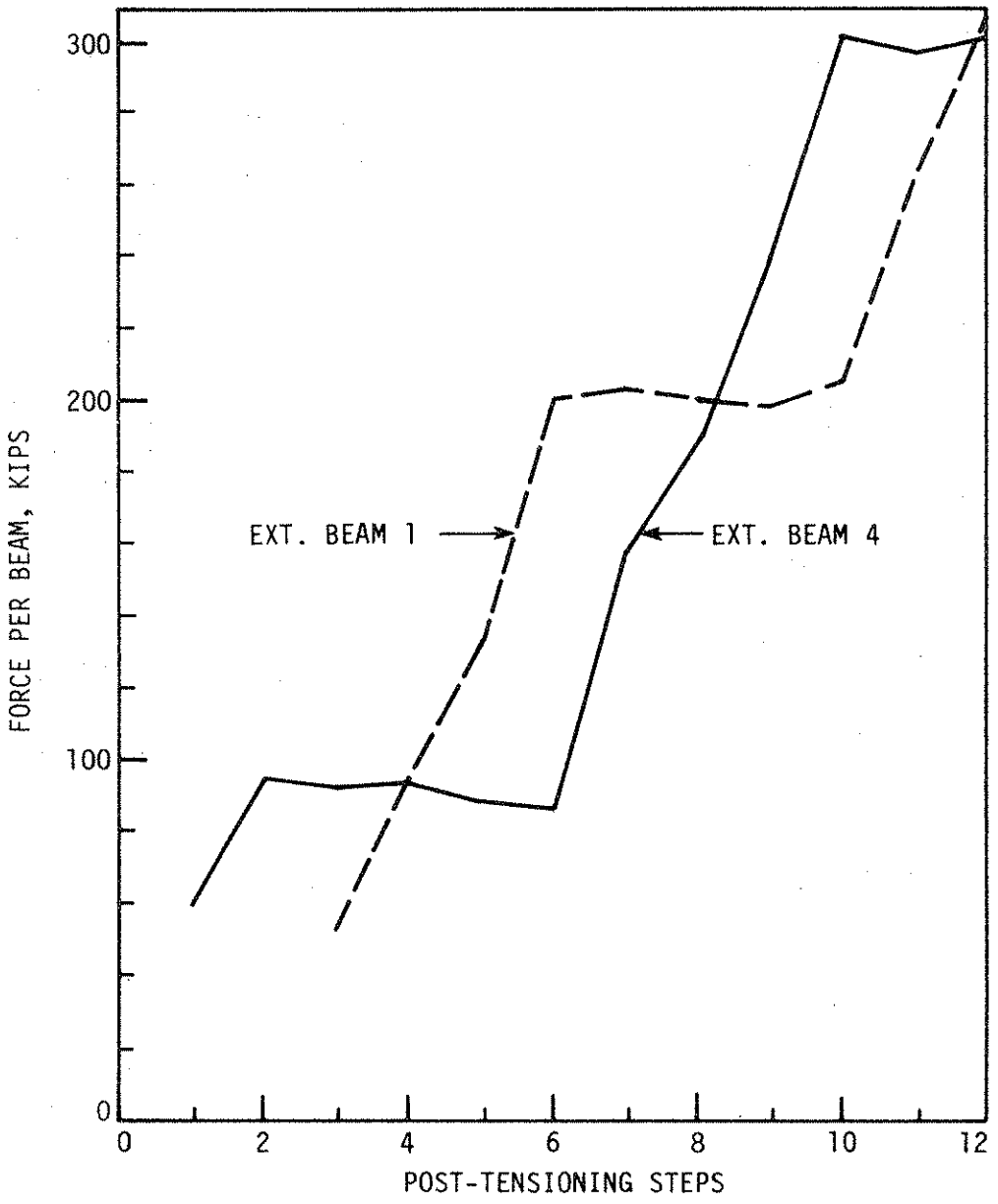

Fig. 36. Variation in post-tensioning force per beam during post-tensioning sequence -- Bridge 2.

After the various losses had been taken into account, Beams 1 and 4 had post-tensioning forces of 303.58 kips and 307.58 kips respectively. Based on an average of these two values, 305.58 kips, the post-tensioning force was 0.1% lower than desired.

The procedure used to obtain data on both bridges for the trucks in the various locations as well as for the various stages of post-tensioning was:

(1) Record zero strain reading for all strain gages utilizing the DAS and Vishay indicator; read and record initial readings of all deflection dials.

(2) Apply loading (truck, post-tensioning, or post-tensioning + truck) at desired location.

(3) Record the strain gage readings as in step 1; record any changes in bridge behavior.

(4) Remove truck loading from bridge and take second zero strain gage and deflection dial reading. Obviously the second zero could not be obtained when the post-tensioning forces were applied.

(5) Repeat steps 1 through 4 until truck loading had been positioned at all desired locations (before and after post-tensioning).

4. TEST RESULTS AND ANALYSIS

Detailed descriptions of the test specimens have been presented in Section 2; detailed information on the various tests (field and laboratory) were presented in Section 3. In subsequent sections of this chapter, experimental results of the various tests performed will be presented. In most instances the experimental results will be compared with theoretical results.

As was done in Phase I, orthotropic plate theory was used in the determination of the theoretical moment coefficients. For details of assumptions made in this analysis, the reader is referred to Ref. 19. The experimental moment fractions are based on bottom flange strains utilizing the same assumptions made during Phase I. As previously mentioned, beam strains measured in the field (Bridges 1 and 2) were on the top of the bottom flange (bottom flange strains) and on the bottom of the top flange (top flange strains). For clarity, the results of each test program will be presented and discussed separately as was done in the previous sections (Sections 2 and 3). Due to the vastness of the various test programs, and thus the resulting data, only the most significant portions of the data will be reported.

4.1 Push-out Test Results and Analysis

The data from the push-out tests consisted of slip and separation measurements, as well as ultimate load values for each specimen. The four slip readings obtained were averaged together to produce the average slip per connector. The load per connector is half the total

load applied to the steel beam. In the case of a stud or high strength bolt, a connector consists of two studs or two bolts.

The separation between the concrete and steel was measured at two locations along the face of the slab. Deflection dials located 1 in. above the bed of the testing machine were used to check for excessive sliding of the specimen on the testing machine platen, as well as separation between the slabs.

The results from these dials indicated movement along the platen was occurring, but was of a small enough magnitude to neglect. Relative separation of the slabs at the base was found by averaging the two deflection dials. The separation at the base does not provide a true value of the uplift on the connectors but was checked to insure that separation or uplift was small; separation was found to be small and thus was not given any further consideration.

The average of the two deflection dials at connector level is referred to as the "uplift" of the slab from the beam. This uplift or separation was checked to insure that it was "less than half the interface slip at the corresponding load level" [32]. Thus, it closely approximated the uplift forces present in an actual composite beam. All but one connector, the angle-plus-bar, met this 50% limit. The rigid nature of the angle-plus-bar connector, which will be discussed in more detail later, probably caused the excessive separation. Because the uplift values obtained in the remaining series were within the 50% limit (see typical load-separation curves in Ref. 9), the effect of uplift was considered to have minimal influence on the behavior of these connectors.

4.1.1 Type A Specimens

As explained in Section 2.1.1, the Type A specimens were tested in order to obtain experimental values for angle-plus-bar connectors (used on bridges built from the 1940's to 1960's), welded studs, and channel connectors. By comparing experimental results to existing design equations [1], a design rationale could be developed for the angle-plus-bar connectors. Values obtained from push-out tests provided a lower limit to those obtained from composite beam tests and thus are conservative when used in design [28,32].

To eliminate several of the variables, concrete compressive strengths were held nearly constant; also the physical dimensions of the push-out specimens were held constant. Tables 10 and 11 present compressive concrete strengths, experimental and theoretical ultimate loads, and types of failure for Series 1 through 5. Theoretical ultimate load values for Series 2, 4, and 5 were obtained by using relationships from AASHTO [1]; those for Series 1 and 3 were obtained by using a modified form of the AASHTO channel formula [1]. Note that within the various specimen series the experimental ultimate load values are very consistent as are the failure mechanisms (except for one case). This same consistency is also true in the load-slip curves for the individual specimens of a given series (see Appendix of Ref. 9).

The connector ultimate load values obtained experimentally compared very well to the predicted values for the half-scale specimens (Series 1 and 2). Table 10 shows that the ratio of predicted to experimental ultimate load for the channel and angle-plus-bar connectors yielded results between 1.00 and 1.13. The slightly low experimental values

Table 10. Push-out tests: Summary of test results and predicted ultimate loads for Type A specimens.

Specimen Designation	Compressive Strength, f'_c (psi)	Observed Connector Ultimate Load, (kips)	Predicted Ultimate Load, (kips)	Ratio of Predicted to Experimental Ultimate Load	Type* of Failure
Series 1					
HA1	4110	38.0	42.1	1.11	D
HA2	4110	41.6	42.1	1.01	D
HA3	4110	42.0	42.1	1.00	D
Series 2					
HC1	4110	40.5	44.2	1.09	C
HC2	4110	39.0	44.2	1.13	C
HC3	4110	41.4	44.2	1.07	A
Series 3					
FA1	4850	125.4	182.8	1.46	C
FA2	4850	129.1	182.8	1.42	C
FA3	5000	129.5	185.5	1.43	C
Series 4					
FC1	4670	87.7	124.7	1.42	A
FC2	4670	84.8	124.7	1.47	A
Series 5					
FS1	5000	58.1	63.9	1.10	B
FS2	4660	56.1	60.6	1.08	B
FS3	4660	60.1	60.6	1.01	B

*See Table 11.

Table 11. Description of type of failures occurring in push-out test specimens.

Letter Designation	Description
A	Tensile cracking of the slab (simultaneous with concrete crushing adjacent to connector)
B	Fracture of the shear connector above the beam flange or weld preceded by cracking of the slab
C	Fracture in weld attaching the connector to the beam flange
D	Shearing of a wedge of concrete from under the connector (concurrent with the separation of the slab from the beam flange)

can be attributed to an unequal distribution of load between the two connectors caused by slight eccentricities of the specimen in the testing machine [31].

In Fig. 37, the load-slip curves for half-scale, angle-plus-bar and channel shear connectors are presented. These load-slip curves (as well as the others which follow) are an average of the individual load-slip curves of the specimens within a given series. The angle-plus-bar connector provided more resistance to slip at all values of load. Compared to the half-scale channel, the angle-plus-bar connector provided a more rigid connection, as well as a slightly higher ultimate strength.

The full-scale, angle-plus-bar shear connector (Series 3), which was previously used on composite bridges in Iowa, was compared to both the channel connectors (Series 4) and the stud connectors (Series 5). Of the full-scale specimens tested, only Series 5 yielded results in good agreement with calculated values (ratios of predicted to experimental ultimate loads between 1.01 and 1.10). The low experimental results most likely can be attributed to slight eccentricity of the specimen in the testing machine. The results from the Series 3 and 4 specimens were in poor agreement with the calculated values (ratios between 1.42 and 1.47), although the low experimental ultimate load values, as well as failure modes, were very consistent within a given series.

The low results for the Series 4 specimens were probably caused by a large number of voids located adjacent to the loaded side of the connectors. After testing, when the slabs were fully separated from

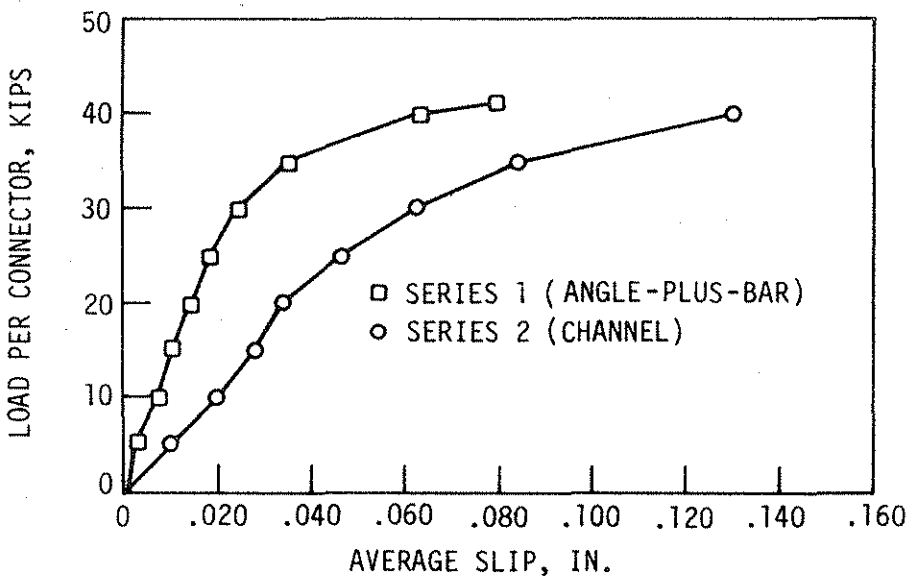

Fig. 37. Comparison of load-slip curves for half-scale connectors.

the connectors, it was discovered that voids comprised approximately 15% of the effective concrete bearing area. The percentage of voids found in the other specimens was found to be considerably less. A considerable number of voids found were located near the channel flange welded to the beam. Previous research [31] has indicated that high stresses exist near the beam flange and that the greatest portion of the load carried by a channel connector is carried by the flange welded to the beam. As is seen in Table 10, Series 4 specimens failed by tensile cracking in the concrete slabs. Since this failure was a function of the dimensions of the slabs, this might also have caused the low experimental values.

Series 3 specimens also experienced failure at loads much lower than calculated. As noted in Table 10, all Series 3 specimens failed through the weld. Inadvertently, a 3/16 in. weld (specified on plans for the laboratory model bridge) was provided rather than the 1/4 in. weld which was specified on Bridge 1 and Bridge 2 plans. The shear and bending capacity of the 3/16 in. weld was calculated and found to be slightly below the observed ultimate load. By providing a 1/4 in. weld, the capacity would have been increased approximately 33%; thus the ratio of predicted to experimental ultimate load would have been lowered considerably. In Section 4.1, it was noted that the separation of the slab from the beam, or uplift, was considered a significant problem on the Series 3 specimens. This is true because the angle-plus-bar connector, being a rigid connector, provides a greater resistance to slip, which increases the tendency of the slabs to separate from

the beam. The failure of the weld at the leading (or first loaded) edge of the angle further influenced the separation tendency.

The load vs. slip curves for the full-scale shear connectors (Series 3, 4, and 5 specimens) are presented in Fig. 38. For comparison, load-slip curves from two other research projects [25,31] are also given. As was the case in the half-scale specimens (Series 1 and 2), the rigid, angle-plus-bar shear connectors provided more resistance to slip than the flexible channel or stud connectors. There is good agreement between Series 5 and the previously tested studs [25]. A lack of agreement at the lower loads can be attributed to the fact that the previously tested specimens were not pre-loaded (Series 5 specimens were pre-loaded to 10% of the ultimate), and some bond between the concrete and steel may have been present. The channel connector (Series 4) did not correlate very well with the previously tested channel connector [31]. Though the channel in Series 4 was larger in size as well as length, it exhibited consistently lower values of load at equivalent values of slip. The presence of voids adjacent to the connector is thought to have caused the difference.

4.1.2 Type B Specimens

Type B specimens (Series 6 and 7), as stated in Section 2.1.1, were tested to determine the effectiveness of using high strength bolts as shear connectors. The two bolt configurations tested (shown in Figs. 5 and 6) produced the results shown in Table 12. Although a limited number of specimens were tested, consistent results were obtained for each connector series. This agreement is evident in the

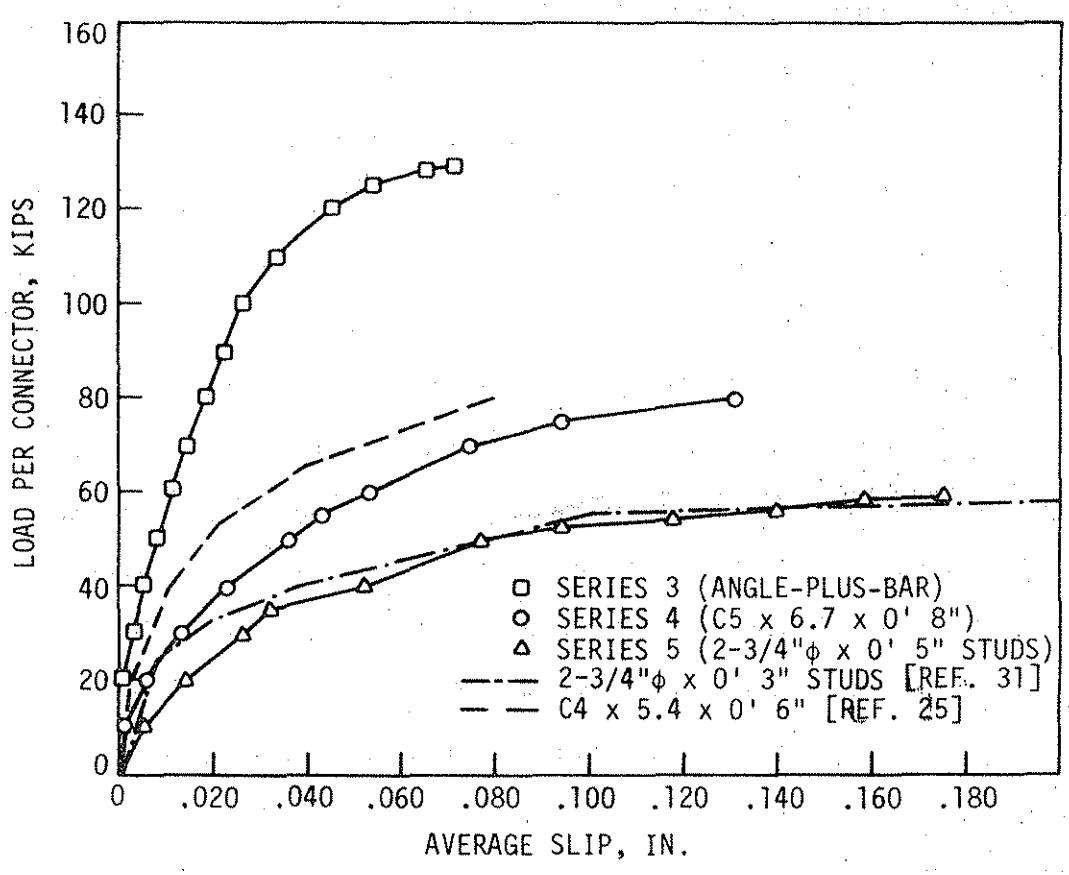

Fig. 38. Comparison of load-slip curves for full-scale connectors, Type A specimens.

Table 12. Push-out tests: Summary of test results and predicted ultimate loads for Type B specimens.

Specimen Designation	Compressive Strength, f'_c(psi) Slab	Grout	Observed Connector Ultimate Load, (kips)	Predicted* Ultimate Load, (kips)	Ratio of Predicted to Experimental Ultimate Load	Type** of Failure
Series 6						
N1	5140	4550	65.4	65.3	1.00	B
N2	5140	4550	71.2	65.3	0.917	B
N3	5140	4550	70.0	65.3	0.933	B
N4	5140	4550	66.9	65.3	0.976	B
Series 7						
E1	5180	5760	75.0	65.6	0.875	B
E2	5180	5760	76.0	65.6	0.863	B
E3	5180	5760	72.2	65.6	0.909	B
E4	5180	5760	72.2	65.6	0.909	B

*Predicted ultimate load based on AASHTO, 1977 formula for welded studs.

**Refer to Table 11, for description of failure types.

ultimate load values in Table 12 and in the specimen load-slip curves (see Appendix of Ref. 9).

In order to evaluate the effectiveness of Type B specimens, welded stud specimens (Series 5) were used for comparison. As may be observed in Figs. 4, 5, and 6, the physical dimensions of the connectors were essentially identical (height was approximately 5 in. and the diameter was 3/4 in.). As previously discussed, the main differences between the bolts and studs were the method of attachment to the beam flange and the tensile strength. The minimum tensile strength of a high strength bolt is 120 ksi, while the tensile strength of a stud is approximately 71 ksi [25], or 40% less than the bolt.

In comparing values from Tables 10 and 12, it is evident that the bolt connectors exhibited consistently higher values of ultimate load than the studs. The Series 6 specimens produced ratios of predicted to experimental ultimate load between 0.917 and 1.00, and the Series 7 ratios were between 0.863 and 0.909. Series 5 connector ratios were consistently greater than 1.01. The deviation in the ultimate strengths may be attributed to the large differences of tensile strength between the connectors, because an increase in the tensile strength is usually accompanied by an increase in shear strength. In Table 12, the ultimate load capacity of the epoxied bolt connector (Series 7) is shown to be slightly higher than the double-nut bolt connector (Series 6). This small difference is very likely due to the reduced cross-sectional area on the double-nut bolts, because the threads were located in the shear plane. Ratios of predicted to experimental ultimate load below 1.00 for the bolt connectors indicate that the AASHTO formula for the

ultimate strength of studs provides a conservative estimate of the ultimate strength of high strength bolt shear connectors.

As shown in Fig. 39, there is good correlation between the Series 5, 6, and 7 specimen load-slip curves. Some of the variation at medium values of load was probably caused by the method of attachment to the beam (bolting versus welding). Up to loads of 15 to 20 kips, the curves have approximately the same slope. From 20 to 45 kips, the effect on the load-slip behavior due to bolting is noticeable. The lower resistance to slip of the bolts is probably related to the seating of the bolt in the hole through the flange.

For loads up to 15 to 20 kips, the bolts provided a higher resistance to slip than the studs. This occurred in the Series 7 specimens, because the slab was clamped down to the beam by the bolt, and thus friction had to be overcome initially. The existence of the nut on the flange in the Series 6 specimens created a more rigid connection than a welded stud, as the nut provided a higher connector stiffness.

Variations in the load-slip characteristics between the double-nutted bolt connector (Series 6) and the epoxied bolt connector (Series 7) were minimal. Any differences can be explained by examining the methods of attachment to the beam flange. The bonding of the slab to the bolt was due to the epoxy. More importantly, the frictional forces from pre-tensioning the bolt probably helped to lower the initial slip values in the epoxied bolt connector. Beyond 30 kips the double-nutted bolt connector was more resistant to slip. The main reason was the upper nut that was tightened against the beam flange. This nut provided more bearing area for the concrete and thereby

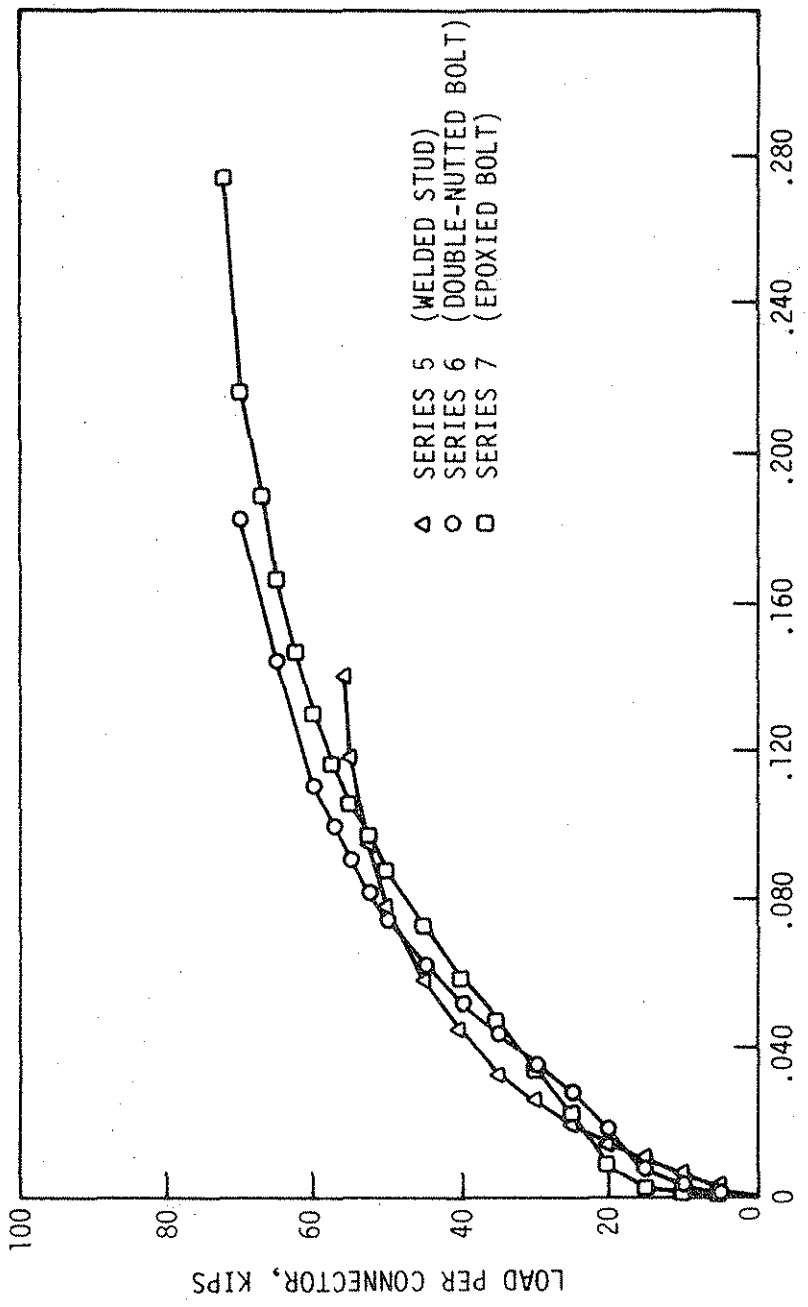

Fig. 39. Comparison of load-slip curves for Series 5, 6, and 7 specimens.

increased the connector stiffness adjacent to the beam where high stresses are known to occur [31]. The double-nutted bolt connector (Series 6) is preferred over the epoxied bolt connector (Series 7), as it is the easier of the two to install for several reasons:

- Fewer installation steps (only one coring operation and no epoxy to apply)
- Quicker (metal shavings do not delay the procedure)
- Fewer materials and equipment (only one core bit and no epoxy is necessary).

Previous studies [7,10] have shown that high strength bolts performed satisfactorily under fatigue loading. Although the bolting configuration in this project was slightly different than the previous studies, in the authors' opinion, there should be no fatigue problems with the bolting configuration proposed (Series 6).

4.2 Composite Beam Test Results and Analysis

As previously mentioned, the main thrust of these tests was to determine the effects of additional shear connectors on post-tensioned composite beams. Results and events in the elastic range tests will be presented in Sec. 4.2.1, and ultimate strength test results and occurrences will be discussed in Sec. 4.2.2.

By post-tensioning a composite beam, the post-tensioning tendons become part of the beam structure, thereby rendering the post-tensioned portion of the beam statically indeterminate to the first degree. In the analysis of the various composite beam specimens, the Δ-T effect

and P-Δ effects were neglected, as these effects were shown to be negligible for the range of loads in this study [19]. The large deflections in the ultimate strength tests normally require the addition of P-Δ effects. However, because the thrust of this testing was to determine the effects of variable amounts of shear connection, the P-Δ effects were also ignored.

4.2.1 Elastic Range Test Results and Analysis

Results presented and discussed in this section are for Tests A, B, and C, all of which involved loading which produced stresses in the steel beams below the elastic limit. Only experimental results are presented in the following paragraphs; comparisons between experimental results and theoretical results will be presented in the following section on ultimate strength. Tests A, B, and C were performed on all of the composite beams without any unusual occurrences.

Experimental midspan deflections due to vertical load only for the interior and exterior composite beams are presented in Figs. 40 and 41 respectively. As seen, there is very little difference in the resulting deflection behavior either due to the post-tensioning force (Test A, B, and C) or the additional shear connectors (Beam 1 vs. Beam 4 and Beam 2 vs. Beam 3). Deflections obtained from Test A (no prestress force locked in the beams) were the most linear of all the tests throughout the entire elastic range. This is expected because, without the post-tensioning force applied, the problem is linear. After the post-tensioning force is locked in, the relation between vertical load and deflection is nonlinear, but Figs. 40 and 41 show this is insignificant throughout the entire elastic range.

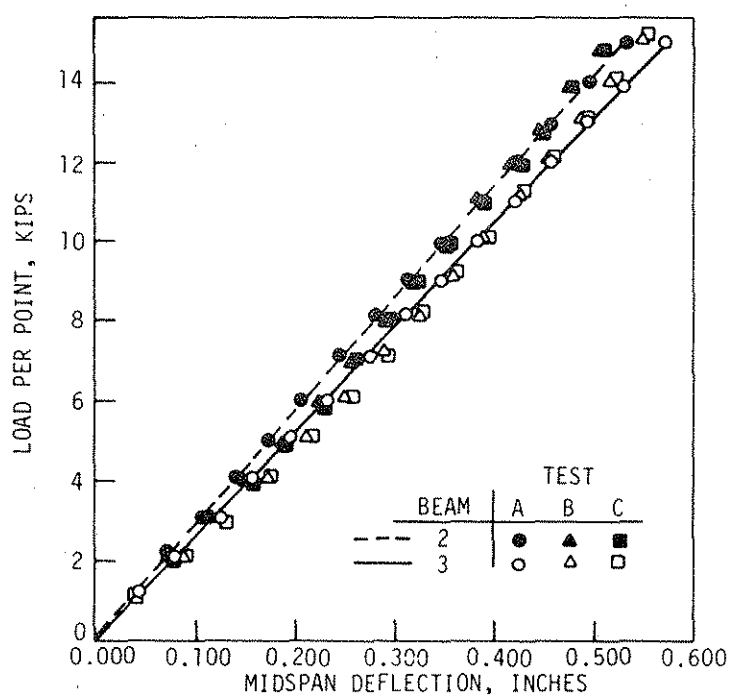

Fig. 40. Interior beam load-deflection curves for Tests A,B, and C.

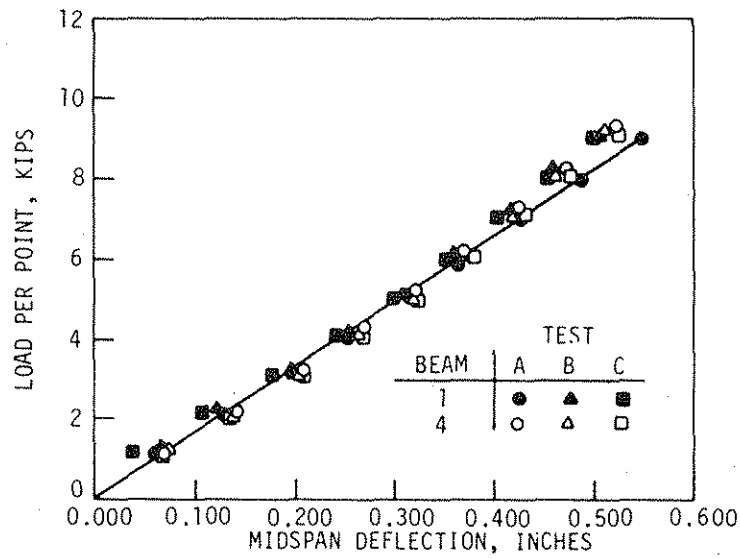

Fig. 41. Exterior beam load-deflection curves for Tests A,B, and C.

The slight differences in deflections at lower values of load are most likely due to the varying degree of bond between the steel beam and concrete slab and variation of prestress force. During Phase I testing, when the beams were part of the half-scale model bridge as well as the cutting process, the movement of the beams for testing and the initial pre-load before each test accounted for the varying degree of bond present. Different values of prestress force also caused a slight variation in deflection (Figs. 40 and 41). At higher values of prestress force, the composite beams tended to deflect more at lower values of vertical load. This was probably due to a lower moment of inertia resulting from cracks in the concrete caused by post-tensioning. At higher values of vertical load, the concrete cracks closed, thus increasing the stiffness of the post-tensioned composite beam.

Strengthening the shear connection in the composite beam slightly lowered the beam's resistance to deflection (Figs. 40 and 41). As shown, the effect was small and not considered to be significant.

4.2.2 Ultimate Strength Test Results and Analysis

The ultimate strength test, Test D, when performed on each composite beam, provided data for vertical loading from 0 kips to ultimate.

The "as fabricated" exterior composite beam (Beam 1) performed uneventfully up to 18 kips per load point in Test 1D. At a vertical load of 18 kips, deformation in the bracket and the flange under the bracket became visible. The beam continued to resist load; however, the rate of slip occurring increased more rapidly (as will be shown later). While loading increased, it was noted that the post-tensioning

tendons remained level as the beam deflected. This phenomena was noted in all the composite beams when loaded to their ultimate strength.

At 30 kips the bottom flange of the steel beam had rotated to within 1/16 in. of the abutment. At 35 kips the angle-plus-bar shear connector sixth from one end failed. The composite beam failed to accept any additional load at this point and testing was terminated. Upon closer examination, it was noted that the slab "rode up" over the shear connector. This phenomenon was similar to that found in the Series 1 push-out specimens. The maximum recorded end slip was 0.238 in., and the midspan displacement was approximately 3.57 in.

The second composite beam tested in the "as fabricated" condition, Beam 2, was loaded to a maximum of 48.3 kips per point. During Test 2D the beam was noticed to have tilted slightly at a load of 18 kips, as one centerspan deflection dial read 0.2 in. lower than the other. This value remained constant throughout the remainder of the test. The deflection dials, along with the other displacement gages, were removed at 37 kips to prevent damage if sudden failure occurred. A ruler at the midspan provided approximate displacement values and the end DCDT's measured relative slip until the test was terminated. At 48.3 kips loading was stopped because of the danger of sudden failure in the testing frame. The maximum slip recorded was 0.015 in., and the midspan displacement was approximately 3 3/8 in. After the load was removed, permanent flange deformation of approximately 2 1/2 in. at midspan was observed. Local buckling of the web under one load point (near the location where the diaphragms were formerly framed in) was evident.

Test 3D, performed on the strengthened, interior composite beam (Beam 3), went according to plan up to a loading of 23 kips. At this point, flange deformation under the brackets was noticeable, and the deflection dials were reset due to the large deflections. Deflection dials and DCDT's, except those measuring slip, were removed at 44.2 kips (midspan displacement equal to 3.34 in.). Using a string line stretched between the beam ends and a ruler, approximate measurement of midspan displacements continued. Testing was terminated at 48.8 kips because the usable stroke of the hydraulic jack was reached. At this point, cracks in the concrete were observed on the underside of the slab, as well as crushing of the concrete on the top side of the slab at the span centerline. However, the beam was still capable of resisting load. At this point the maximum midspan deflection and end slip was 5 9/16 in. and 0.009 in., respectively.

In order to fail the composite beam, it was decided to release the load, add 3 in. of steel plate at the load points, and resume loading. Occasional readings were taken with a deflection dial and string line at midspan and two DCDT's to record end slip. At a maximum load of 50.4 kips, a sudden compressive failure in the slab occurred at the span centerline. During reloading, the maximum deflection never exceeded 5 9/16 in., and the final end slip was 0.009 in. The shear connectors showed no signs of distress; however, web buckling was noted in the same location as in Beam 2.

The fourth ultimate strength test, Test 4D, proceeded uneventfully up to 22 kips, where it was noted that the lower beam flange in the vicinity of the post-tensioning load brackets had deformed similarly

to the previous composite beams. At 24 kips, near one load point, concrete was visibly peeling away from the flange on the underside of the slab. The chipping of the concrete was noticeable later (at approximately 28 kips) under the other load point but eventually ceased at both locations around 30 kips. A loud cracking sound occurred at 33 kips, and a sudden drop in load of 2 kips followed. The load was held constant until it was discovered that the block of concrete under one of the jacks had cracked. It was then decided to continue the test. Just before the ultimate load of 38.1 kips was reached, a lateral bow of approximately 1/2 in. was observed. A sudden failure occurred simultaneously in the slab and curb approximately 16 in. from the span centerline. The compressive failure of the concrete was accompanied by local buckling of the top flange directly below the distressed concrete.

A comparison of theoretical and experimental ultimate bending moment values is presented in Table 13. As may be seen, the experimental moment was within 9.5% of the predicted capacity for all four composite beams. The predicted ultimate bending moments were based on a plastic stress distribution, which was modified when a state of inadequate shear connection existed [28]. The exterior-type composite beams, Beams 1 and 4, provided experimental values that agreed very well with the predicted values. Addition of shear connectors increased the experimental ultimate moment capacity only 8.8%. Beams 3 and 4, provided with an adequate shear connection, failed by slab (and curb) crushing, while Beam 1, with inadequate shear connection, failed through the shear connection. Beams 2 and 3, interior-type beams,

Table 13. Summary of composite beam ultimate strength tests.

Beam No.	Type of Failure	Ultimate Vertical Load, (kips)	Ultimate Bending Moment, (in.-kips)				$\frac{M_u}{*}$
			M_u	M'_u	M''_u	M'''_u	
1	Shear connection	35.0	4140	3918	4529	4186*	0.989
2	Test stopped before failure (apparent yielding)	48.3	5813	5780	6529	6367*	0.913
3	Crushing of concrete slab	50.4	6102	5780	6534*	N.A.	0.934
4	Crushing of slab and curb	38.1	4503	3918	4585*	N.A.	0.982

N.A. - not applicable

* - use the theoretical bending moment as marked

M_u - experimental test moment (dead load included)

M'_u - theoretical moment, based on no post-tensioning and adequate shear connection

M''_u - theoretical moment, based on post-tensioning and adequate shear connection

M'''_u - theoretical moment, based on post-tensioning and inadequate shear connection

also provided reasonable results. Though Test 2D was terminated, the maximum experimental moment was close to the predicted value. The experimental moment obtained in Test 3D most likely was influenced by stopping the test to extend the stroke on the hydraulic jack before testing to failure. Some crushing of the concrete was noted before stopping the test, and the reduction in cross-sectional area of the slab probably reduced the ultimate moment slightly. As shown in Table 13, including the effects of post-tensioning in the theoretical analysis increased the theoretical ultimate moment capacity of the exterior and interior beams approximately 17% and 13% respectively.

Figure 42 presents the effects of different levels of shear connection on the bottom flange strains. As may be seen, there was small variation, especially at low loads, due to the amount of shear connection. This agrees with the fact that the difference in relative slip between "as fabricated" and strengthened beams was very small. Reasonable correlation between experimental and computed strains is also shown in Fig. 42. The theoretical strains were based on full interaction between the beam and slab.

Profiles of strain at the span centerline are given in Fig. 43 for the various beams at several levels of loading. Once again the observed strains agree well with calculated strains (based on full interaction), as well as between beams with different amounts of shear connection. The strains at the higher values of load did not correlate as well with the theoretical strain profiles. These differences were most noticeable at the steel-concrete interface where slip may occur, thus creating a localized effect at the gages.

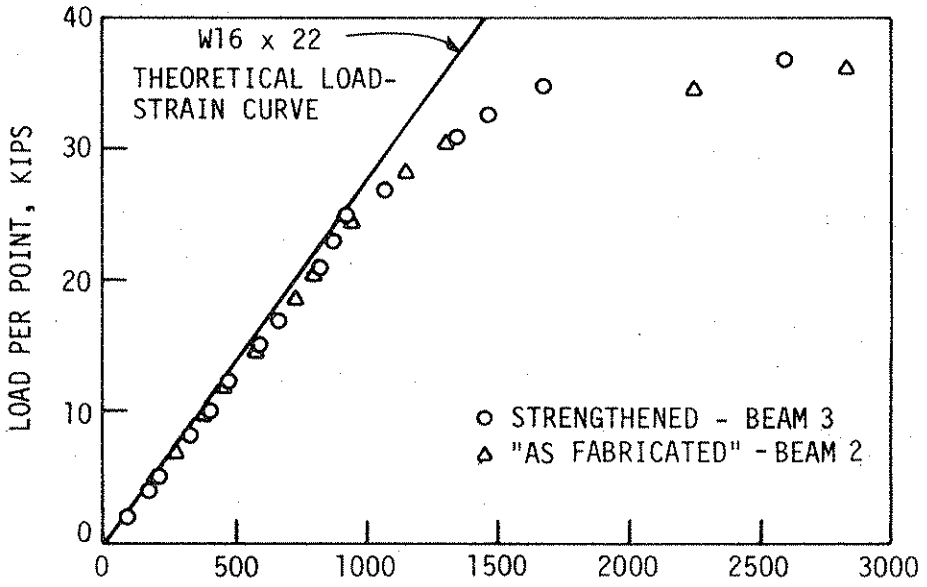

a. Comparison of interior beams and theory.

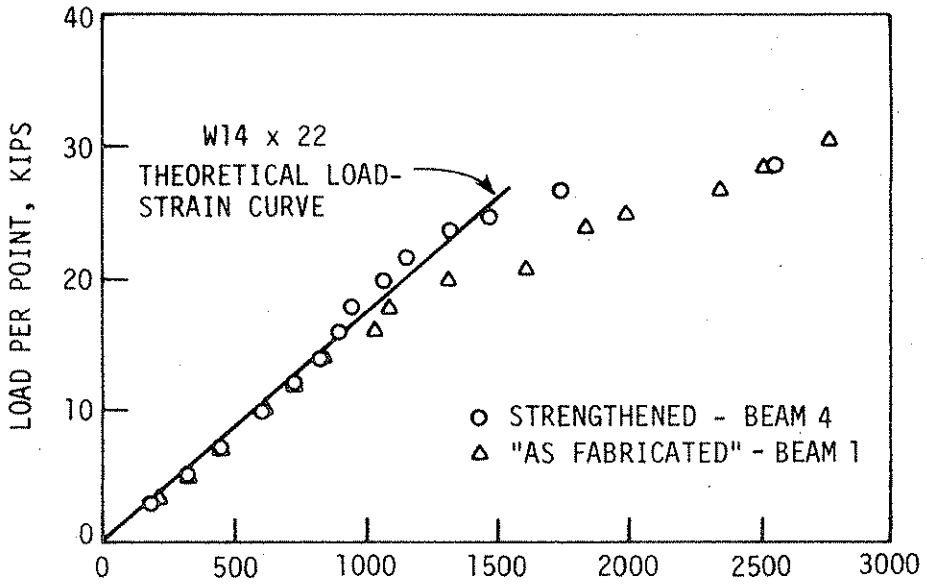

b. Comparison of exterior beams and theory.

Fig. 42. Load-midspan strain curves for composite beams.

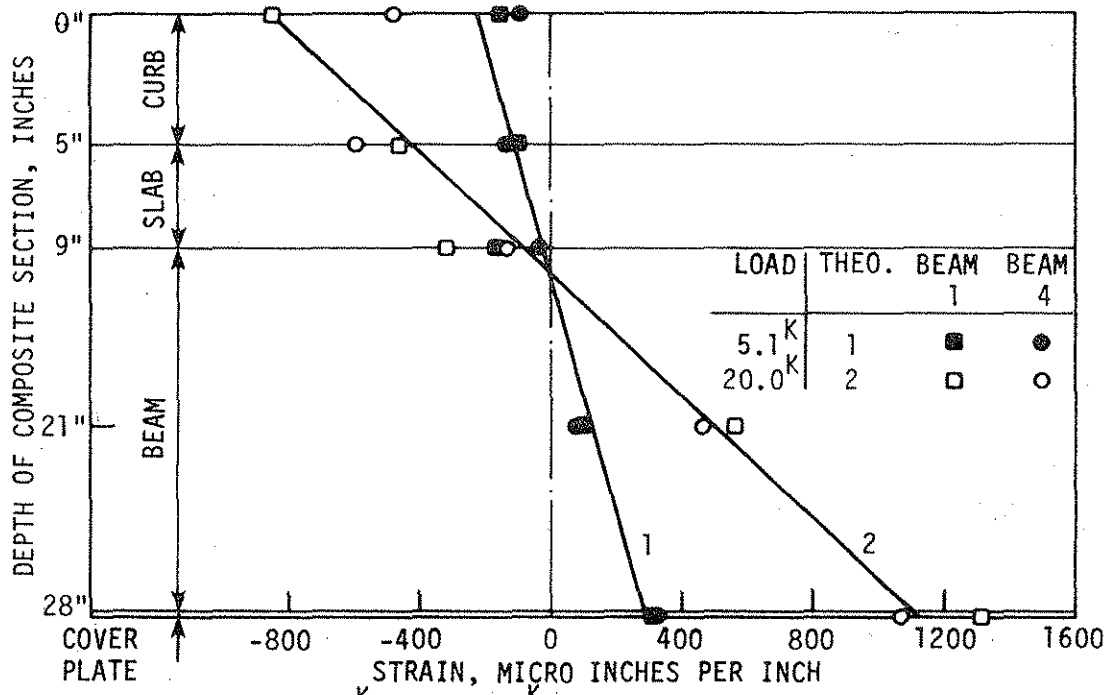

a. $P = 5.1^K$, $P = 20.0^K$ for exterior-type beams.

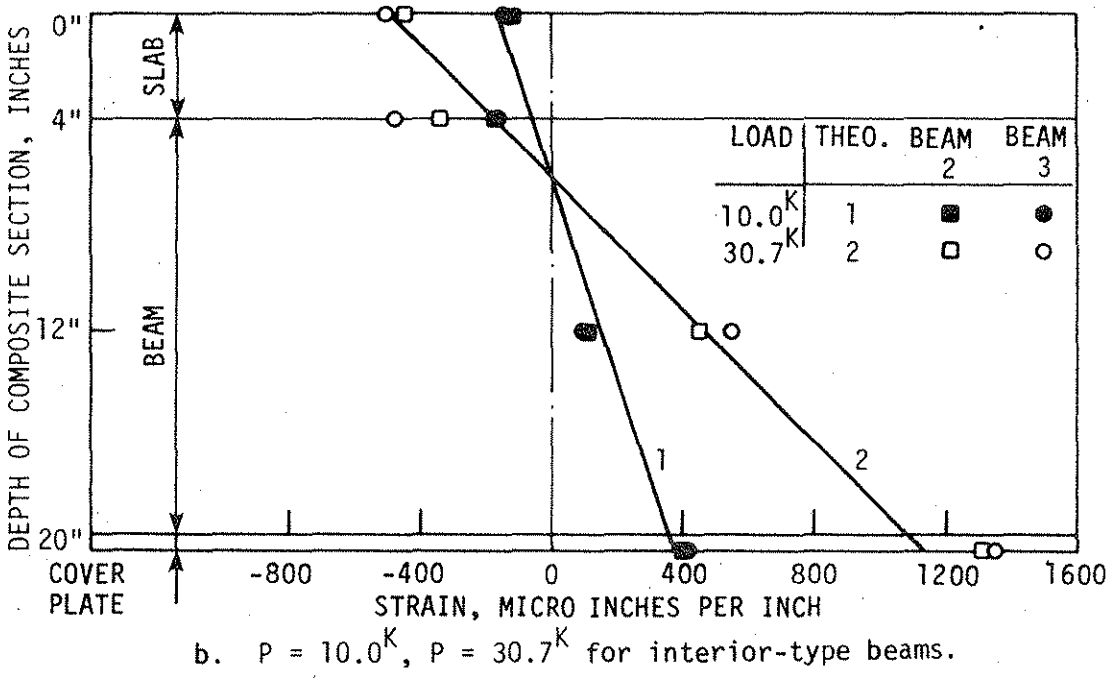

b. $P = 10.0^K$, $P = 30.7^K$ for interior-type beams.

Fig. 43. Midspan strain profiles at various values of load per point.

In all tests, the measured deflection exceeded the theoretical composite section bending deflection, as illustrated in Fig. 44. The theoretical deflections are based on 100% interaction between the concrete and steel beam and on the steel beam acting alone. As shown in Fig. 44, the experimental values are closer to the 100% interaction line. This high degree of interaction agrees with the low relative slips obtained experimentally. The theoretical curves in Fig. 44 are based on deflections due to bending effects only (no shear deformation effects, P-Δ effects, or the like) and therefore underestimate the observed deflections.

Figure 45 shows the load vs. end slip curves for each of the composite beams. As can be seen, the difference in slip between the strengthened and "as fabricated" beams at low loads is small. The rigid nature of the angle-plus-bar connectors resulted in low values of slip, which might have lowered the difference in slips, especially at small values of load. At approximately 70% of the ultimate load, the "as fabricated" beams tended to exhibit more slip as a result of having less shear connectors. Though Beam 2 was not taken to failure, it can be noted that the slip was increasing at approximately the same rate as Beam 1, which failed through the shear connectors.

Figure 46 presents the experimental force per connector vs. relative slip for each of the composite beams and the average load-slip curve for the Series 1 push-out specimens. The approximate force in the shear connector was found by expressing the vertical load in terms of horizontal shearing force. Because Beams 3 and 4 had two different types of shear connectors (angle-plus-bar and high strength double-nutted

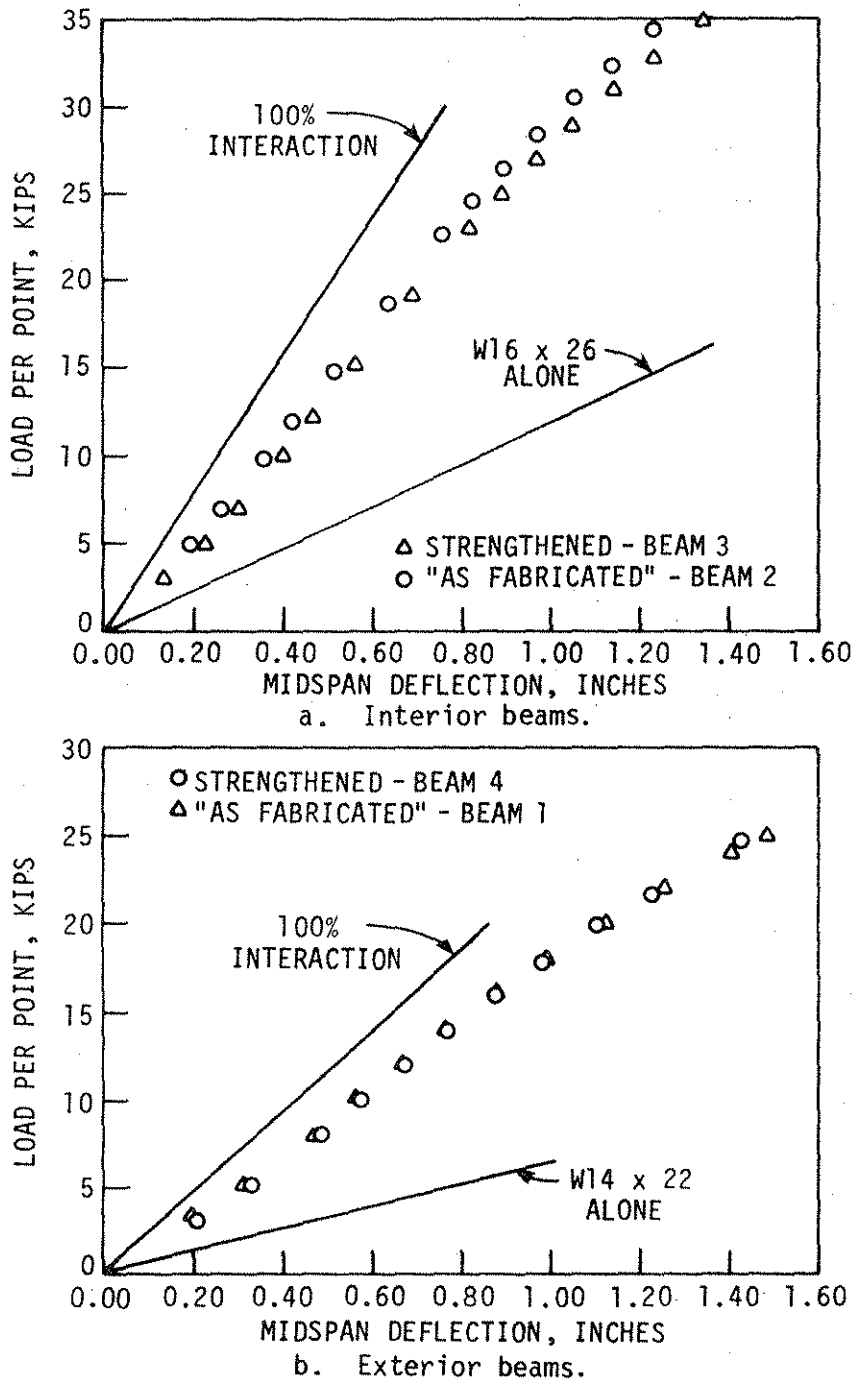

Fig. 44. Comparison of theoretical and experimental load-deflection curves.

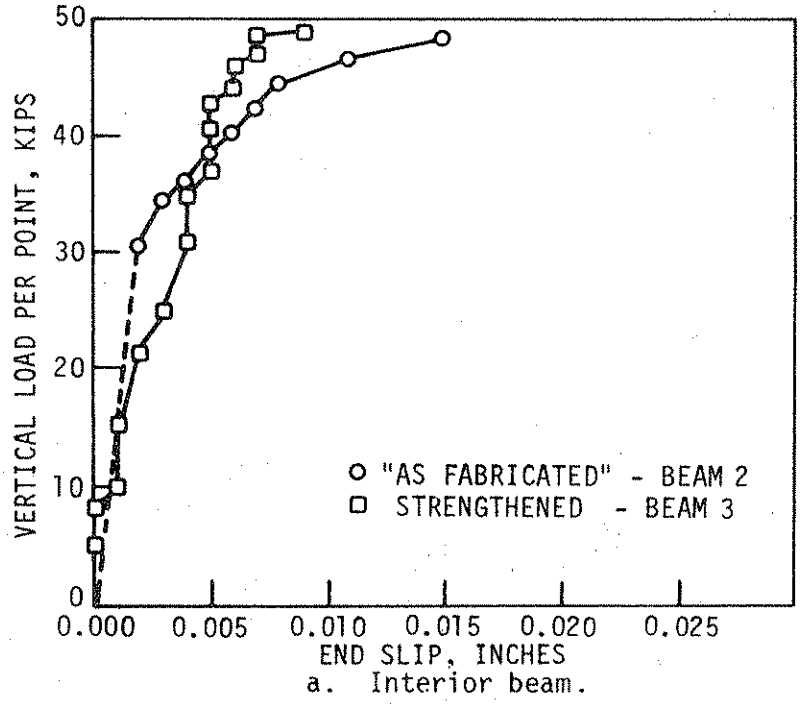

a. Interior beam.

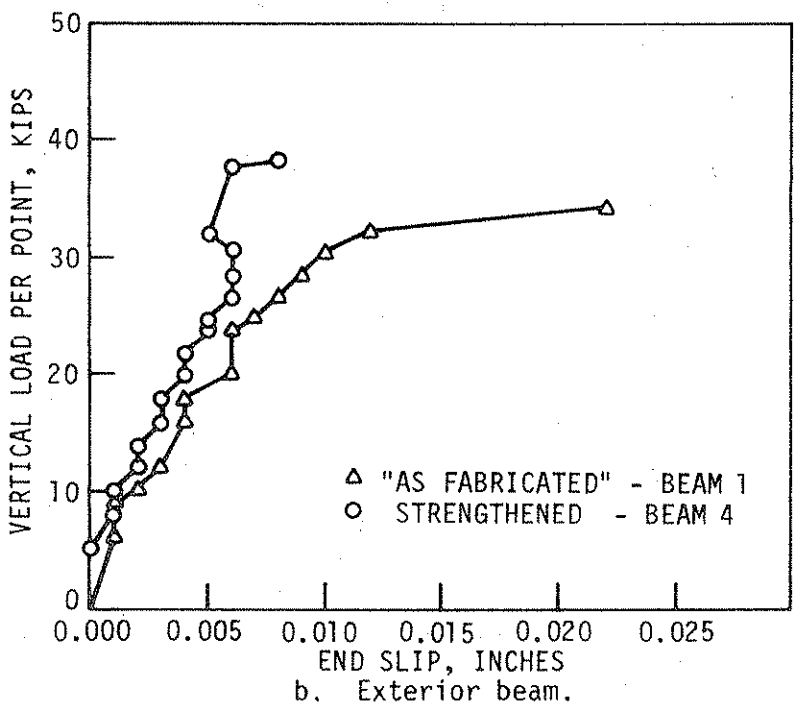

b. Exterior beam.

Fig. 45. Load-end slip curves.

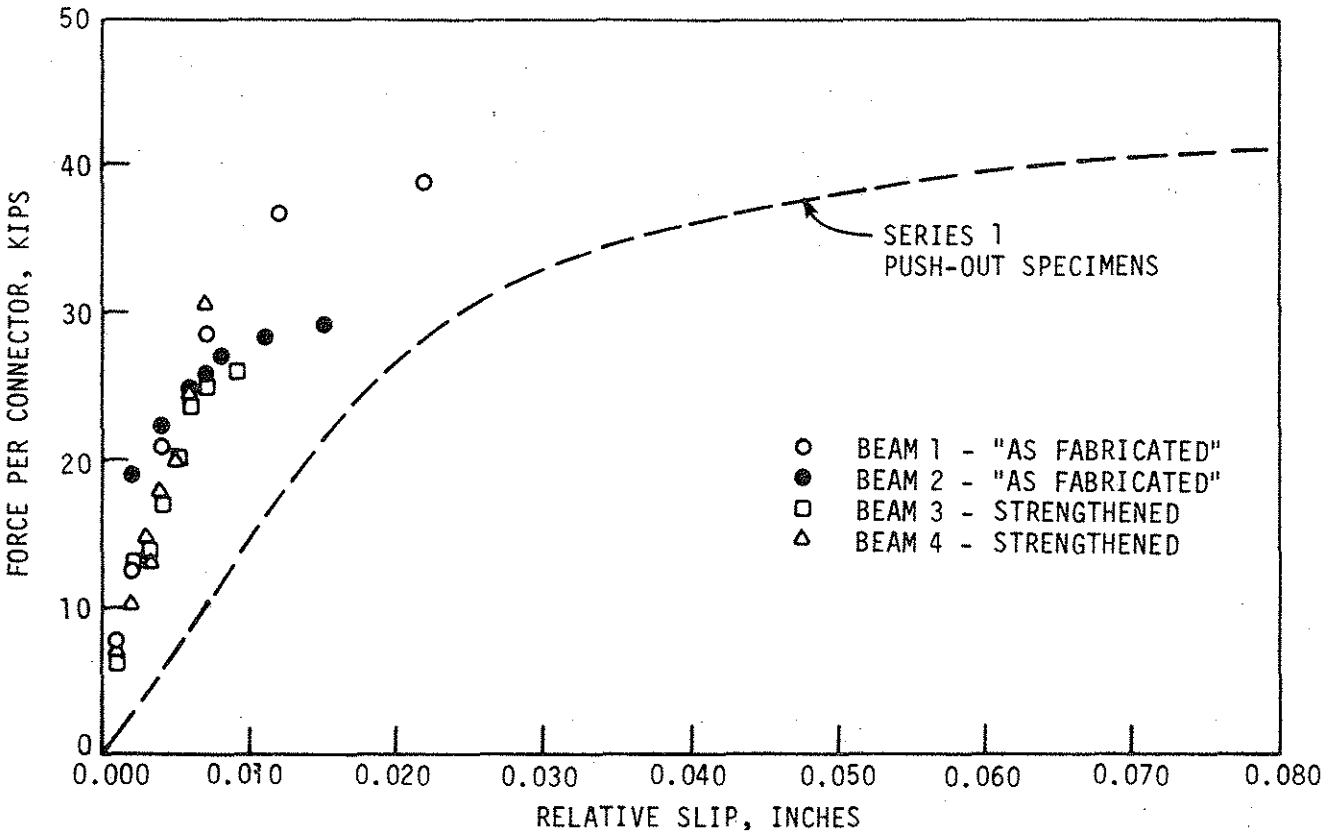

Fig. 46. Load-slip curves for each composite beam.

bolt), a value for the bolt connectors in terms of the angle-plus-bar was approximated. As shown in Fig. 46, a typical connector in each of the composite beams provided roughly the same amount of resistance to slip at equal values of force. The load vs. slip curves from the composite beams were of the same shape as the Series 1 curve, even though the values of slip were much lower. As previously noted for the same connector, results from push-out tests are more conservative than composite beam results. It may also be noted in Fig. 46 that the connector in Beam 1 had a maximum calculated force of 39.9 kips, which is similar to that found experimentally by the push-out tests (6% higher). All other beams had connector forces lower than the push-out test connectors. This agrees with the fact that only Beam 1 failed in its shear connection while the other beams (except Beam 2) failed by crushing of the concrete.

4.3 Elastic Tests of the Plexiglas Model

Figure 47 shows how the centerline bottom flange strains in each beam changed as the post-tensioning force in Beam 1 was increased. There was essentially no change in the bottom flange strain in the other exterior beam (Beam 4). However, the strains in Beams 1, 2, and 3 increased in somewhat of a linear fashion. Figure 48 illustrates the variations in the midspan bottom flange strains that occur when 50.0 lbs of post-tensioning force are locked on Beam 1, and the post-tensioning force on Beam 4 is increased in increments (PTS-2). The strains in question increase most significantly in the beam being

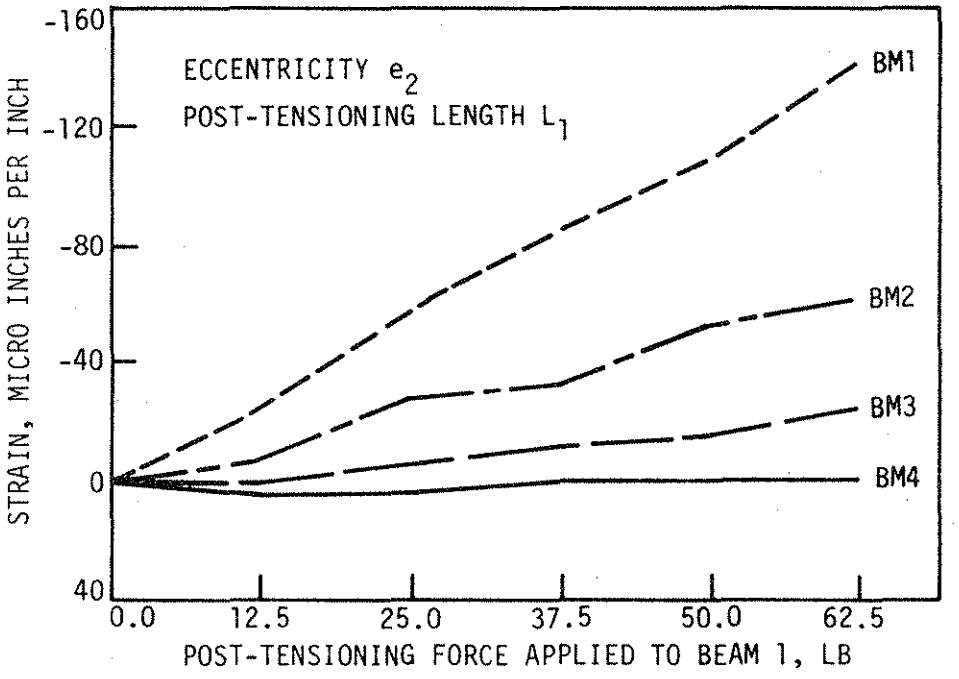

Fig. 47. Span centerline bottom flange strain vs. post-tensioning force applied to Beam 1 -- plexiglas model.

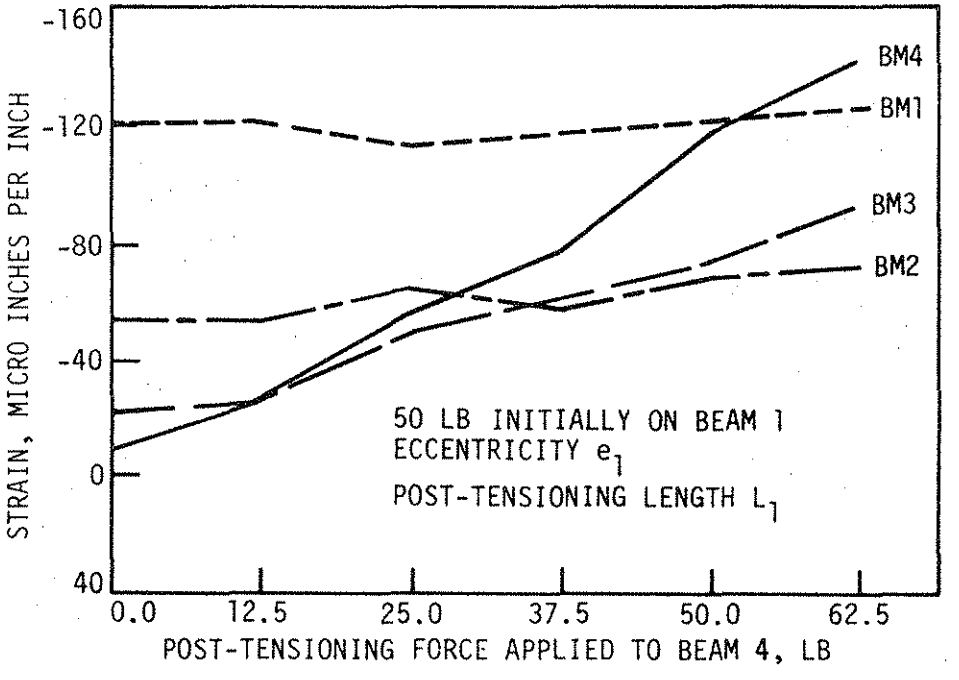

Fig. 48. Span centerline bottom flange strain vs. post-tensioning force applied to Beam 4 -- plexiglas model.

post-tensioned (Beam 4) and in the one adjacent to it (Beam 3); however, there are small increases in the other two beams also. Results similar to these were found during the testing of the model bridge of Phase I.

The moment fractions for the model beams subjected to PTS-1 are shown in Fig. 49. The strains upon which these fractions were calculated resulted from the following conditions: (1) eccentricity e_2, (2) post-tensioning length L_1, and (3) and post-tensioning force of 50 lbs (PTS-1: e_2, L_1, PF = 50 lbs). The dashed line shown is the distribution obtained using orthotropic plate theory assuming the bridge to be right angled rather than skewed. Based on theory, a slightly larger fraction of the post-tensioning remains with the exterior beams than is distributed to the interior beams. The experimental results indicate an essentially equal distribution to the four beams, even though the post-tensioning was only applied to the exterior beams (PTS-1).

Post-tensioning the model bridge (PTS-1: e_2, L_1, PF = 50 lbs) did not significantly affect the vertical load distribution. Figure 50 compares the moment fractions for the bridge before (depicted with circular dots) and after (depicted with triangular dots) post-tensioning. As can be seen, there is excellent agreement (except for one point) not only between the before and after post-tensioning values, but also with the theoretical values given. A similar excellent agreement between theoretical and experimental results is shown in Fig. 51, which illustrates the moment fraction for the simulated truck loading. In a later section (Sec. 4.3.2.1) these distribution results (which were obtained in testing the model) are compared with the results obtained from the prototype, Bridge 2.

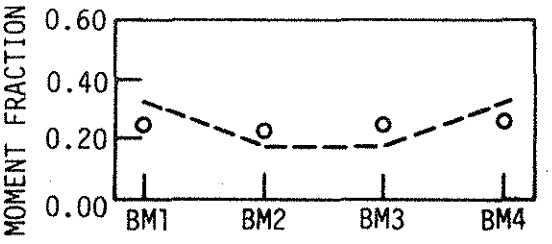

BEAMS 1 & 4 POST-TENSIONED (PTS-1: e_2, L_1, PF = 50 LBS)

Fig. 49. Moment distribution due to post-tensioning (PTS-1)--plexiglas model.

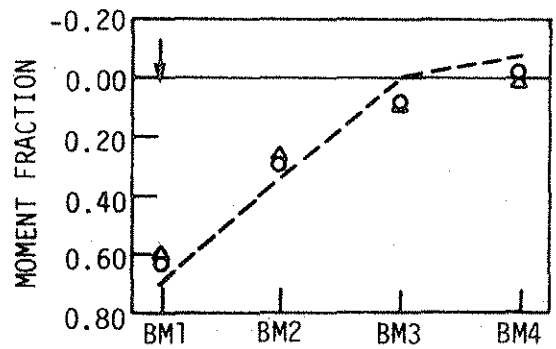

a. 14.2 lb, load at LP-1.

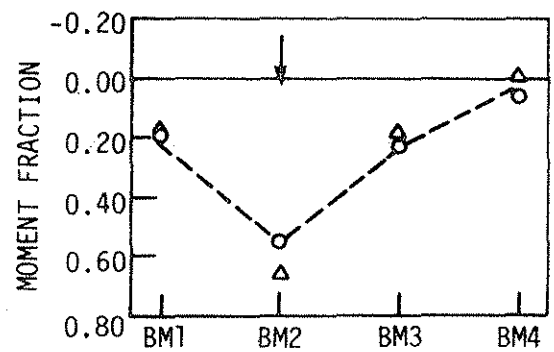

b. 14.2 lb, load at LP-2.

o BEFORE POST-TENSIONING

Δ AFTER POST-TENSIONING

Fig. 50. Moment distribution due to vertical load before and after post-tensioning (PTS-1) -- plexiglas model.

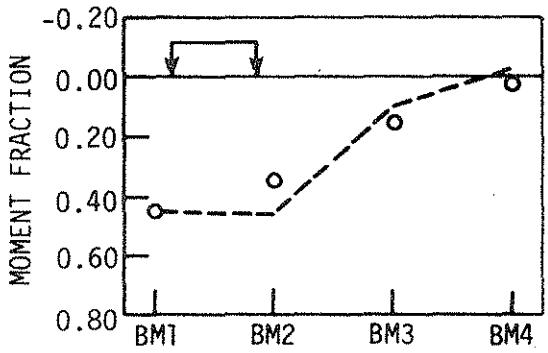

a. Truck in Lane 1.

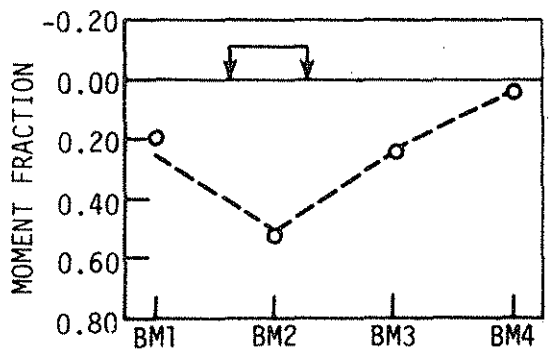

b. Truck in Lane 2.

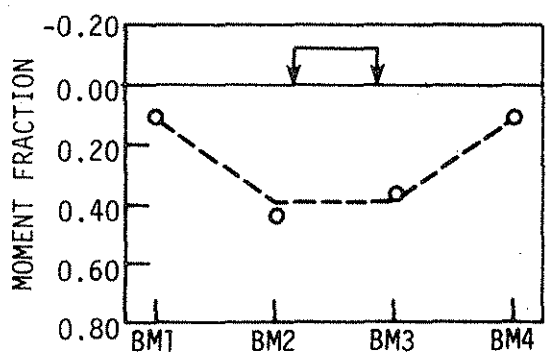

c. Truck in Lane 3.

Fig. 51. Moment distribution due to truck load after post-tensioning (PTS-1) -- plexiglas model.

Shown in Fig. 52 are the variations in centerline deflections resulting from an increase in the post-tensioning forces (PTS-1:L_1) and the eccentricity ($e_3 > e_2 > e_1$) at which the force is applied. For the post-tensioning forces applied (0 lbs to 62.5 lbs) at eccentricities e_1 and e_2, the nonlinear (P-Δ) effects were not significant, as indicated by the straight lines for these two eccentricities. However, for the third eccentricity e_3, the nonlinear effects were significant, as indicated by the curved load-deflection relationship, and thus could not be neglected in design.

Although moment fractions were not included here, they were obtained for the post-tensioning (PTS-1) at the three different eccentricities. The smallest eccentricity e_1 resulted in slightly more of the post-tensioning remaining in the exterior beams; however, for all practical purposes, there is no difference in the moment fractions at any of the three eccentricities.

Similar results (although not included in this report) were obtained for the moment fractions determined by utilizing the three different post-tensioning lengths, L_1, L_2, and L_3 (i.e., moment fraction essentially the same for all three lengths). One small difference was that slightly more of the post-tensioning force remained in the exterior beams when the shortest length L_3 was used. This can be explained in that with the shortest length L_3 there was less of the bridge subjected to post-tensioning and, thus, less length over which lateral distribution could occur.

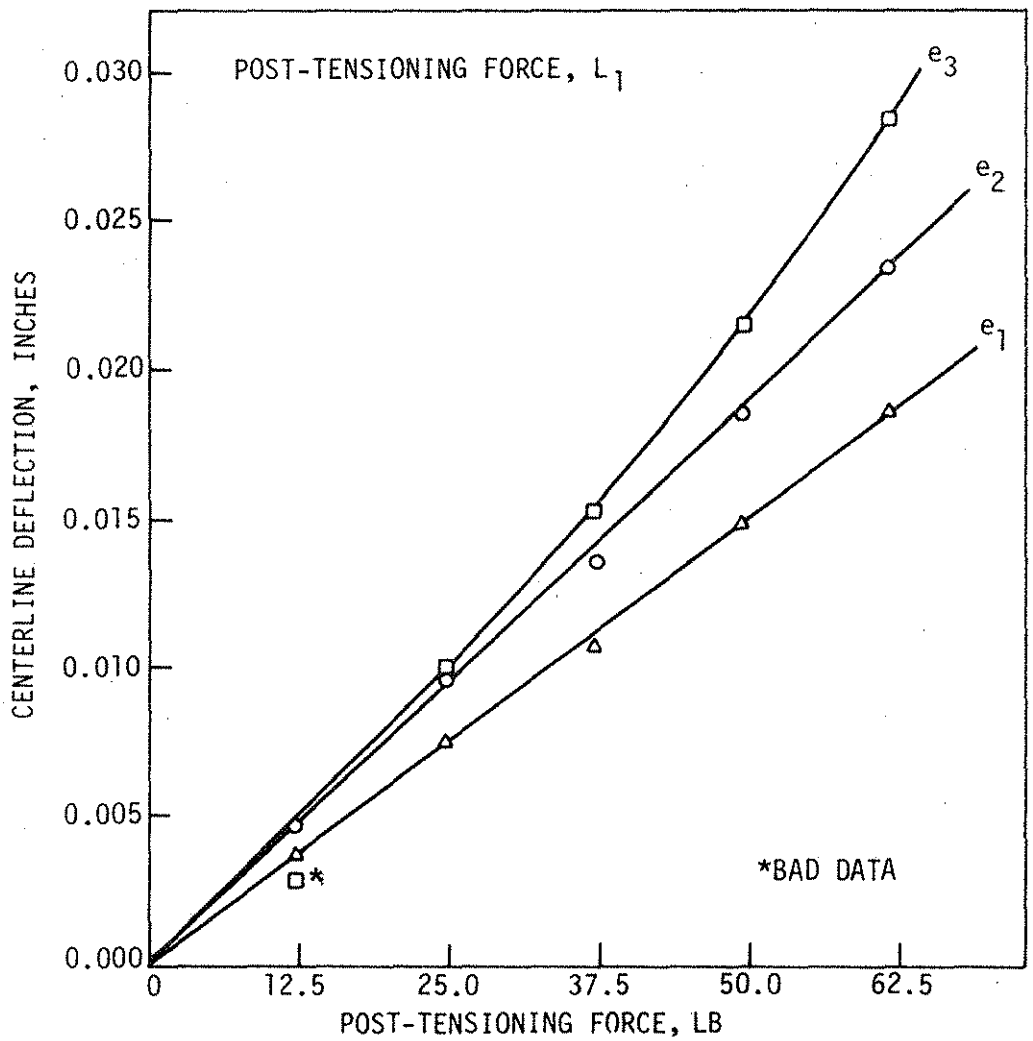

Fig. 52. Centerline deflection vs. post-tensioning force (PTS-1)--plexiglas model.

4.4 Field Bridge Tests

4.4.1 Bridge 1

4.4.1.1 Effect of Post-tensioning

As stated in Sec. 3.4, the post-tensioning force was applied to Bridge 1 in six steps. The strains occurring after each step of post-tensioning are shown in Fig. 53. Note that although the post-tensioning force was only 1% low, the resulting strain in the exterior beams was 33% low, assuming the bridge to be simply supported. Similar results were found in all other data in Table 14. Review of the data indicated that the bridge actually was not simply supported but had some end restraint. Additional information on the end restraints is given in Sec. 4.4.1.2.

Moment fractions computed from orthotropic plate theory and from field-measured beam strains are given in Fig. 54. For post-tensioning, orthotropic plate theory predicts that the moment fraction for an exterior beam will be approximately twice the moment fraction for an interior beam. Figure 54a shows, however, that the moment fractions for the exterior beams, based on measured strains, were smaller than the predicted values. Interior beams, consequently, had larger than predicted moment fractions. The laboratory model tests in Phase I gave much better correlation between theoretical and measured moment fractions. It is very likely that the discrepancy was due to restraint at the ends of exterior beams in Bridge 1 (to be discussed in Section 4.4.1.2).

Table 14. Comparison of experimental and theoretical data--Bridge 1.

	Deflection at ℄ due to Post-tensioning (in.)	Deflection at ℄ due to Truck in Lane 1 (in.)	Change in Post-tensioning Force due to Truck in Lane 1 (kips)
Based on Simple Span	0.340	0.335	7.47
Measured	0.199	0.187	5.23
Based on Fixed Ends	0.060	0.085	1.29

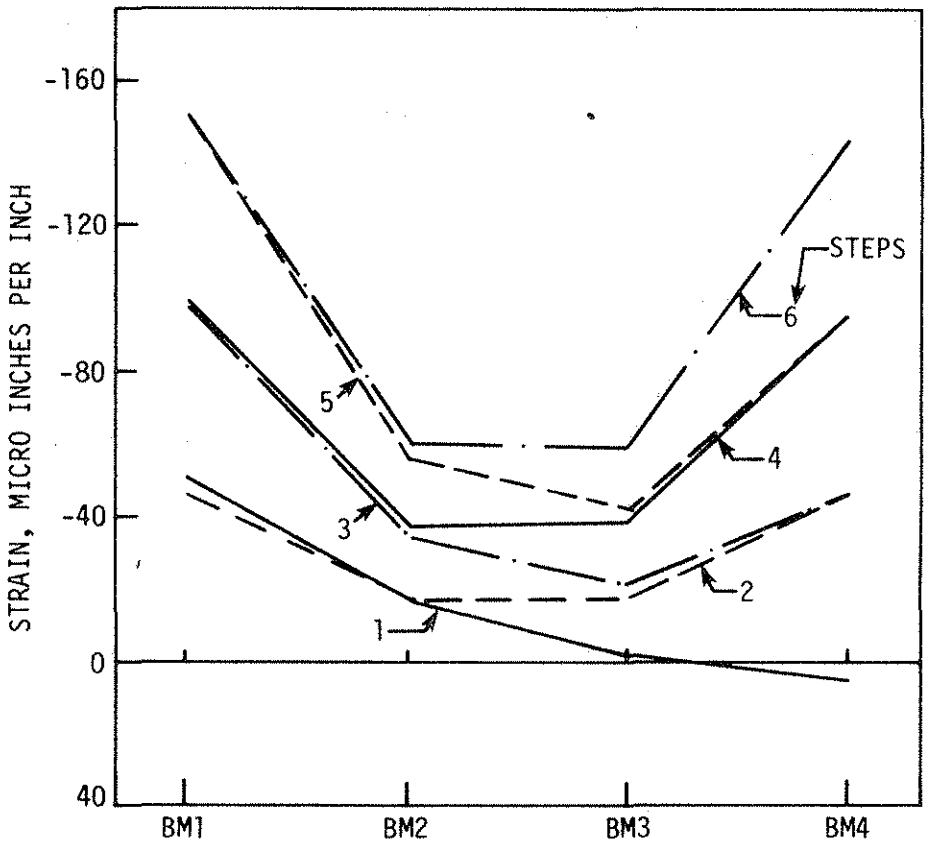

Fig. 53. Variation in midspan bottom flange strains as post-tensioning is applied to Beams 1 & 4. --Bridge 1.

For a truck in each of the three lanes (Fig. 54b, c, and d), theoretical and measured moment fractions are in excellent agreement. The figure shows no significant difference in truck load distribution after post-tensioning, as also was indicated by the model testing in Phase I.

Although theoretical and measured moment fractions are in fair to excellent agreement, the computed strains for simply supported bridge beams do not agree as well with field-measured strains. Figure 55 indicates that strains measured as a result of post-tensioning were only about two-thirds of the strains computed. Strains measured with a truck near the midspan of Bridge 1, in Lanes 1, 2 or 3 (Fig. 56a, b, or c), also are approximately two-thirds of the computed, simple span strains. The two-thirds ratio holds for exterior beams when the post-tensioning and truck strains are added; that ratio also holds for the change in post-tensioning force in the tendons (Table 14). Measured strains, in general, were less than strains computed for simple span bridge beams.

4.4.1.2 Effect of End Restraint

In order to check the discrepancy between measured and computed strains noted above, theoretical strains for both simple span and fixed beam ends were plotted in Figs. 55 and 56. Also, theoretical deflections for both simple span and fixed beam ends were plotted in Figs. 57 through 59. An examination of the figures showed that the measured strains and deflections were almost always bracketed by the simple span and fixed end conditions. Furthermore, there was excellent correlation between strain and deflection measurements as described

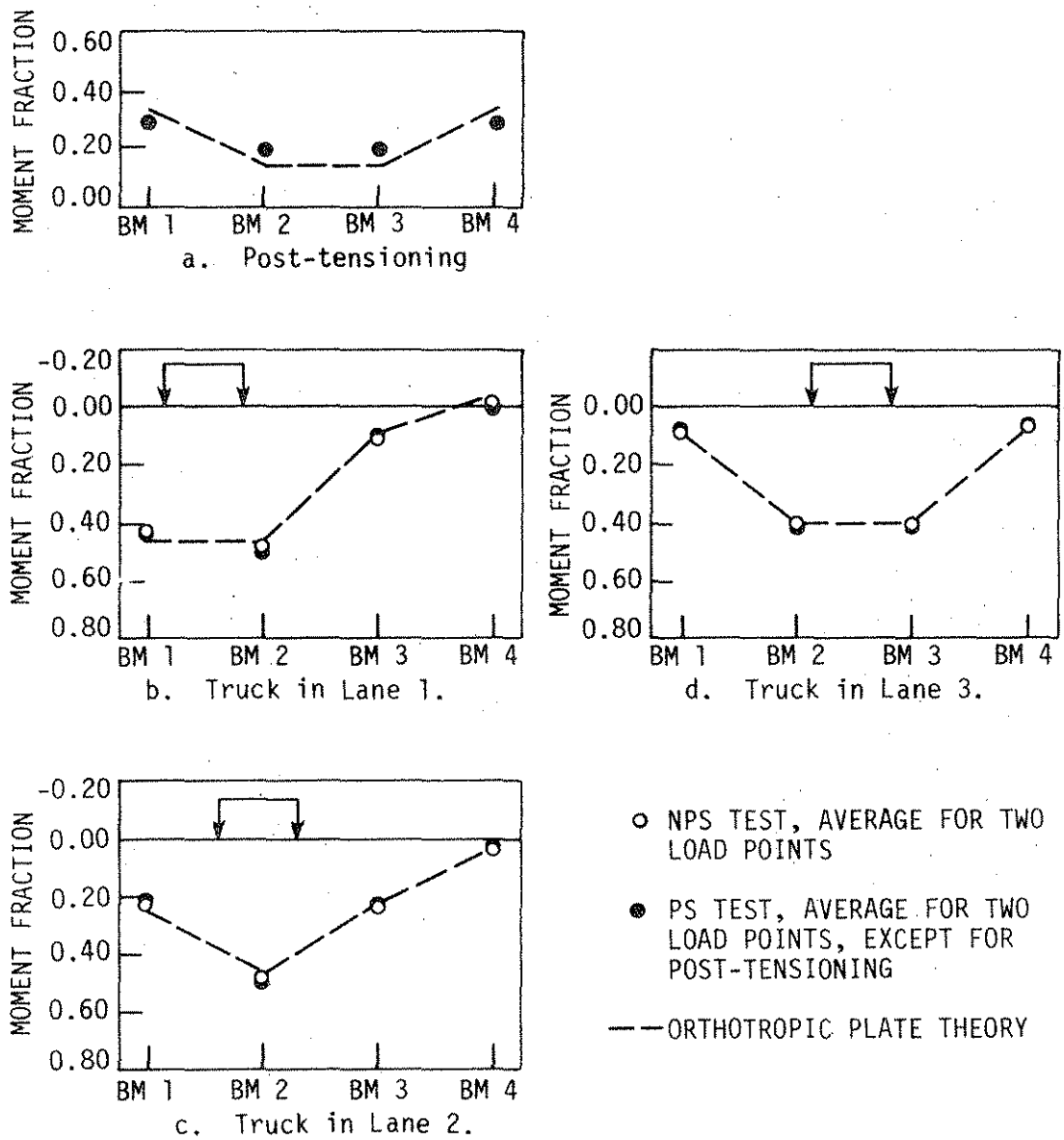

Fig. 54. Moment fractions based on midspan, bottom flange beam strains -- Bridge 1.

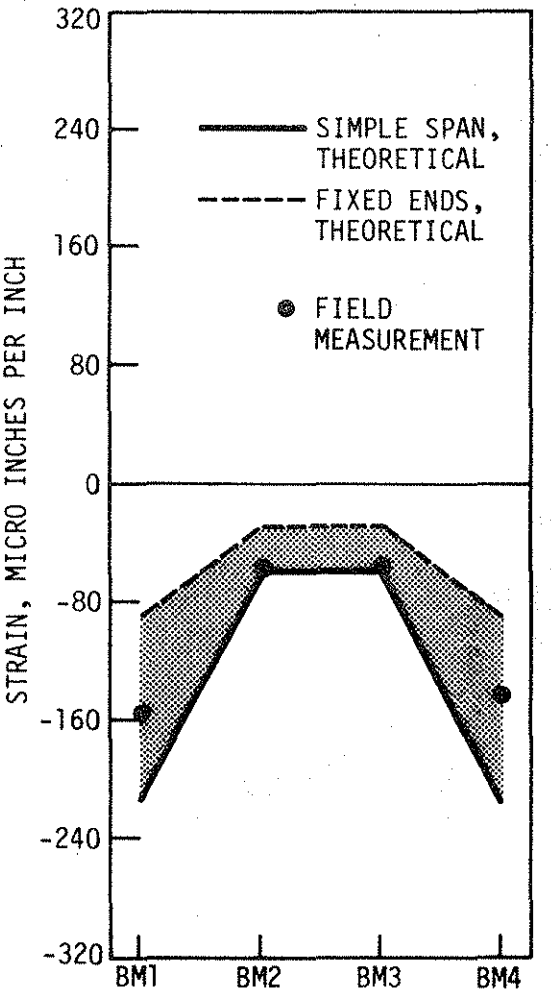

Fig. 55. Post-tensioning, midspan, bottom flange beam strains -- Bridge 1.

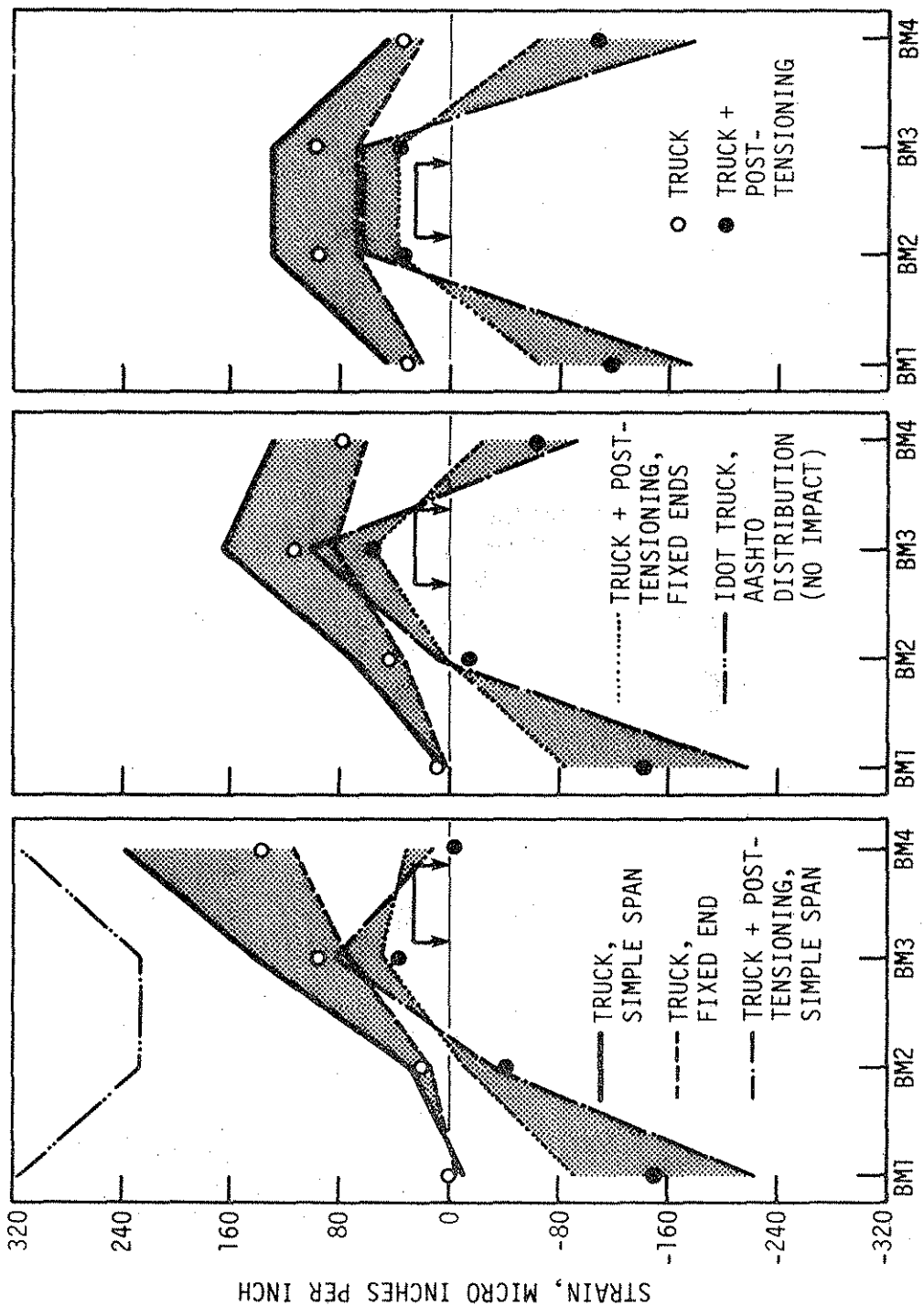

a. Truck in Lane 1. b. Truck in Lane 2. c. Truck in Lane 3.

Fig. 56. Reduction of bottom flange midspan strain as a result of post-tensioning Bridge 1.

below. Post-tensioning strain measurements fell approximately midway between simple span and fixed end extremes for exterior beams, but measured strains approached the simple span condition for interior beams (Fig. 55). The same positions with respect to the extremes can be observed for measured deflections in Fig. 57. The measured strains for a truck in Lane 1 (Figure 56a) are between extremes, but closer to the fixed end condition for all beams. Measured deflections illustrated in Fig. 58 also fall between the extremes, but toward the fixed end condition. The combined post-tensioning and truck strains for the more heavily strained exterior beams lie about halfway between simple span and fixed end conditions (Fig. 56a). Measured deflections for the same beam (Fig. 59) also lie about halfway between extreme conditions.

Both strain and deflection measurements seemed to indicate the presence of some end restraint at Bridge 1 beam ends. The check of deck strength in the next section notes that the actual, higher than assumed, deck strength did not affect strain and deflection measurements significantly. The bridge plans show reinforcing bars to be extended from the bridge deck into the abutment and from the curbs into the abutments, thereby assuring some end restraint for exterior beams.

Compression restraint at the tops of the exterior beams could explain why, for post-tensioning, the exterior beams appeared to have end restraint, whereas the interior beams appeared to have no significant end restraint. The negative, post-tensioning moment caused the bridge deck to elongate. The elongation was effectively restrained by abutments

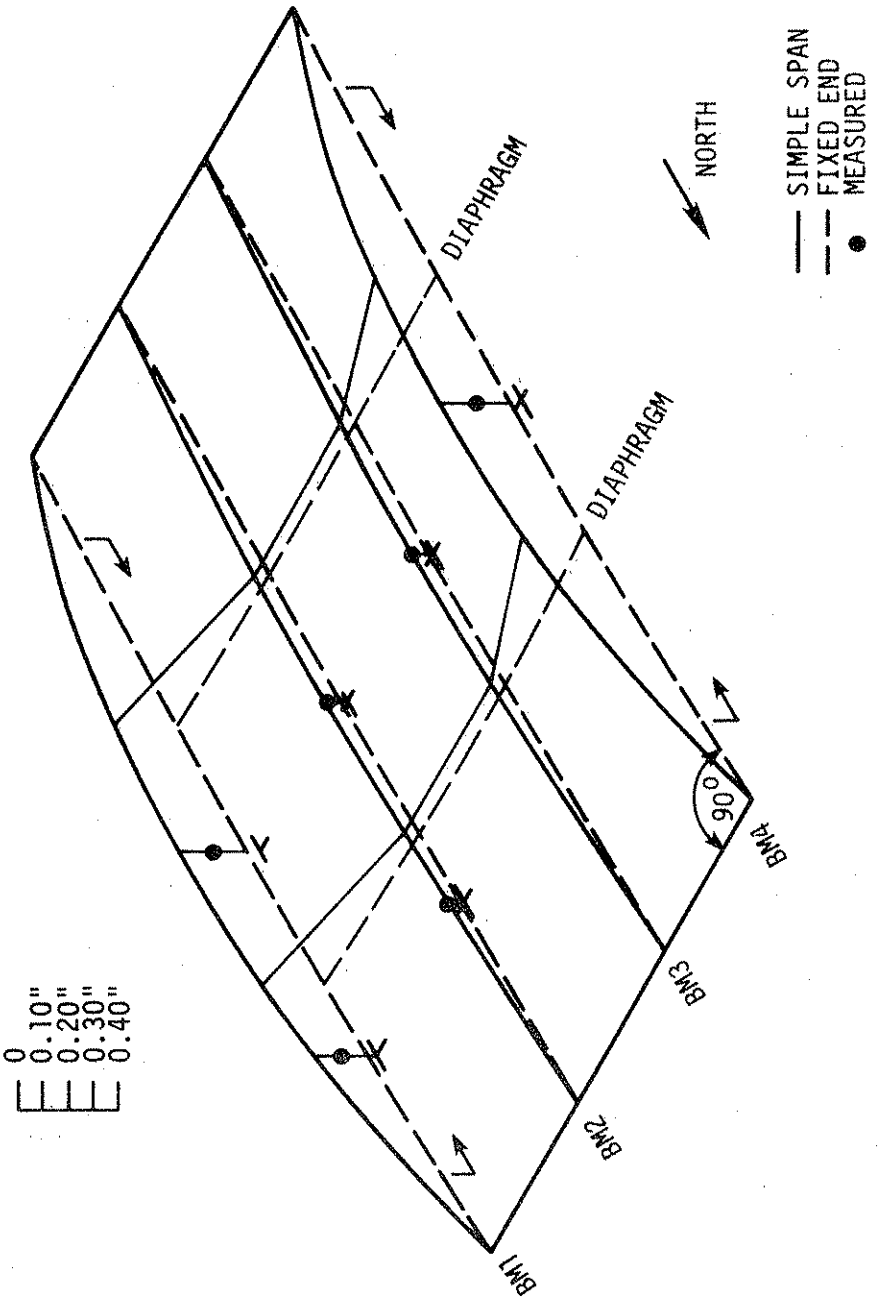

Fig. 57. Deflected shape for Bridge 1 with post-tensioning.

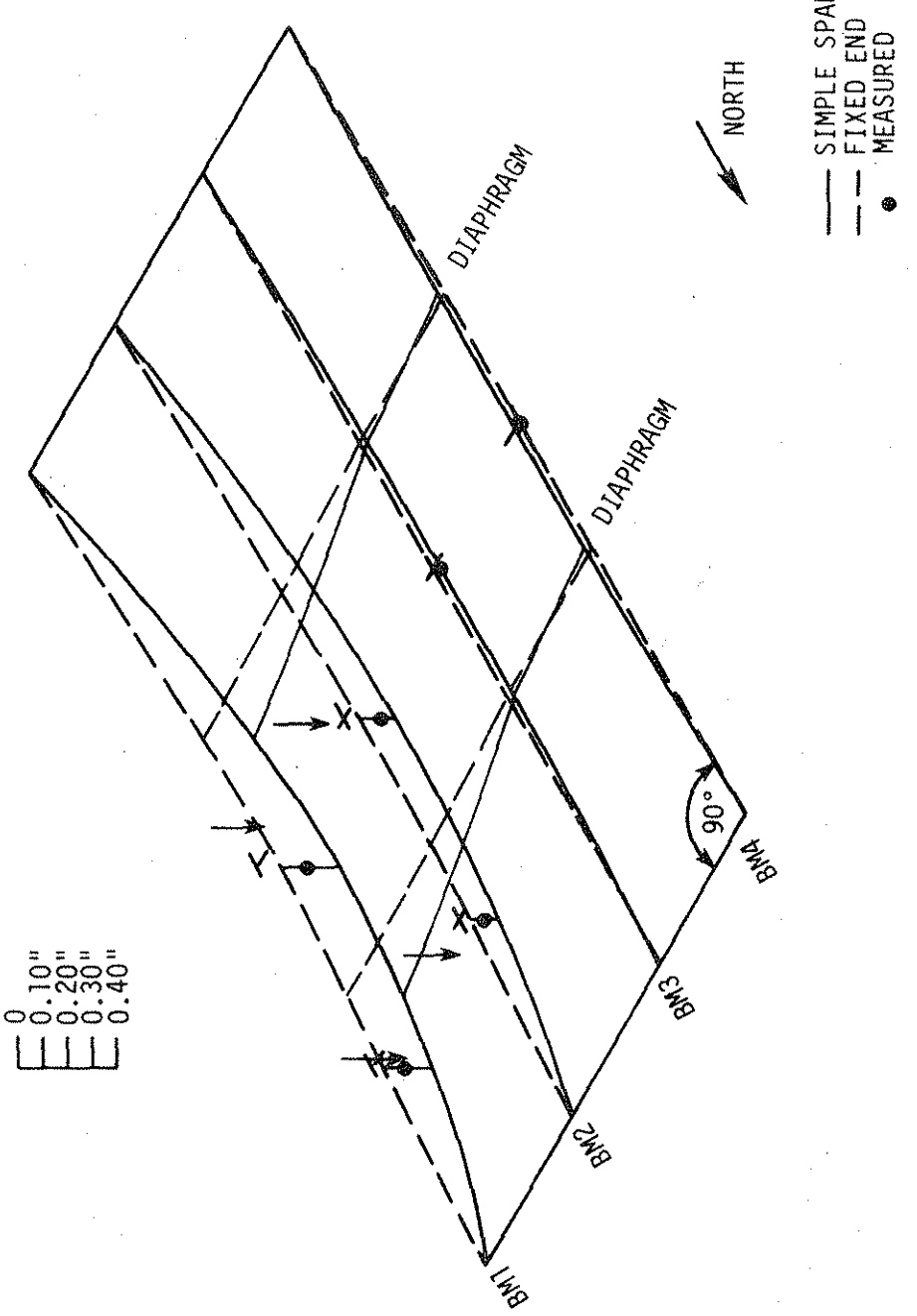

Fig. 58. Deflected shape for Bridge 1 with truck in Lane 1.

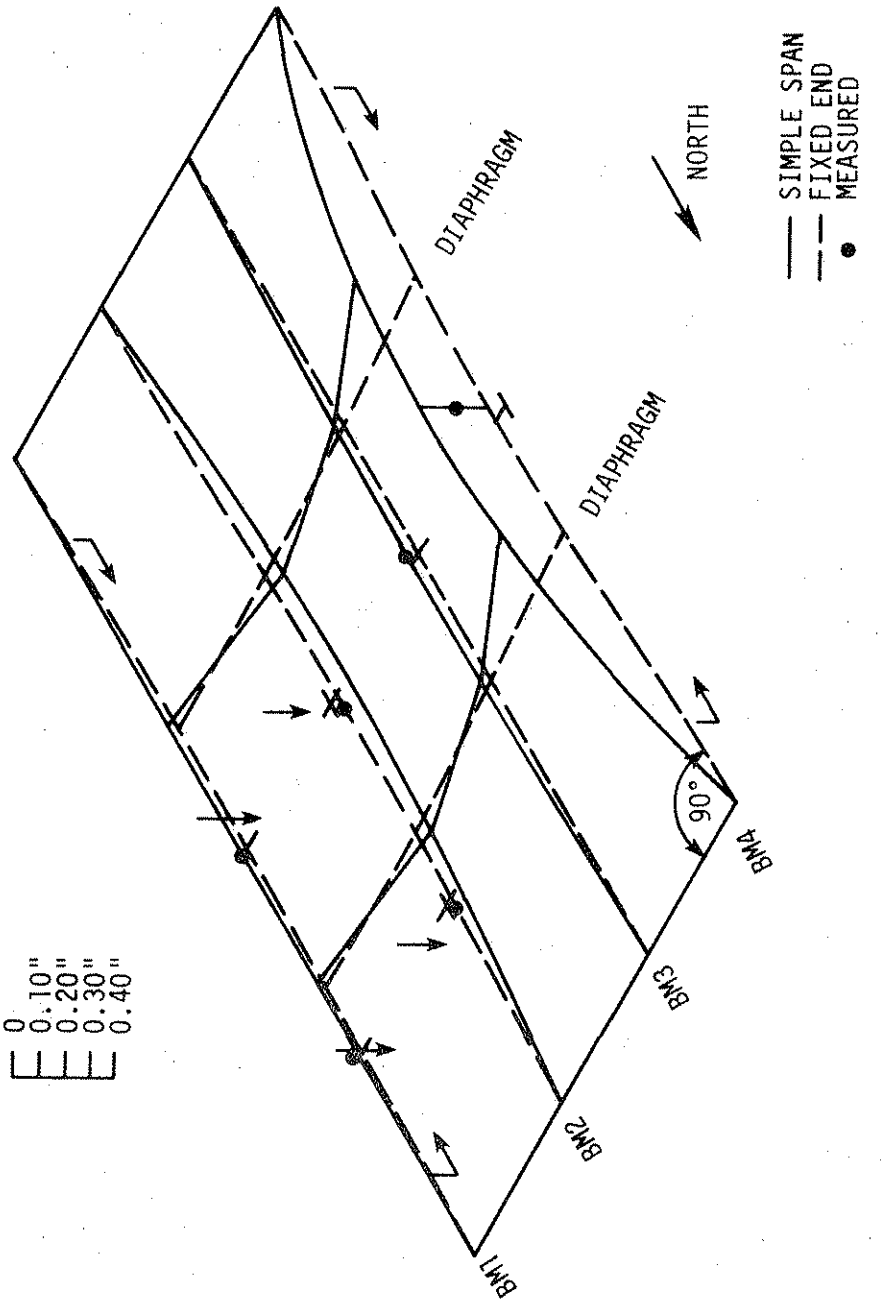

Fig. 59. Deflected shape for Bridge 1 with post-tensioning and truck in Lane 1.

at exterior beams, but the elongation was not restrained at the interior beams.

For the positive truck moments, the bottoms of the beams elongated, and the elongation could be restrained in a more uniform manner by beam bearings and the end diaphragm detail. This would explain why beam strains for truck loads in Fig. 56 indicated some restraint for both exterior and interior beams.

Both strain and deflection field measurements indicated some end restraint, which seemed to be greater for exterior beams than for interior beams. Although the restraint reduced the effects of post-tensioning, it also reduced the effects of the truck. Differences in end restraint from exterior to interior beams affected the load distribution behavior of Bridge 1.

4.4.1.3 Effect of High Strength Deck Concrete

For purposes of design and computations within this report, deck concrete strength was taken as 3000 psi. (Iowa DOT experience has indicated that strength seldom is less than 3000 psi.) Testing of deck cores from Bridges 1 and 2 gave strengths in excess of 6000 psi. Due to the large difference between assumed and actual strengths, the effect of the difference was examined for Bridge 1.

All comparisons given below were made for f'_c = 6000 psi and n = 6 with respect to f'_c = 3000 psi and n = 10. For overall stresses (including dead, long term dead, live, and impact loads), midspan beam cover plate tension stresses were reduced a maximum of 3%. Orthotropic plate theory moment fractions were affected by a small, relatively constant amount. For the largest fractions, the change was only a few

percent. The required post-tensioning force was reduced by 6%. Theoretical stresses comparable to field-measured stresses were reduced by 6% or less, and deflections were reduced by 13% or less.

Angle-plus-bar shear connector capacity, based on the AASHTO channel formula, was increased substantially; however, weld capacity computed from welds on bridge plans permitted only a 29% increase in capacity.

The stronger than assumed concrete deck did not affect the basic bridge rating or post-tensioning computations noticeably. The deck strength did, however, affect shear connector capacity significantly. Testing of the concrete deck strength could very well be worthwhile as a means of reducing the number of shear connectors required to be added to the bridge as part of a strengthening program.

4.4.2 Bridge 2

4.4.2.1 Effect of Post-tensioning

The post-tensioning force was applied to Bridge 2 in 12 steps (see Sec. 3.4). Figure 60 illustrates the change in bottom flange strain after each step. Although the post-tensioning force applied to the exterior beam was only 0.1% low, assuming the bridge to be simply supported, the resulting strains in the exterior beams were 52% low. As was the case on Bridge 1, Bridge 2 also had considerable end restraint present. This may be seen by reviewing the data in Table 15. Section 4.4.2.2 presents additional information on the end restraint. Although the deck on Bridge 2 had a considerable amount of spalling, no additional cracks were observed as a result of the post-tensioning.

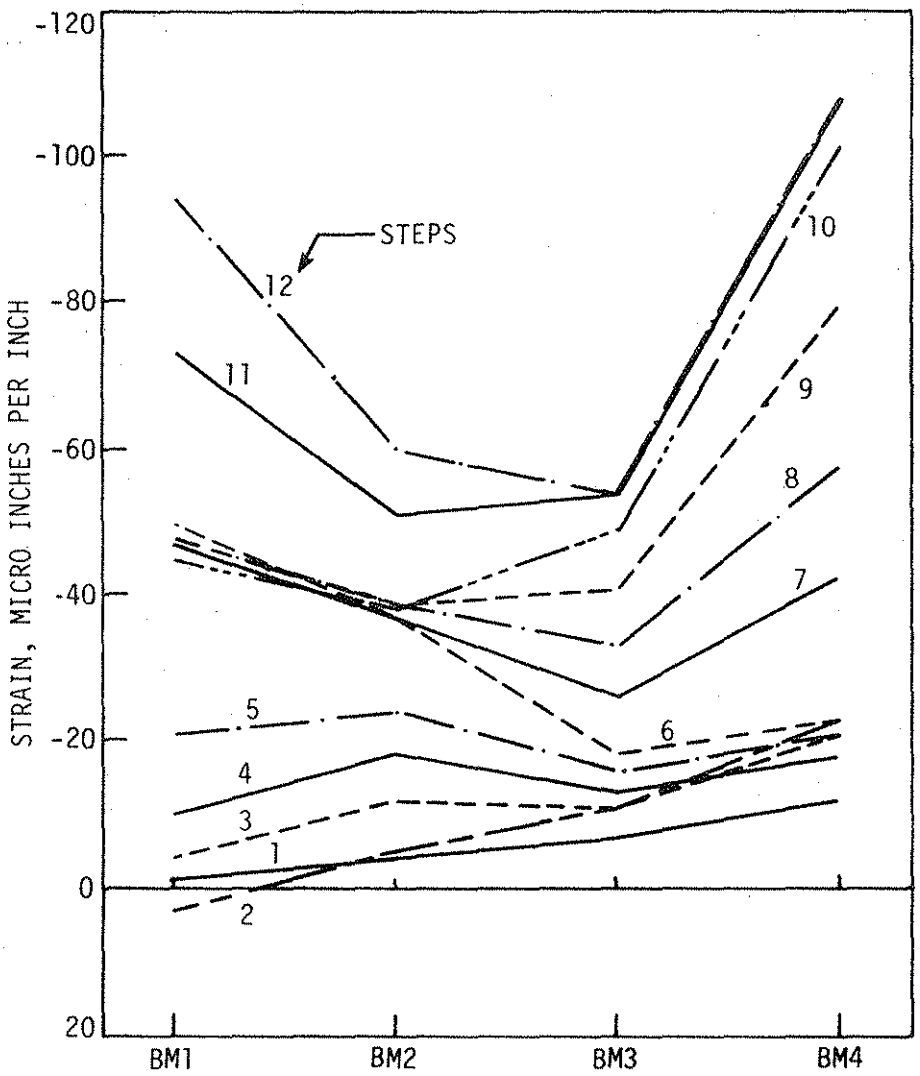

Fig. 60. Variation in midspan bottom flange strains as post-tensioning is applied to Beams 1 & 4 -- Bridge 2.

Table 15. Comparison of experimental and theoretical data--Bridge 2.

Values	Deflection at ℄ due to Post-tensioning (in.)	Deflection at ℄ due to Truck in Lane 1 (in.)	Change in Post-tensioning Force due to Truck in Lane 1 (kips)
Based on Simple Span	0.547	0.472	8.25
Measured	0.318	0.233	*
Based on Fixed Ends	0.061	0.136	0.91

*Bad data, due to strain indicator

Figure 61 gives the moment fractions computed by orthotropic plate theory and moment fractions computed from strains measured on beam bottom flanges for post-tensioning and for trucks in each of the three lanes. For post-tensioning only, Fig. 61a shows that orthotropic plate theory predicted higher moment fractions for exterior beams than were measured and predicted lower moment fractions for interior beams than were measured. The predicted vs. measured behavior was similar to that for Bridge 1 (Fig. 54a), but for Bridge 2 the predicted vs. measured deviations were greater. The results for Bridge 2, however, were in good agreement with the results for the plexiglas model (Fig. 49). Because the plexiglas model did have simple span end conditions, the deviation between predicted and measured moment fractions should be attributed primarily to the effect of skew on Bridge 2.

Figure 61b, c, and d showed generally good to excellent agreement between theoretical and measured moment fractions for the truck. The results here also compared well with the results given in Fig. 51a, b, and c for the plexiglas model. The moment fractions computed from beam strains in Bridge 2 deviated most from moment fractions computed on the basis of orthotropic plate theory when the truck was located in Lane 1. The greater deviation could be expected, since in Lane 1 the truck is farthest from the center of the bridge and closest to the one skewed end.

Figure 62a shows that strains measured in the exterior beams of Bridge 2 for post-tensioning were only about one-half those predicted from theory for a simple span, right-angle bridge. For the truck in Lanes 1, 2, and 3, Fig. 62a, b and c shows that measured strains are

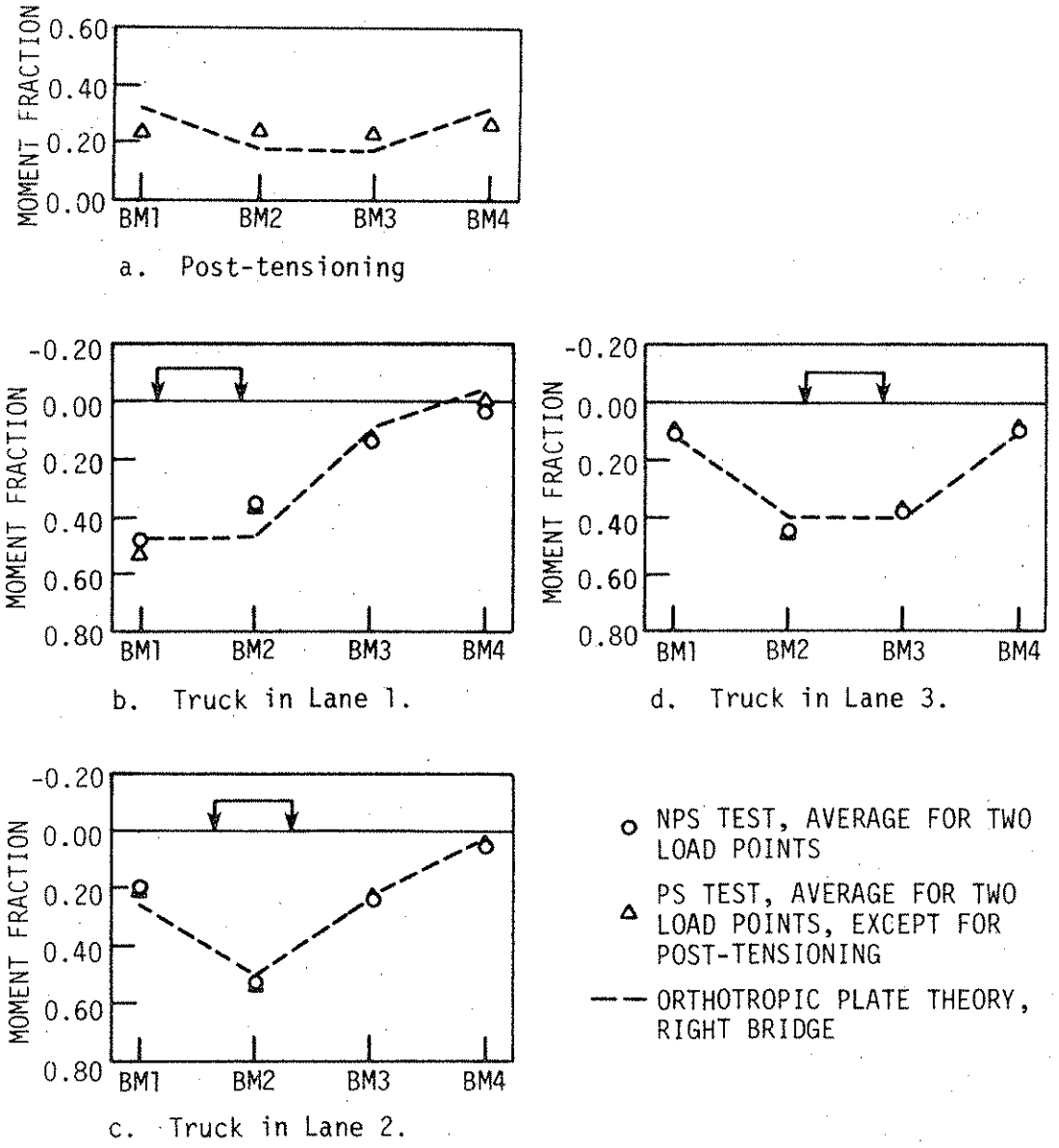

Fig. 61. Moment fractions based on midspan, bottom flange beam strains--Bridge 2.

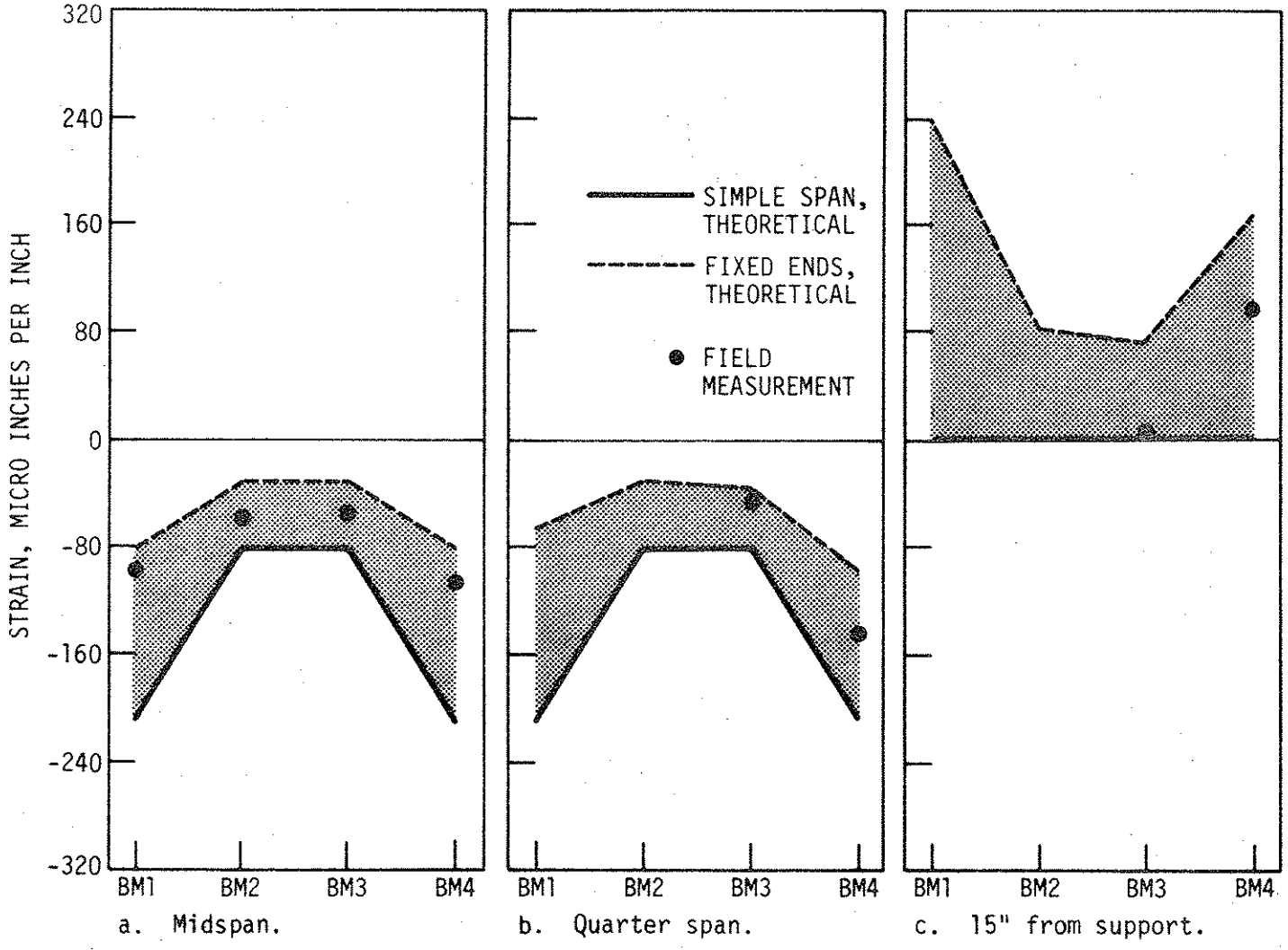

Fig. 62. Post-tensioning bottom flange beam strains -- Bridge 2.

generally one-half to two-thirds of those predicted for a simple span, right angle bridge. Although the change in the post-tensioning force when a truck is in Lane 1 could not be measured accurately due to strain indicator problems, the measured values were between the simple span and fixed end extreme conditions. Again, as was the case with Bridge 1, measured and theoretical moment fractions are in better agreement than measured and theoretical strains.

4.4.2.2 Effect of End Restraint

As noted in the literature review, beam end restraint is one of the consequences of skew. Comparisons of the results from the plexiglas model and Bridge 2 in the previous section were favorable, and thus, a large portion of measured end restraint could be attributed to skew. In addition, the plans for Bridge 2 showed construction that provided a greater degree of restraint and more uniform restraint from exterior to interior beams than the end restraint for Bridge 1.

In all of the figures in which measured strain was presented, both extreme conditions for a right angle bridge, simple span, and fixed end are drawn. In almost every case, the measured strains fell within the simple span, fixed end range. For post-tensioning alone, Fig. 62a indicated that all measured midspan strains lay within the range but were closer to the fixed end condition. In contrast to Fig. 55 for Bridge 1, the measured strains for Bridge 2 implied considerable end restraint for all beams, not just exterior beams. Strains measured at the quarter point of Bridge 2 (Fig. 62b) also implied end restraint. For the end restraint to exist, strains near the support would have to change from compression to tension for the post-tensioning.

This strain reversal is shown, at least for the exterior beam, in Fig. 62c.

Further evidence of end restraint in exterior beams is given in Fig. 63. At midspan, the quarter point, and 15 in. from the support, the measured strains generally approach the fixed end condition. For post-tensioning, strains reversed from compression to tension from midspan to the support (Fig. 63a). For the truck in Lane 1, strains reversed from tension to compression (Fig. 63b). Strains also reversed, for combined post-tensioning and the truck, usually coming closest to the fixed end condition (Fig. 63c). The midspan strains for combined post-tensioning and the truck in Lanes 1, 2 and 3 (Fig. 64a, b, and c) also approached the fixed end condition.

A comparison of the post-tensioning strains in Fig. 62a and the post-tensioning deflections in Fig. 65 showed good agreement. In both cases the measured values were approximately halfway between the simple span and fixed end conditions. With the truck in Lane 1, measured strains in Fig. 64a lay near the fixed end condition; the measured deflections in Fig. 66 also lay near the fixed end condition. Although the combined post-tensioning and truck strains in Fig. 64a generally lay near the fixed end condition, the same generalization did not fit the deflection data in Fig. 67 as well. The measured deflections exhibited more variability with respect to the simple span and fixed end conditions.

In the case of truck loading, the plexiglas model and Bridge 2 measured bottom flange strains were compared directly in Fig. 68. The magnitudes of the strains were in good to excellent agreement. This

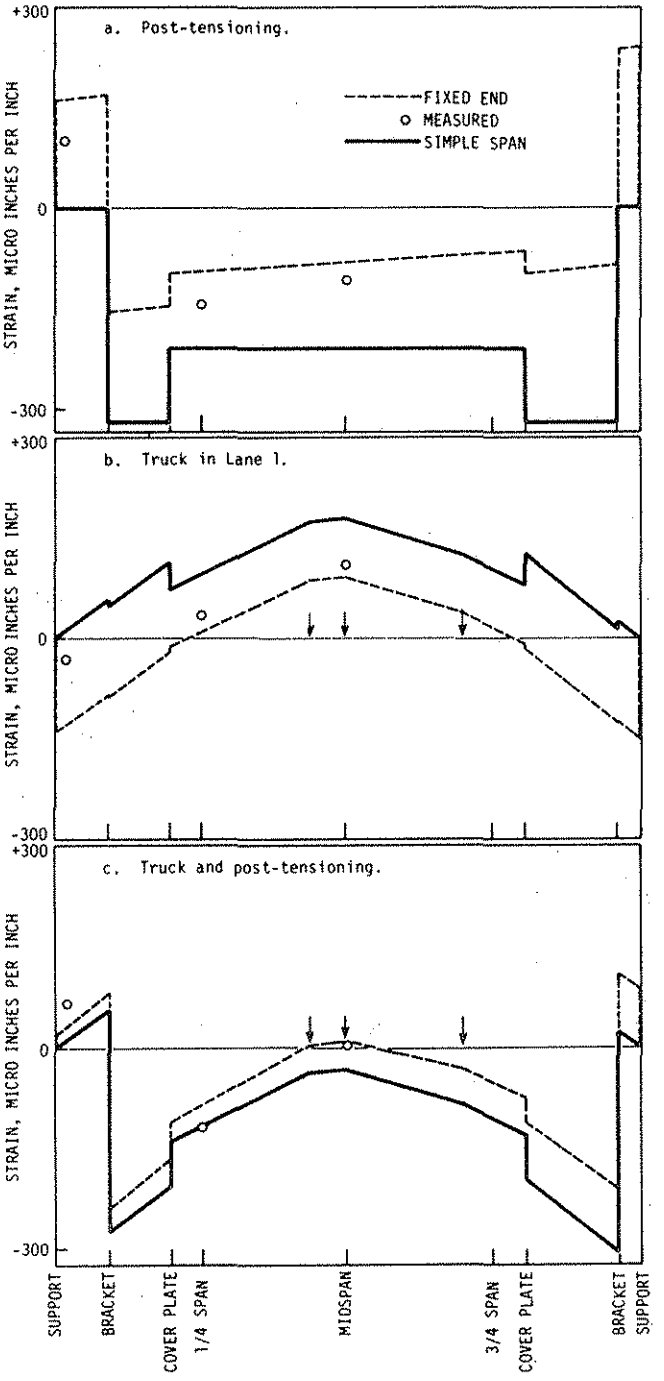

Fig. 63. Bottom flange strains, exterior beam--Bridge 2.

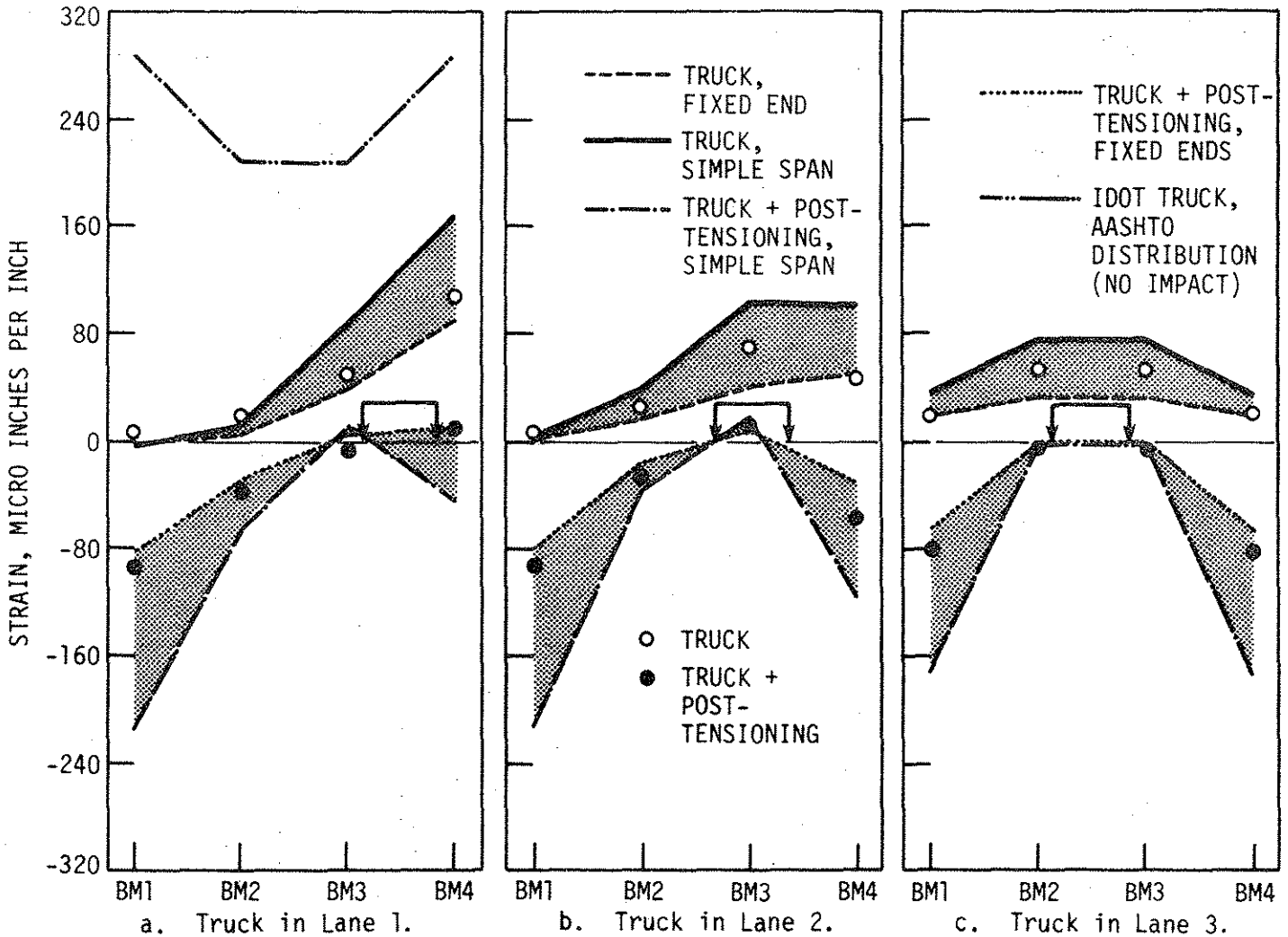

Fig. 64. Reduction of bottom flange midspan strain as a result of post-tensioning Bridge 2.

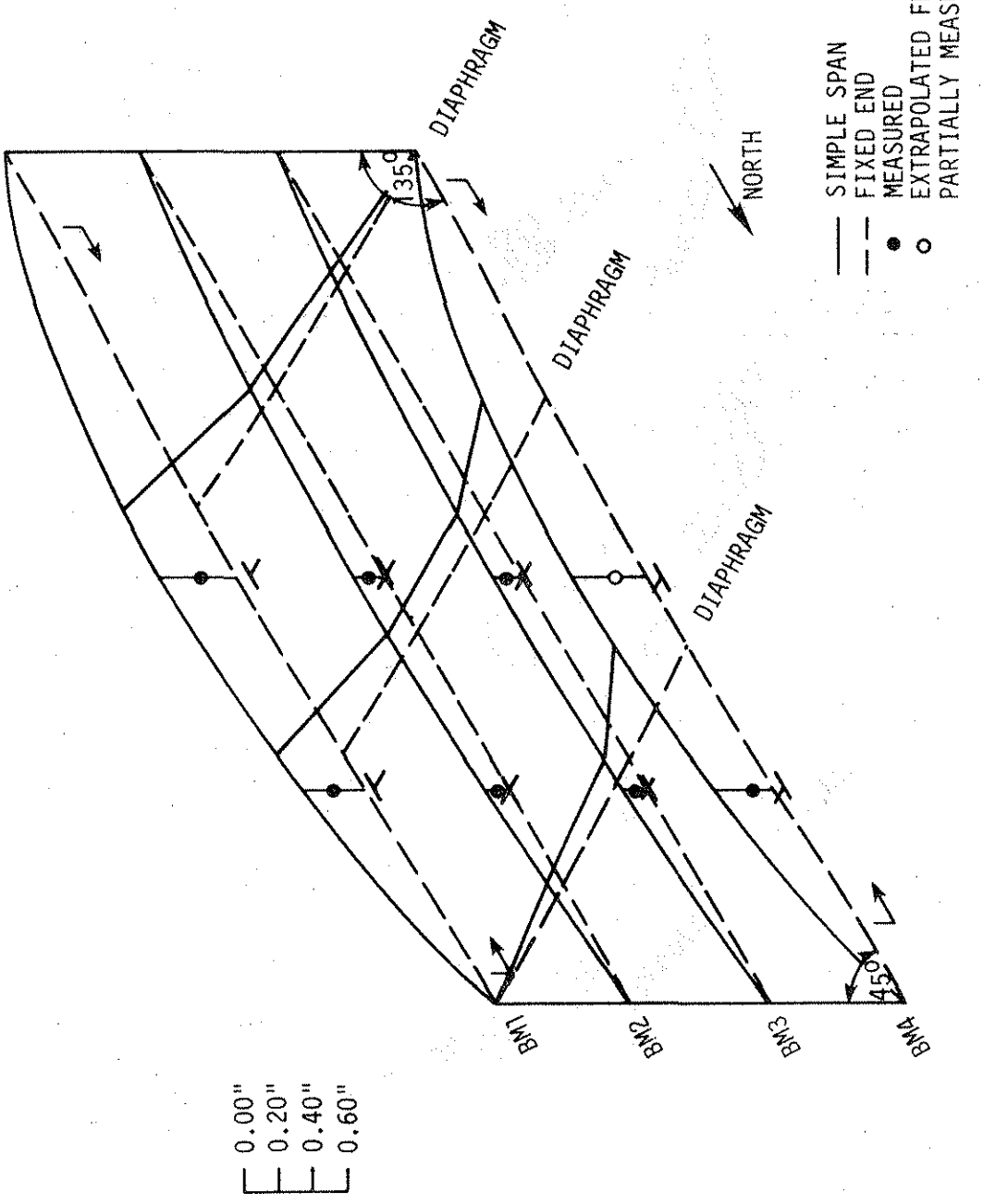

Fig. 65. Deflected shape for Bridge 2 with post-tensioning.

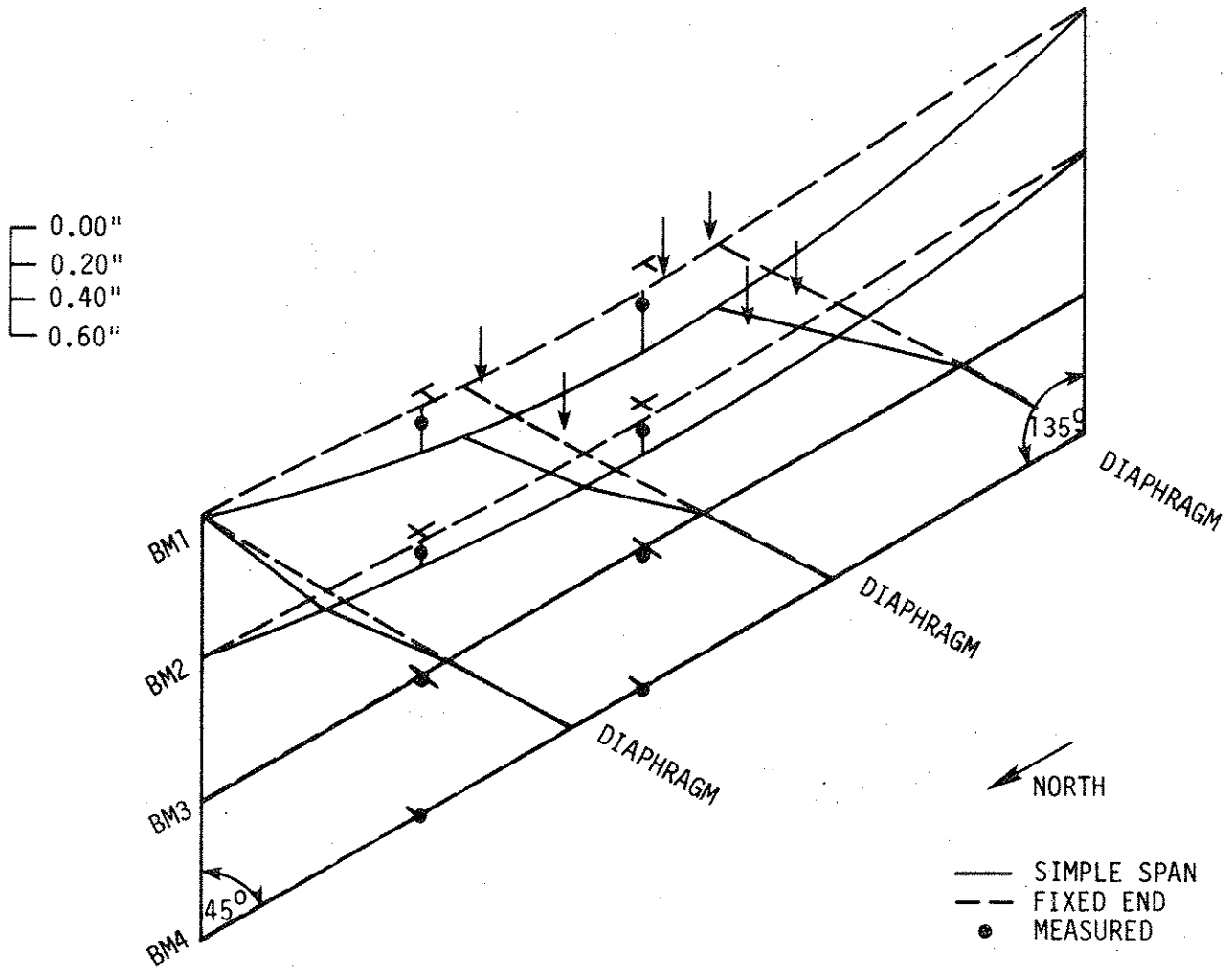

Fig. 66. Deflected shape for Bridge 2 with truck in Lane 1.

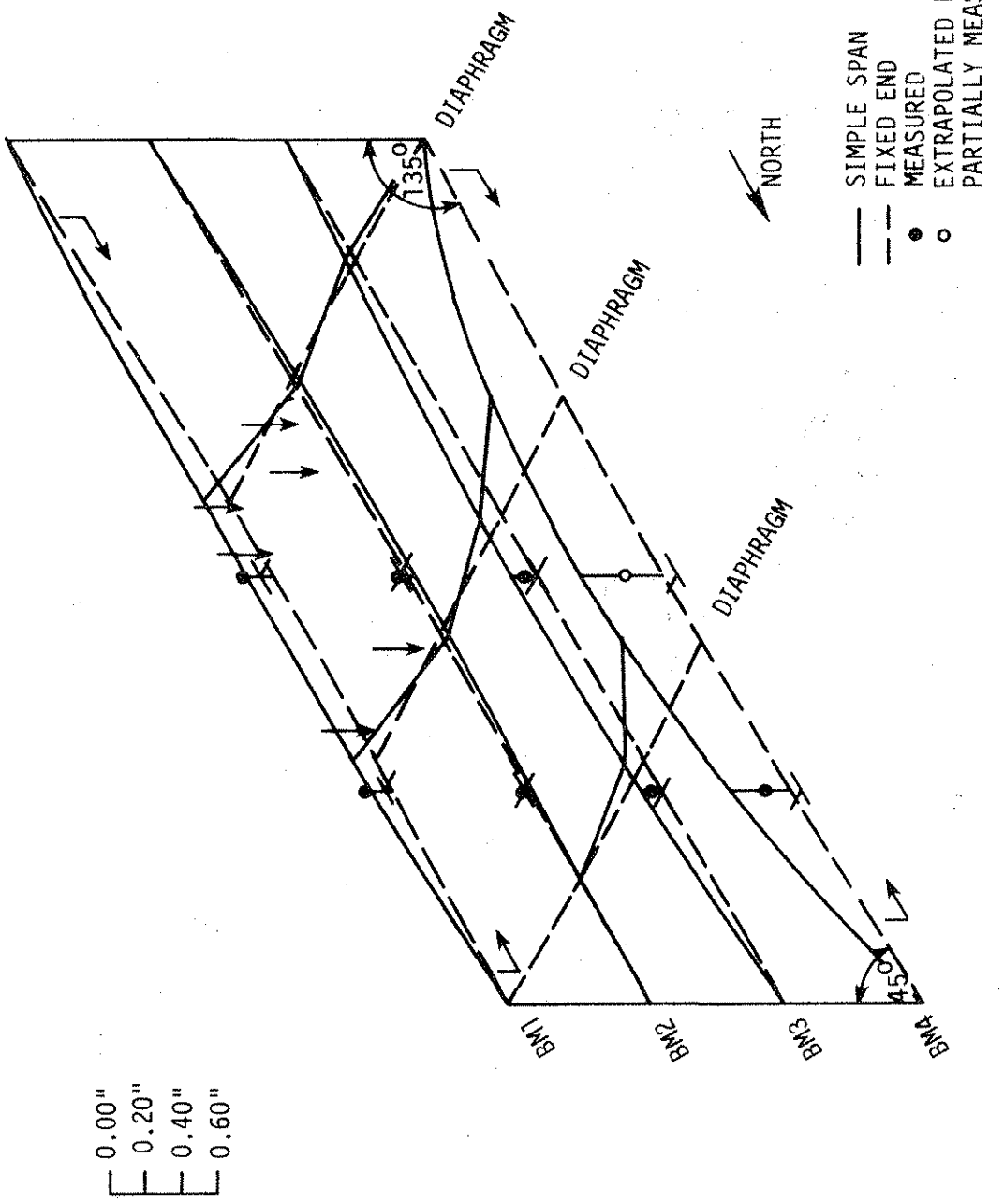

Fig. 67. Deflected shape for Bridge 2 with post-tensioning and truck in Lane 1.

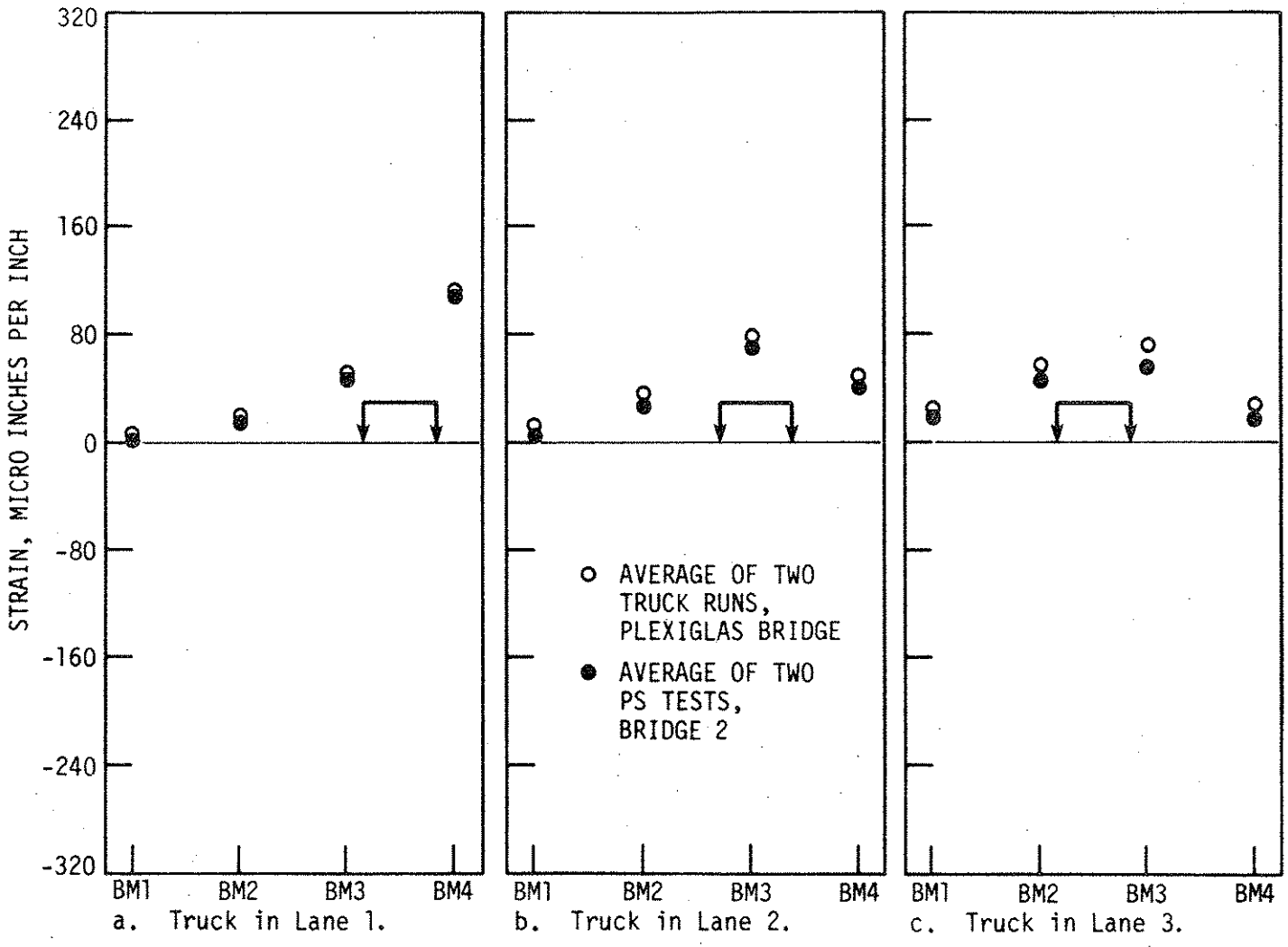

Figure 68. Measured bottom flange midspan strains--plexiglas bridge and Bridge 2.

validated the model, as well as indicated that end restraint was due more to skew than construction details at beam ends.

In almost all of the cases described above, strain and deflection measurements indicated considerable beam end restraint. The measured strains and deflections usually approached the theoretical fixed end condition for a right angle bridge. Both the plexiglas model and Bridge 2 exhibited end restraint, although the restraint for Bridge 2 was greater, due to construction details. The end restraint reduced post-tensioning effects but at the same time reduced truck live load effects.

4.4.2.3 Effect of Skew

In addition to causing end restraint for bridge beams, skew created a twist within the bridge deck. To give an indication of this twist, theoretical moment fractions for a truck in Lane 1 on a right angle bridge were plotted (Fig. 69), along with moment fractions computed from midspan bottom flange strains. Except for the exterior beam on the far side of the bridge, measured moment fractions from the three truck positions bracketed the theoretical moment fractions. The skew shifted moment toward the beams for which the truck was closest to midspan. Even with the twist, however, the measured moment fractions were reasonably close to theoretical.

4.4.3 Field Test Summary

The field testing program demonstrated that strengthening of composite bridges by post-tensioning is feasible and can be accomplished successfully. When existing shear connectors are inadequate, high strength bolt shear connectors can be added to the bridge relatively

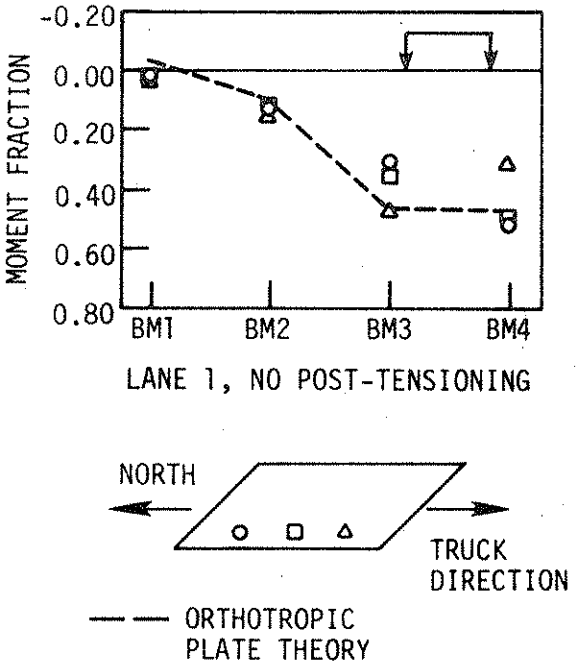

Fig. 69. Effect of truck position on moment fractions -- Bridge 2.

easily and economically. Although methods for post-tensioning utilized in Phase II were labor intensive, these methods were dictated by instrumentation and the need to check the sequence of tendon stressing. The overall strengthening process, in practice, could be accomplished with much less effort. Measurement of post-tensioning forces, for example, could be accomplished with jack pressures and checked by tendon elongation measurements.

Design methods used in Phase II adequately predicted the distribution of post-tensioning to the bridge. However, orthotropic plate theory was found to be more suitable for use with right-angle bridges (Bridge 1) than with skewed bridges (Bridge 2), as more discrepancy between experimental and theoretical results was found in Bridge 2. End restraint did affect load distribution and flexural stresses for both right-angle and skewed bridges. In addition to the effects of end restraint, in skewed bridges the effects of several other factors are unknown, such as the effect of angle of skew on reactions and shear stresses. Thus, a more exact analysis should be developed for skewed bridges. This new analysis, along with orthotropic plate theory for right-angle bridges, could then be used to develop a simplified design methodology. The methodology would permit the practicing engineer to refer to design tables or charts for post-tensioning data for right-angle and skewed bridges rather than spend considerable amounts of design time with exact theories.

5. SUMMARY AND CONCLUSIONS

5.1 Summary

The literature review indicated that behavior of skewed, orthotropic bridges was reasonably close to that for right-angle bridges, if the angle of skew did not exceed 45°. At a 45° skew, however, load distribution was affected somewhat, in that exterior beams tended to carry more load and interior beams less load. Several of the skew effects noted in the literature, such as increased moments and reactions near obtuse corners, were not checked in Phase II.

The literature review also established the validity of push-out tests for determining strength of shear connectors. Previous research had indicated that high strength steel bolts might be substituted for welded stud connectors of equal diameter with no loss in fatigue or ultimate capacity.

Laboratory testing of shear connectors established the capacity of existing angle-plus-bar connectors. Although the angle-plus-bar connectors were stiffer and exhibited less slip under load than comparable channel shear connectors did, the angle-plus-bar connectors did not have an ultimate capacity significantly larger than a comparable channel. On the basis of testing of Phase II, it was determined that the ultimate capacity of the angle-plus-bar connector could be determined from a modified AASHTO channel connector formula, provided that the weld capacity between the angle and bridge beam was not exceeded.

Two methods of adding connectors to existing bridge beams were tested, both of which involved high strength bolts. The double-nutted

bolt method (Series 6) and the epoxied bolt method (Series 7) of attaching bolt connectors gave load-slip characteristics similar to those for welded studs (Series 5). Both methods for attaching bolts provided connectors which gave a higher ultimate strength than a welded stud of the same diameter. Consequently, the AASHTO formula for ultimate strength of welded studs was conservative for high strength bolt connectors installed by either method. The double-nutted method was judged easier to install in the laboratory and consequently was used in the field with no difficulty.

The composite beams, which were cut from the half-scale bridge model of Phase I and tested to failure, gave an indication of the overall performance of post-tensioned composite beams. Although the beams deformed in the region of the brackets and the post-tensioning tendons deformed at the brackets at high loads, the post-tensioning system did not fracture. Instead, the observed beam failures occurred due to failure of the shear connectors or crushing of the slab concrete. In all cases the experimental ultimate moments were within 10% of computed ultimate moments.

The tests demonstrated that the addition of shear connectors to the model beams did increase ultimate capacity by an amount up to approximately 9%. In the case of the exterior beams, addition of shear connectors also changed the failure mode from shear connector failure to a flexural, slab/curb concrete crushing failure. Computations for the model bridge beams indicated that the addition of post-tensioning could increase ultimate capacity by up to 17%.

The plexiglas skewed bridge model duplicated the behavior of Bridge 2 very closely in terms of load distribution. Application of post-tensioning to the model caused beam moment fractions which deviated from moment fractions computed by orthotropic plate theory in the following manner: A greater fraction of the post-tensioning moment was shifted to interior beams than expected. The measured and computed moment fractions for post-tensioning of Bridge 2 deviated in the same manner. Moment fractions measured for model truck loads fell closer to moment fractions computed by orthotropic plate theory for a right angle bridge than those for post-tensioning. The model behavior again was duplicated in Bridge 2. Post-tensioning of the plexiglas model essentially did not affect model truck load distribution. Post-tensioning also did not affect truck load distribution in Bridge 2.

Somewhat unexpectedly, field-measured strains and deflections for Bridge 1 were less than those computed on the basis of orthotropic plate theory and simple span beam end conditions. The field results, however, were bracketed by simple span and fixed end beam conditions. All of the data indicated that end restraint at bridge abutments was greater than might be expected.

For post-tensioning only, measured strains and deflection at midspan of Bridge 1 indicated considerable end restraint for exterior beams, but almost no restraint for interior beams. For truck loading, with or without post-tensioning, measured strains and deflections indicated significant restraint at both interior and exterior beam ends. The difference in restraint from post-tensioning to truck loading might be explained by the fact that post-tensioning applied a

negative moment to the bridge, whereas truck loading applied a positive moment to the bridge. Abutment and support details for Bridge 1 most likely caused the difference in end restraint from negative to positive moment.

Because strains as a result of post-tensioning were only two-thirds of those computed to be required for strengthening the bridge, there could be concern that the strengthening was ineffective. However, strains measured for truck loading were also only two-thirds of those computed. The unexpected post-tensioning strain loss essentially was compensated by the also smaller than expected truck strains.

Testing of deck concrete cores from Bridges 1 and 2 gave strengths greater than 6000 psi vs. the 3000 psi assumed for analytical purposes. The higher deck strength had a very minor effect on the need for strengthening and the required post-tensioning force. The higher deck strength did, however, significantly increase the capacity of shear connectors and thereby had an effect on the need for additional shear connectors as part of a strengthening program.

As a result of the unexpected end restraint for Bridge 1, Bridge 2 was more extensively instrumented with strain gages and deflection dials. The additional instrumentation confirmed the existence of end restraint in Bridge 2.

For post-tensioning alone, field measured strains and deflections for Bridge 2 were only about one-half those computed for a simple span, right angle bridge. Essentially there was no difference between exterior and interior beams; for both types of beams the measured quantities were very close to those computed on the basis of fixed end

conditions. Comparison with the plexiglas model indicated that more of the end restraint was due to skew than to construction details at the abutments of Bridge 2.

For the truck loading, measured strains and deflections were one-half to two-thirds of those expected. The measured quantities generally lay midway between simple span and fixed end conditions or closer to the fixed end condition. For Bridge 2, post-tensioning did not affect truck load distribution.

Again, as was the case for Bridge 1, the post-tensioning did not cause as much compression strain as desired, but truck loading also did not cause as much tension strain as expected. The two effects essentially compensated.

As a result of the field work for both Bridge 1 and Bridge 2, it appeared that significant end restraints existed as a result of construction details for single span, right angle composite bridges and as a result of both skew and construction details for single span, skewed composite bridges. The restraint reduced the effect which truck loading had on the bridge beams and also reduced the effect which post-tension strengthening had on bridge beams.

5.2 Conclusions

The following conclusions were developed as a result of this study:

(1) The capacity of existing shear connectors must be checked as part of a bridge strengthening program. Since strength of

deck concrete has a significant effect on the need for additional shear connectors, determination of the concrete deck strength in advance of bridge strengthening is recommended.

(2) The ultimate capacity of angle-plus-bar shear connectors can be computed on the basis of a modified AASHTO channel connector formula and an angle-to-beam weld capacity check.

(3) Existing shear connector capacity can be augmented by means of double-nutted high strength bolt connectors. Ultimate capacity of a high strength bolt connector can be computed directly from the AASHTO formula for a welded stud.

(4) Post-tensioning did not significantly affect truck load distribution, either for right angle or for 45° skewed bridges.

(5) Approximate post-tensioning and truck load distribution for actual bridges can be predicted by orthotropic plate theory for vertical load; however, the agreement between actual distribution and theoretical distribution is not as close as that measured for the laboratory model in Phase I.

(6) The right angle bridge (Bridge 1) exhibited considerable end restraint at what would be assumed to be simple support. The construction details at bridge abutments seem to be the reason for the restraint.

(7) The 45° skewed bridge (Bridge 2) exhibited more end restraint than Bridge 1. Both skew effects and construction details at the abutments accounted for the restraint.

(8) End restraint in Bridges 1 and 2 reduced tension strains in the steel bridge beams due to truck loading, but also reduced the compression strains caused by post-tensioning. In effect, the truck tension strain losses compensated for the post-tensioning compression strain losses.

6. RECOMMENDED CONTINUED STUDIES

On the basis of the literature review and testing program, the following should be checked:

(1) End restraint and differences in end restraint among bridge beams affect load distribution and the performance of a bridge. A study of the variables involved in end restraints should be undertaken to insure that reasonable combinations of end restraints do not cause excessive flexural or shear stresses. Theoretical results should be substantiated by measurement of the end restraint in several bridges.

(2) Skew does affect shears and reactions for both post-tensioning and truck loading. At this point the extent of skew effects are unknown and should be determined to insure that allowable shear stresses in bridge beams are not exceeded.

(3) Although orthotropic plate theory has been shown to predict load distribution in right angle bridges, there are greater differences between orthotropic results and experimental results in skewed bridges. Thus, skewed bridges should be analyzed in more detail and a design methodology developed, in which the design engineer simply uses design curves, charts, and so forth for load distribution rather than the more involved theories.

(4) The concept of utilizing the post-tensioning tendons in a "king-post" arrangement rather than straight should be investigated. The "king-post" arrangement has the advantage

of providing a vertical lift component, as well as making possible the required jacking operation from the top of the bridge rather than under it.

(5) Post-tension strengthening has successfully been applied to simple-span bridges. The problems associated with utilizing similar strengthening in the positive and negative moment regions of continuous bridges should be investigated.

(6) Presently there are no data on the effects of dynamic loading on the post-tension strengthened beams or on the fatigue strength of these beams. In a laboratory study, the same specimens could be used to determine both of these properties.

(7) As previously stated, in the author's opinion, there should be no fatigue problems with the bolting configuration proposed. However, there are no data available concerning the fatigue strength of the core patching grout in combination with the existing concrete. A relatively small study should be undertaken to determine if there are any problems in utilizing the high strength bolt shear connectors in combination with the two different concretes.

7. ACKNOWLEDGMENTS

The study presented in this report was conducted by the Engineering Research Institute of Iowa State University and was sponsored by the Highway Division, Iowa Department of Transportation, and the Iowa Highway Research Board under Research Project HR-238.

The authors wish to extend sincere appreciation to the engineers of the Iowa DOT for their support, cooperation, and counseling. A special thanks is extended to the following individuals for their help in various phases of the project:

- Charles A. Pestotnik, Bridge Engineer, Iowa DOT
- John P. Harkin, Bridge Rating Engineer, Iowa DOT
- Vernon J. Marks, Research Engineer, Iowa DOT
- Richard D. Smith, Research Technician, Iowa DOT
- Jimmy Wooters, Resident Maintenance Engineer (Gowrie area), Iowa DOT
- Kenneth D. Westergard, County Engineer, Dickinson County.

Appreciation is also extended to Eugene A. Lamberson of Dywidag Systems International (DSI), who donated all the Dywidag Threadbars used on the bridges. The epoxy coating of the bars by Midwest Pipe Coating, Inc. is also appreciated.

Special thanks are accorded the following students for their assistance in various phases of the project: graduate students Benjamin J. Biller, Michael J. Herlihy III, and Douglas L. Wood; and undergraduate students Tim A. Dedic, Bruce J. Hattig, Scott Thompson, and Brad Beck.

8. BIBLIOGRAPHY

1. American Association of State Highway and Transportation Officials. Standard Specifications for Highway Bridges, 12th Edition. Washington, D.C.: American Association of State Highway and Transportation Officials, 1977.

2. American Association of State Highway and Transportation Officials. Manual for Maintenance Inspection of Bridges 1978. Washington, D.C.: American Association of State Highway and Transportation Officials, 1978.

3. Bakht, Baidar, M. S. Cheung and T. S. Aziz. "Application of a Simplified Method of Calculating Longitudinal Moments to the Ontario Highway Bridge Design Code." Canadian Journal of Civil Engineering. Vol. 6, 1979. pp. 36-50.

4. Clark, L. A. and R. West. The Behaviour of Solid Skew Slab Bridges under Longitudinal Prestress. London: Cement and Concrete Association, 1974.

5. Cook, John P. Composite Construction Methods. New York: John Wiley and Sons, 1977.

6. Dallam, Lawrence N. "Pushout Tests With High-Strength Bolt Shear Connectors." Missouri Cooperative Highway Research Program Report 68-7. Engineering Experiment Station, University of Missouri-Columbia, 1968.

7. Dallam, Lawrence N. "Static and Fatigue Properties of High-Strength Bolt Shear Connectors." Missouri Cooperative Highway Research Program Report 70-2. Engineering Experiment Station, University of Missouri-Columbia, 1970.

8. deCastro, Ernesto S. and Celal N. Kostem. Load Distribution in Skewed Beam-Slab Highway Bridges, Fritz Engineering Laboratory Report No. 378A.7. Bethlehem: Fritz Engineering Laboratory, Lehigh University, 1975.

9. Dedic, David J. "Push-out and Composite Beam Tests of Shear Connectors," M.S. Thesis, Iowa State University, Ames, Iowa, 1983.

10. Dorton, Roger A. "The Conestoga River Bridge Design and Testing." A paper presented at Canadian Structural Engineering Conference, 1976.

11. Gaylord, E. H., Jr. and C. N. Gaylord, Editors. Structural Engineering Handbook, Second Edition. New York: McGraw-Hill Book Company, 1979.

12. Goble, G. G. "Shear Strength of Thin Flange Composite Specimens." American Institute of Steel Construction, Engineering Journal. Vol. 5, No. 2, April 1968. pp. 62-65.

13. Gustafson, William C. and Richard N. Wright. "Analysis of Skewed Composite Girder Bridges." American Society of Civil Engineers, Journal of the Structural Division. Vol. 94, No. ST4, April 1968. pp. 919-941.

14. Heins, C. P. and D. A. Firmage. Design of Modern Steel Highway Bridges. New York: John Wiley and Sons, 1979.

15. Hondros, G. and J. G. Marsh. "Load Distribution in Composite Girder-Slab Systems." American Society of Civil Engineers, Journal of the Structural Division. Vol. 86, No. ST11, November 1960. pp. 79-109.

16. Johnson, R. P. Composite Structures of Steel and Concrete, Volume 1. New York: John Wiley and Sons, 1975.

17. Kennedy, John B. and Davalath S. R. Gupta. "Bending of Skew Orthotropic Plate Structures." American Society of Civil Engineers, Journal of the Structural Division. Vol. 102, No. ST8, August 1976. pp. 1559-1574.

18. Klaiber, F. W., K. F. Dunker and W. W. Sanders, Jr. "Strengthening of Single Span Steel Beam Bridges." American Society of Civil Engineers, Journal of the Structural Division. Vol. 108, No. ST12, December 1982. pp. 2766-2780.

19. Klaiber, F. W., K. F. Dunker and W. W. Sanders, Jr. Feasibility Study of Strengthening Existing Single Span Steel Beam Concrete Deck Bridges. Final Report, ISU-ERI-Ames-81251. Ames: Engineering Research Institute, Iowa State University, 1981.

20. Klaiber, F. W., W. W. Sanders, Jr. and D. J. Dedic. "Post-Tension Strengthening of Composite Bridges." Final Report, IABSE Symposium on Maintenance Repair and Rehabilitation of Bridges, Vol. 39, 1982. International Association of Bridge and Structural Engineering. pp. 123-128.

21. Knowles, P. R. Composite Steel and Concrete Construction. New York: John Wiley and Sons, 1973.

22. Lee, D. J. and E. C. Chaplin. "Design and Analysis of Skew Bridge Structures." Symposium on Prestressed Concrete in Short to Medium Span Bridges--Proceedings. FIP/Concrete Institute of Australia. Sydney, August 30/31, 1976.

23. Newmark, N. M., C. P. Siess and W. M. Peckham. "Tests of Simple-Span Skew I-Beam Bridges." Studies of Slab and Beam Highway Bridges, Part II. University of Illinois Bulletin, Vol. 45, No. 31, Bulletin Series No. 375, January 1948.

24. Ollgard, Jorgen G. "The Strength of Stud Shear Connectors in Normal and Lighweight Concrete." M.S. Thesis, Lehigh University, Bethlehem, Pennsylvania, 1970.

25. Ollgard, J. G., R. G. Slutter and J. W. Fisher. "Shear Strength of Stud Connectors in Lightweight and Normal-Weight Concrete." American Institute of Steel Construction, Engineering Journal. Vol. 8, No. 2, April 1971. pp. 55-64.

26. Sabnis, Gahanan M., Editor. Handbook of Composite Construction Engineering. New York: Van Nostrand Reinhold Company, 1979.

27. Siess, C. P., N. M. Newmark and I. M. Viest. "Small Scale Tests of Shear Connectors and Composite T-Beams." Studies of Slab and Beam Highway Bridges, Part III. University of Illinois Bulletin, Vol. 49, No. 45, Bulletin Series No. 396, February 1952.

28. Slutter, R. G. and G. C. Driscoll. "Flexural Strength of Steel-Concrete Beams." American Society of Civil Engineers, Journal of the Structural Division. Vol. 91, No. ST2, April 1965. pp. 71-99.

29. Viest, I. M. "Investigation of Stud Shear Connectors for Composite Concrete and Steel T-Beams." Journal of the American Concrete Institute. Vol. 27, No. 8, April 1956. pp. 875-891.

30. Viest, I. M. and C. P. Siess. "Design of Channel Shear Connectors for Composite I-Beam Bridges." Public Roads. Vol. 28, No. 1, April 1954. pp. 9-16.

31. Viest, I. M., C. P. Siess, J. P. Appleton and N. M. Newmark. "Full Scale Tests of Channel Shear Connectors and Composite T-Beams." Studies of Slab and Beam Highway Bridges, Part IV. University of Illinois Bulletin, Vol. 50, No. 29, Bulletin Series No. 405, December 1952.

32. Yam, L. C. P. Design of Composite Steel-Concrete Structures. London: Surrey University Press, 1981.

9. APPENDIX A.

DETAILS OF POST-TENSIONING BRACKETS USED ON BRIDGES 1 AND 2.

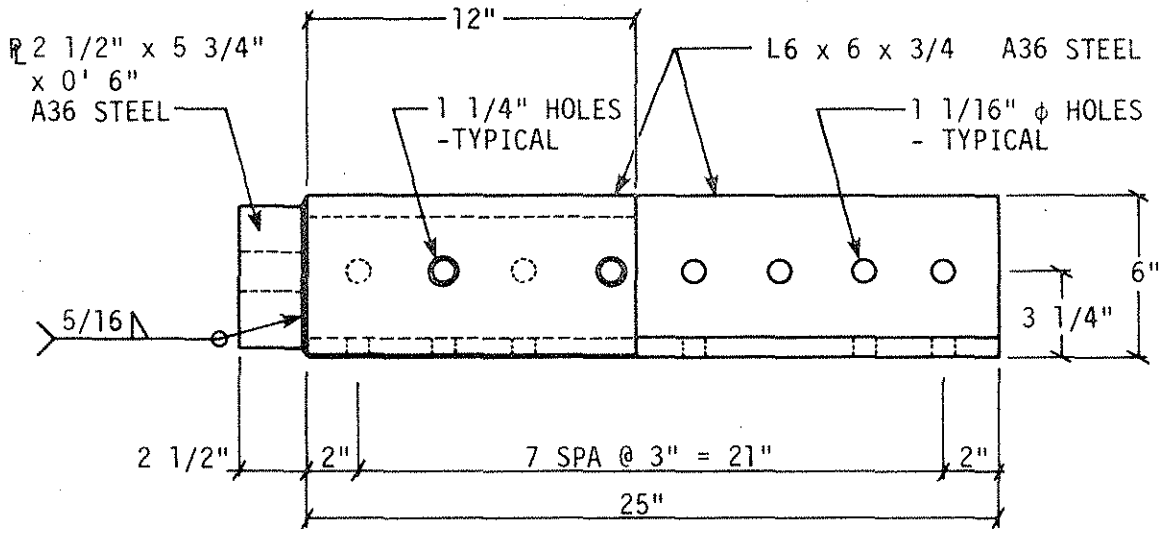

a. Side view.

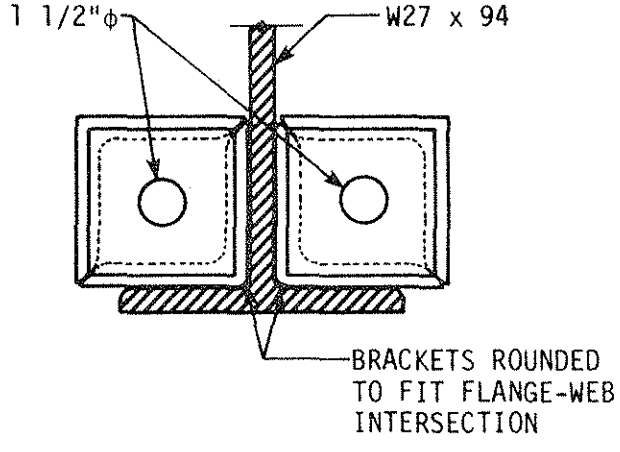

b. End view.

Fig. A-1. Post-tensioning bracket -- Bridge 1.

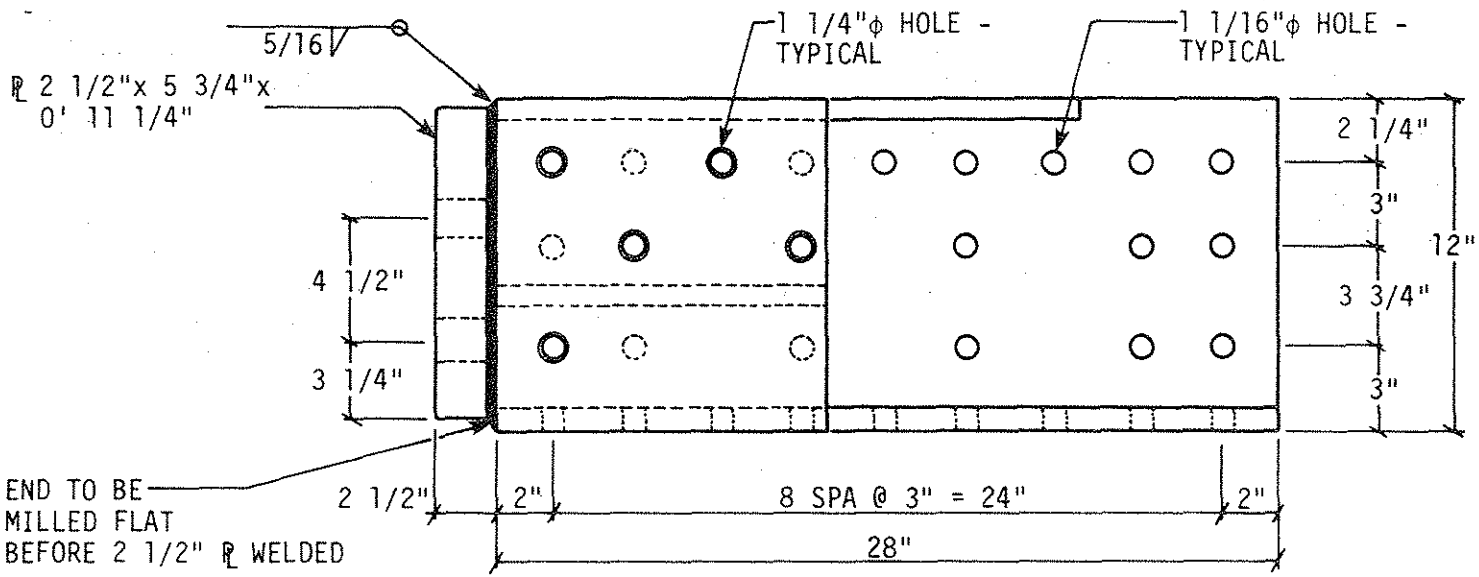

a. Side view.

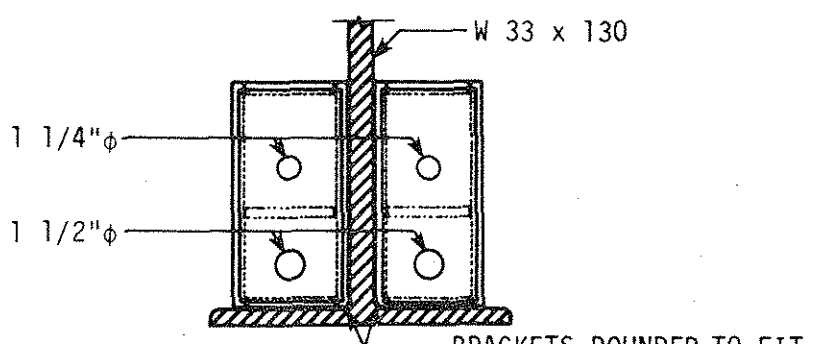

b. End view.

NOTES:

ALL STEEL A36.

EXCEPT AS NOTED,
ALL STEEL 3/4" ℄

Figure A-2. Post-tensioning bracket--Bridge 2.